A Theory for Track Maintenance Life Prediction

JUNE 1981
DOT/RSPA/DPB-50/81/25

FINAL REPORT
UNDER CONTRACT:
DOT-05-70058

Washington, D.C. 20590

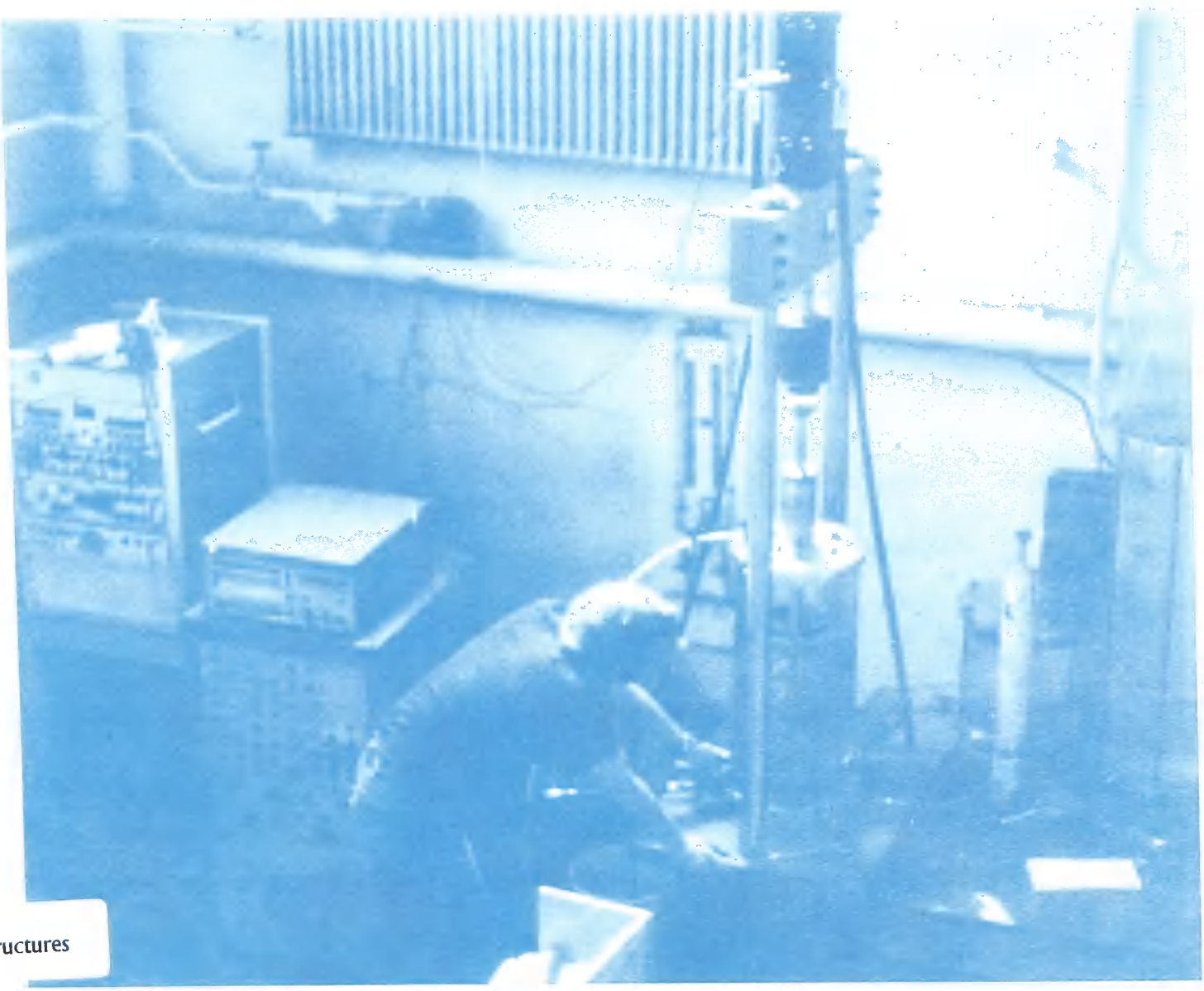

U.S. Department of Transportation
Research and Special Programs Administration

ack & Structures

(inside front cover)

NOTICE

This document is disseminated under the sponsorship of the Department of Transportation in the interest of information exchange. The United States Government assumes no liability for the contents or use thereof.

NOTICE

The United States Government does not endorse products or manufacturers. Trade or manufacturer's names appear herein solely because they are considered essential to the object of this report.

Technical Report Documentation Page

1. Report No.	2. Government Accession No.	3. Recipient's Catalog No.
DOT-RSPA/DPB-50/81/25		

4. Title and Subtitle	5. Report Date
A Theory for Track Maintenance Life Prediction	June 1981
	6. Performing Organization Code
	8. Performing Organization Report No.
7. Author(s) Ernest T. Selig, Ching S. Chang, Jorge E. Alva-Hurtado, and Clement W. Adegoke	
9. Performing Organization Name and Address Department of Civil Engineering, State University of New York at Buffalo, and University of Massachusetts, Marston Hall Amherst, Massachusetts 01003	10. Work Unit No. (TRAIS) 11. Contract or Grant No. DOT-OS-70058
12. Sponsoring Agency Name and Address Office of University Research Research & Special Programs Administration U. S. Department of Transportation Washington, D.C. 20590	13. Type of Report and Period Covered July 1977-July 1980 Second Year Final Report 14. Sponsoring Agency Code DPB-50

15. Supplementary Notes

This report is the final report covering the work for the second year of the research contract. Technical Monitor: Philip Mattson, DTS-741 Transportation Systems Center

16. Abstract

The objective of this study is to develop a methodology for predicting cumulative permanent deformation of track structures under traffic loading as a basis for maintenance life determination. This report presents the progress achieved in the second year of the research. A computer model named GEOTRACK was developed that represents the nonlinear elastic deformation of the track system. On the basis of a comparison of the elastic predictions with this model and the dynamic measurements from FAST, the model was considered to provide a reasonable representation of the track response. Available information on the elastic and inelastic properties of ballast and subgrade materials under cyclic load was reviewed as a basis for selecting the form of material constitutive relationships required for the track performance predictions. Static and cyclic triaxial tests were then carried out on granite ballast with equivalent stress states determined from the GEOTRACK model. The method of predicting permanent strain accumulation in the ballast layer under the track is then described and predictions using this approach are illustrated by comparing them to measured inelastic strains in the FAST track.

17. Key Words	18. Distribution Statement
Computer model, cyclic properties, dynamic response, material characterization, permanent deformation, track model, track maintenance	Document is Available to the U.S. Public through the National Technical Information Service, Springfield, VA 22161

19. Security Classif. (of this report)	20. Security Classif. (of this page)	21. No. of Pages	22. Price
Unclassified	Unclassified		

METRIC CONVERSION FACTORS

Approximate Conversions to Metric Measures

Symbol	When You Know	Multiply by	To Find	Symbol
	LENGTH			
in	inches	*2.5	centimeters	cm
ft	feet	30	centimeters	cm
yd	yards	0.9	meters	m
mi	miles	1.6	kilometers	km
	AREA			
in^2	square inches	6.5	square centimeters	cm^2
ft^2	square feet	0.09	square meters	m^2
yd^2	square yards	0.8	square meters	m^2
mi^2	square miles	2.6	square kilometers	km^2
	acres	0.4	hectares	ha
	MASS (weight)			
oz	ounces	28	grams	g
lb	pounds	0.45	kilograms	kg
	short tons (2000 lb)	0.9	tonnes	t
	VOLUME			
tsp	teaspoons	5	milliliters	ml
Tbsp	tablespoons	15	milliliters	ml
fl oz	fluid ounces	30	milliliters	ml
c	cups	0.24	liters	l
pt	pints	0.47	liters	l
qt	quarts	0.95	liters	l
gal	gallons	3.8	liters	l
ft^3	cubic feet	0.03	cubic meters	m^3
yd^3	cubic yards	0.76	cubic meters	m^3
	TEMPERATURE (exact)			
°F	Fahrenheit temperature	5/9 (after subtracting 32)	Celsius temperature	°C

*1 in = 2.54 (exactly). For other exact conversions and more detailed tables, see NBS Misc. Publ. 286, Units of Weights and Measures, Price $2.25, SD Catalog No. C13.10:286.

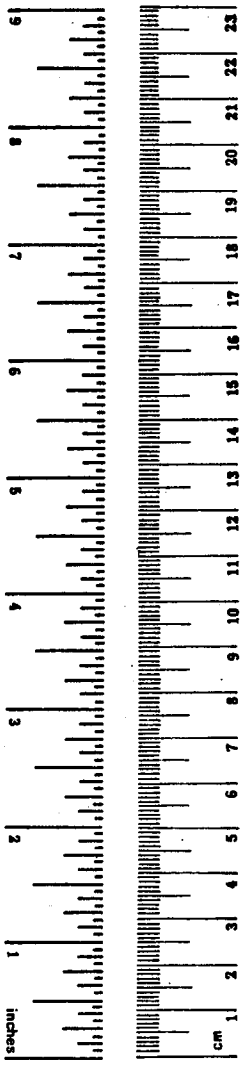

Approximate Conversions from Metric Measures

Symbol	When You Know	Multiply by	To Find	Symbol
	LENGTH			
mm	millimeters	0.04	inches	in
cm	centimeters	0.4	inches	in
m	meters	3.3	feet	ft
m	meters	1.1	yards	yd
km	kilometers	0.6	miles	mi
	AREA			
cm^2	square centimeters	0.16	square inches	in^2
m^2	square meters	1.2	square yards	yd^2
km^2	square kilometers	0.4	square miles	mi^2
ha	hectares (10,000 m^2)	2.5	acres	
	MASS (weight)			
g	grams	0.035	ounces	oz
kg	kilograms	2.2	pounds	lb
t	tonnes (1000 kg)	1.1	short tons	
	VOLUME			
ml	milliliters	0.03	fluid ounces	fl oz
l	liters	2.1	pints	pt
l	liters	1.06	quarts	qt
l	liters	0.26	gallons	gal
m^3	cubic meters	35	cubic feet	ft^3
m^3	cubic meters	1.3	cubic yards	yd^3
	TEMPERATURE (exact)			
°C	Celsius temperature	9/5 (then add 32)	Fahrenheit temperature	°F

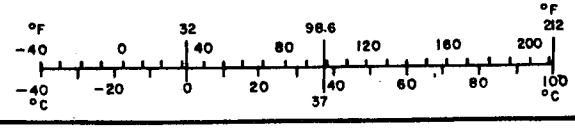

EXECUTIVE SUMMARY

Problem Studied

This is the final report covering the work for the second year of a research contract under sponsorship by the Office of University Research. The objective of this research is to develop a methodology for predicting maintenance life of track structures as governed by the cumulative permanent deformation developed under traffic loading in the ballast and underlying soil layers.

The research included: 1) a review of the relevant behavior of ballast and soil material, 2) development of a mathematical model of the track system, 3) a laboratory program of static and cyclic tests on ballast, and 4) establishing and evaluating a method for permanent strain prediction in track structures. The approach is similar to that which has been used for predicting the deterioration of highway pavements resulting from soil permanent deformation.

Basically, the track structure, including the ballast and soil components, responds elastically under each load application. However, permanent strain can become significant after a large number of cycles. An elastic track system model which incorporates the effects of the train loading, the rail, the tie, the ballast and the soil layers can be used for determining the stresses in any particular situation. Appropriate laboratory property tests are used to establish the relationship between these elastic stresses and the resulting plastic strains, as a function of the number of load applications. The resulting strains after any number of cycles are then summed to estimate the track permanent settlement for the equivalent traffic level.

Results Achieved

Based on a review of available computer models for the track structure, and an evaluation of the model requirements for maintenance life prediction, a new model, GEOTRACK, was developed. This model incorporates the essential features

of the system and is also economical to run on the computer.

Both static and cyclic tests were conducted on granite ballast from FAST. These tests helped establish the appropriate representation of the material properties for use in the prediction method. The tests also provided ballast property values for the Facility for Accelerated Service Testing track (FAST) in Pueblo, Colorado, from which data were obtained for evaluating the model predictions. An important result of these property test experiments was the establishment of an approximate method to predict cyclic permanent strains from static tests.

A methodology for permanent strain prediction in ballast and underlying soil layers was formulated. This approach gave results that were in reasonable agreement with observed field performance at FAST. However, the method represents uniform track settlement rather than the differential settlement that causes the need for track maintenance. Further research is planned to establish a means for nonuniform settlement prediction.

Utilization of Results

The methodology has been developed to the point that it can be used to provide a rational basis for decision making in maintenance planning and track design. Along with continued development and evaluation of the methodology, an effort will be made to advise potential users of the capabilities of the model and assist in its implementation in practice.

PREFACE

The work described in this report was begun at the State University of New York at Buffalo (SUNYAB) and completed at the University of Massachusetts (UMass). The work was conducted for the U. S. Department of Transportation, supported by funds from the Office of University Research. This report is a summary of the results of the second year of investigation under Contract No. DOT-OS-70058.

The objective of this research, which was begun in July, 1977, is to develop a theory for predicting track maintenance life. Work on this project was conducted under the direction of Dr. Ernest T. Selig, Professor of Civil Engineering and Principal Investigator, and Dr. Ching S. Chang, Assistant Professor of Civil Engineering and Co-Principal Investigator. The technical monitor for the research was Mr. Philip Mattson of the DOT Transportation Systems Center in Cambridge, Massachusetts.

Graduate students at the State University of New York and the University of Massachusetts participated in the research. Doctoral dissertations by Clement W. Adegoke and Jorge E. Alva-Hurtado cover the majority of the work and provide most of the material contained in the first and second year reports. Harry E. Stewart participated in the FAST track dynamic data preparation and the property tests on the ballast and subgrade materials. Michael J. Mann participated in the FAST static data preparation and performed computer analysis using the GEOTRACK model. Deh C. Ho also assisted with the computer analyses. Donald R. McMahon assisted with the static ballast property tests. Brian C. Dorwart aided in the set up of the cyclic testing machines and the associated instrumentation. Thomas J. Siller assisted with the cyclic tests. In addition, a considerable effort in the FAST data analysis was contributed

by Dr. Tai-Sung Yoo, Research Assistant Professor at SUNYAB.

A primary factor in the success of the research during the transition of staff from SUNYAB to UMass was the administrative assistance provided by Janet V. Prosser at SUNYAB and the administrative assistance and responsibility for preparation of the final report manuscript provided by Kristin J. Currier at UMass.

CONTENTS

CONTENTS (cont'd)

LIST OF FIGURES

LIST OF TABLES

CHAPTER 1. INTRODUCTION

The specific objective of this research is to develop a methodology for predicting cumulative permanent deformation of track structures under traffic loading as a basis for maintenance life determination. The approach involves:

1. A study of available information to develop a means of characterizing the behavior of ballast and track roadbed soils that causes the permanent deformation.

2. Development of an appropriate mathematical model of the track structure for use in permanent deformation prediction.

3. Constructing a cyclic test facility and using this facility for conducting property tests on ballast and subgrade soils for obtaining needed properties.

4. Establishing a preliminary methodology for permanent deformation prediction and assessing the validity of the model by a comparison with available field data.

Over the past few years, considerable amount of attention has been directed towards the application of analytical methods in the design of railroad track structures. Such effort has resulted in the development of various computer models for predicting the stress, strain and deflection in the track structures under transient loads. Attempts were made to more realistically incorporate the properties of the roadbed materials, that is the ballast and subgrade, into the mathematical models. Simultaneously, an appreciable amount of data have been generated from repeated load tests performed on ballast and subgrade materials to provide material characterization for input to the models.

The general approach for predicting track response has been fashioned after

the approach developed for highway and airfield pavements. It is assumed that under moderate stress levels, the response of most subgrade and granular materials becomes relatively elastic and constant after a few hundred load repetitions. Under each load application, the transient response of the track system thus can be predicted using a linear or a non-linear, elastic analytical model. The permanent inelastic deformations which accumulate upon repeated application of such stresses are obtained from a relationship between the plastic strains, elastic stress and number of load applications.

While this approach has been applied with some degree of success in pavement research, the suitability of this approach for track structures had not been determined. It is likely that the accuracy of the model will depend critically on the ability to represent in the laboratory tests the effects of stress states to which the roadbed elements are subjected in the field. As a result of insufficient field data in the past, the available analytical models previously developed had not been validated. However, a significant advance in the state of understanding of track response has been possible as a result of an instrumentation program conducted at the DOT Facility for Accelerated Service Testing (FAST) track in Pueblo, Colorado, to monitor the response of the ballast and subgrade layers under traffic.

This report presents the progress achieved in the second year of the research. A previous report (Ref. 1) covered the first year of the research. In the first year, an examination was made of the dynamic and cumulative strains in the ballast, subballast and subgrade at the FAST track to determine the general characteristics required of the prediction models. Then the available computer programs MULTA, PSA and ILLITRACK were evaluated. Dynamic measurements from several track sections at FAST were compared with the predicted results from the three models. Based on the assessment of the models and the computer

program performance, MULTA was selected for further modification into a non-linear elastic, stress-dependent model. This new model was used as a basis for stress state determination in the maintenance life prediction methodology.

Cyclic triaxial test equipment with associated control apparatus was designed and fabricated for measuring the material behavior for the track model. The triaxial cell can handle either 6 or 8-in. diameter samples. With this apparatus, the resilient modulus and permanent deformation behavior of ballast and subgrade materials can be studied, including the effects of initial stresses and cyclic stress increases from the train loads.

A survey of existing permanent deformation prediction procedures was described in this report. It was concluded that the most promising procedure uses the stress path approach for property determination in a manner analogous to the recently developed approach for predicting rut depth in pavement applications.

In the second year, the model for the elastic deformation of the track system was further refined and evaluated. This new model, GEOTRACK, is described in this report and a comparison of predictions with FAST dynamic measurements is made. A review of cyclic behavior of ballast and some soil materials is also made to establish an appropriate material characterization for the track model. The method of defining the stress conditions for the ballast property tests using the equivalent stress path approach and the GEOTRACK model is then described. The observed cumulative strains in the ballast, subballast and subgrade at the FAST track are briefly described. Then the results of static and cyclic triaxial tests on the FAST granite ballast are also presented. Finally, the approach for prediction of ballast cumulative strain is described and the results, based on the triaxial property tests, are compared to the field behavior.

CHAPTER 2. GEOTRACK MODEL

2.1 Introduction

In the first year final report (Ref. 1), three analytical models for the track system were described. These were MULTA, PSA and ILLITRACK. The characteristics of the models were examined, and their accuracy checked by numerical comparisons with field data (Refs. 2, 5). The field data (Refs. 4, 6) were obtained from the instrumented FAST track in Pueblo, Colorado.

The observed dynamic response of the track roadbed as a function of various track parameters such as ballast type, ballast depth, tie type and wheel loads was shown from the FAST experiments (Table 2-1). The dynamic responses of the ballast, subballast and subgrade were consistent, showing a distinctive peak for each wheel load. However, because of the rail stiffness, sufficient interaction existed between adjacent wheels of a truck to make the axle pair on a truck cause the dominant cyclic frequency, rather than a single axle. This is an important consideration in the determination of the proper shape and duration of the stress pulse and the number of cycles employed in repeated load property tests for track performance prediction. Depending on the wheel loaction, interaction between adjacent axles, and tie bending, the dynamic ballast and subballast strains exhibited compressive and/or extensional responses. The dynamic response of the roadbed under each application of an axle load at FAST was elastic. This observation is used to justify the use of elastic models and resilient soil properties for predicting the resilient response of track structures under train loads. However, the strains and deformations were not proportional to wheel load, although the relationship was approximately linear in the range of 10 to 33 kips. Thus the elastic model must be nonlinear for adequate representation.

Table 2-1. Sets of Conditions for Instrumented Track Sections

Section	Set	Tie Type	Ballast Type	Ballast Depth (in.)	Track Geometry	Tie Spacing (in.)
17C	1	Concrete	Granite	16 - 19	Curved	24
17E	2	Concrete	Granite	14	Tangent	24
18A	3	Hardwood	Granite	21	Tangent	19.5
18B	4	Hardwood	Granite	15	Tangent	19.5
20B	5	Hardwood	Limestone	15	Tangent	19.5
20G	6	Hardwood	Traprock	15	Tangent	19.5

Subballast Depth = 6 in. of well-graded gravelly sand in all cases.

Subgrade = silty, fine to medium sand.

Tie Properties =

Wood: 7-in. high x 9-in. wide x 8.5-ft long, A = 63 $in.^2$, E = 1.5 x 10^6 $lb/in.^2$, I = 257.25 $in.^4$

Concrete: 9-in. high x 8.5-in. wide (top) and 10.75-in. wide (bottom) x 8.5-ft long, A = 86.6 $in.^2$, E = 3 x 10^6 $in.^2$, I = 582 $in.^4$

Rail Properties = 136-lb steel rail, A = 13.35 $in.^2$, E = 30 x 10^6 psi, I = 94.9 $in.^4$

The following conclusions were made as a result of the study of the three track models:

1. For a set of chosen roadbed properties, MULTA and PSA predict a similar trend of behavior in comparison to the field measurements. On the basis of the similarity of PSA and MULTA in the mathematical representation of the three-dimensionality of the track system, it is believed that both PSA and MULTA can reasonably predict the response of the track system.
2. The pseudo plane-strain assumption in ILLITRACK may not be representing the three-dimensionality of the track system as desired. The parameters involved for this assumption are angle of distribution and effective tie bearing length. Both of them are problem-dependent and therefore experience is required for specifying these two parameters. The usefulness of this model may be enhanced through a systematic study of these two parameters which will provide a guideline for selecting the proper values.
3. The PSA model is an order of magnitude more expensive to run than MULTA or ILLITRACK.
4. The linear elastic assumption presently adopted in MULTA and PSA is not considered adequate for representing the actual non-linear, stress-dependent behavior of roadbed materials.

From these conclusions, the decision was made to develop a new model, GEOTRACK, which is based on MULTA but which accounts for the stress-dependent nature of the roadbed materials (Ref. 2). The model emphasizes the geotechnical aspects of track behavior. In addition to the more fundamental question of material modelling, certain other deficiencies were encountered in using the MULTA model. In order to obtain a more efficient and practical model, the following additional

modifications were made:

1. The roadbed layers are composed of linear elastic materials in GEOTRACK as well as in MULTA; however, the modulus in GEOTRACK is a function of stress state rather than a constant.
2. The MULTA model repeats calculations of identical influence coefficients generated by loading on the tie segments. This repetition is eliminated in GEOTRACK with the result that the input data has been reduced by four-fifths, and the calculation time has been reduced.
3. The MULTA model computes parameters for only three depth locations within three layers, while GEOTRACK can compute results for six depth locations within five layers.
4. Because truck loading (i.e., a pair of axles) constitutes the dominant cyclic load frequency, automatic superposition of adjacent axle loads is incorporated into the GEOTRACK model.
5. The BURMISTER and LAC codes are combined in GEOTRACK to form a single model, thus eliminating the need for two separate runs which for MULTA required an external magnetic tape.
6. Based on the track geometry information (which is specified by the length of tie, tie spacing and number of ties), the radii locations of the points of interest where stress and displacement information are desired are computed automatically in GEOTRACK, thus eliminating the need for manual computation and reducing the input data requirements appreciably.
7. The cartesian coordinate system was varied from the original version of MULTA and a corrected transformation matrix was employed to convert influence coefficients from cylindrical to cartesian coordinates.

8. For the determination of stresses in the roadbed materials, a correction for the sign of the shear stresses was accomplished, resulting in a smaller stress state in the roadbed in comparison to the MULTA model.
9. Correct consideration of symmetry in the direction parallel to the rails is now incorporated, eliminating the center "hump" in stress distribution across the ties produced by the MULTA model, particularly with stiff ties.

2.2 Material Characterization

The three basic requirements in the solution of any boundary value problem are 1) satisfaction of the equilibrium equations, 2) satisfaction of the compatibility equations which ensures admissible displacement fields, and 3) the selection of appropriate constitutive laws for the materials, which relate the components of the stress tensor to the components of the strain tensor. The third requirement has been the most difficult in geotechnical engineering, since soil does not behave as a linear elastic material.

Roadbed elements under in-service conditions are generally subjected to repeated application of sub-failure stress levels (i.e., stresses lower than the static strength). A number of investigators (Refs. 7 to 15) have used the repeated load triaxial test to study the behavior of roadbed materials under repeated loading.

As a result of all this extensive research, the concepts of resilient strain and resilient modulus have evolved. Fig. 2-1 shows a schematic of a typical repeated load behavior of roadbed material, and Fig. 2-2 shows actual stress-strain data for ballast material obtained by Olowokere (Ref. 13). In each load application, the element experiences both resilient (recoverable or

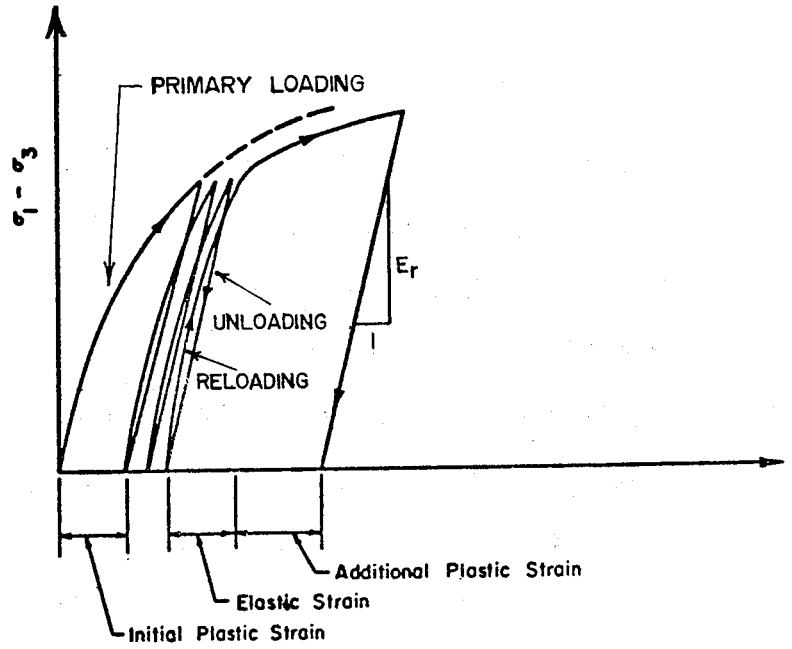

Fig. 2-1. Schematic of Repeated Load Response of Roadbed Material

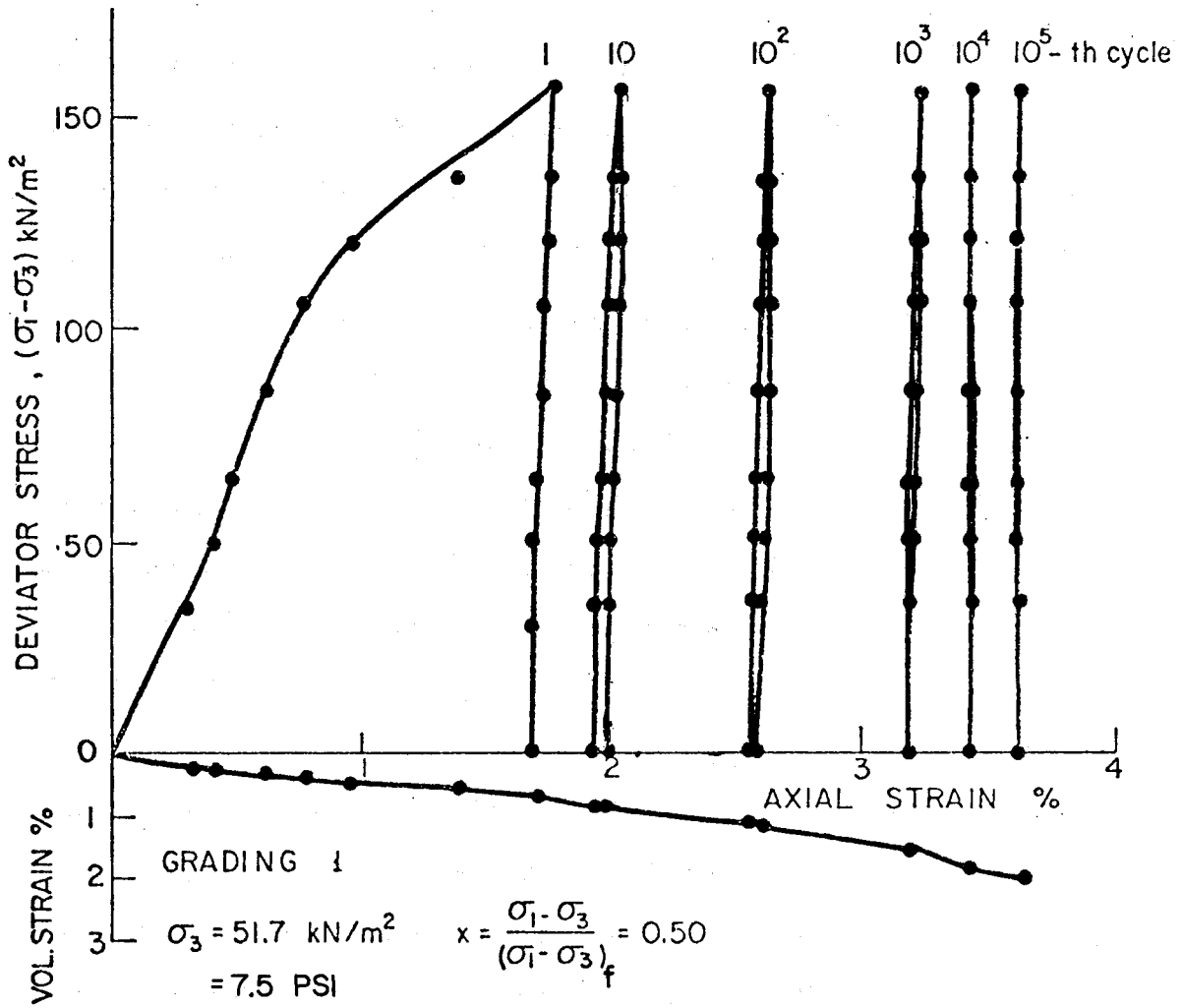

Fig. 2-2. Observed Stress-strain Behavior of Ballast Material under Triaxial Repeated Loading. (Ref. 13)

elastic) and residual (non-recoverable, inelastic or plastic) strains. At any load cycle, the resilient modulus (E_r) is defined as the ratio of the deviator stress to resilient strain. As shown in Fig. 2-2, the greatest amount of inelastic strain occurs in the first load and unload cycle. After about ten to one hundred cycles, the response of the material has become relatively elastic and constant, although some small residual strains will continue to occur at a decreasing rate with each cycle.

The observed behavior of ballast material as shown in Fig. 2-2 indicates that an elasto-plastic behavior is exhibited by the ballast up to some number of load cycles, after which the inelastic behavior disappears almost completely. The behavior during the primary loading can be approximated by the well-known hyperbolic relations proposed by Kondner and Zelasko (Ref. 16) and formalized by Duncan and his co-workers (Ref. 17). The parameters representing the elastic or resilient state, however, have been found to be strongly dependent on the state of stress (Refs. 17, 18, 19, 20). This stress-state dependency of the elastic parameters has generally been recognized as a form of material non-linearity which may be accounted for by making the Young's modulus (E) and Poisson's ratio (ν) functions of the stress state.

The resilient modulus of roadbed materials (E_r) as defined previously has been related to the stress state by various functions of either the confining pressure (σ_3), the deviator stress ($\sigma_d = \sigma_1 - \sigma_3$), or the sum of the principal stresses ($\Theta = \sigma_1 + \sigma_2 + \sigma_3$). Due to the different effects of Θ and σ_d, the resilient modulus of soils may increase or decrease with stresses, depending on the type of soil. It has been found experimentally by Seed, et al. (Ref. 21) that for coarse-grained materials, Θ has a greater effect than σ_d, and the modulus increases with stress according to either Eq. 2-1 or Eq. 2-2:

$$E_r = K_1 \Theta^{K_2} \quad , \qquad (2\text{-}1)$$

$$E_r = K_1' \sigma_3^{K_2'} \quad , \tag{2-2}$$

where E_r = resilient modulus,

θ = the bulk stress = $\sigma_1 + \sigma_2 + \sigma_3$,

$\sigma_1, \sigma_2, \sigma_3$ = the major, intermediate and minor principal stress, respectively, and

K_1, K_2, K_1', K_2' = experimentally determined constants.

On the other hand, for fine-grained materials, σ_d has a greater effect than θ, and the modulus generally decreases with increase in σ_d. The above relationships have been verified by more recent investigators (Refs. 12, 14, 18, 22, 23). Equations 2-1 and 2-2 are analogous to the following dependency of initial tangent modulus on confining pressure as obtained by Duncan and Chang (Ref. 17) for static analysis of soils:

$$E_i = K\, p_a (\sigma_3/p_a)^n \quad , \tag{2-3}$$

where E_i = initial tangent modulus,

σ_3 = confining pressure,

P_a = atmospheric pressure expressed in the same pressure units as E_i and σ_3, and

K,n = experimentally determined constants.

The GEOTRACK model can be used with any of the proposed relationships between resilient modulus and stress state. However, based on a review of available information and the results of preliminary analysis with the model, the relationship defined by Eq. 2-1 was selected. The equations for the FAST materials are given in Table 2-2, together with assumed values for Poisson's ratio. The values of parameters K_1 and K_2 were obtained from tests conducted by Thompson (Ref. 24).

Because of the problems associated with measuring accurate values of ν, as well as the fact that the response of the pavement and track systems is relatively insensitive to reasonable variations of ν, estimated and constant values of ν are often used as engineering approximation (Ref. 25). Poisson's

Table 2-2. Resilient Equations for FAST Roadbed Materials (Ref. 24)

Material	Resilient Equations, $E_r = K_1\Theta^{K_2}$ (lb/in.^{2})		Poisson's Ratio, ν (Assumed)
	K_1	K_2	
Granite Ballast	7735	0.509	0.37
Limestone Ballast	5423	0.559	0.37
Traprock Ballast	2509	0.686	0.37
Subballast	2182.0	0.687	0.37
Subgrade	523.0	1.08	0.4

ratio appears to vary between 0.3 and 0.4 for granular materials, and between 0.4 and 0.5 for cohesive subgrades. Values within this range are used in this study.

2.3 GEOTRACK Description

The components of a conventional track structure system are represented by GEOTRACK. These components are: 1) the roadbed materials consisting of the ballast, subballast and subgrade, 2) the track structure consisting of the ties, the rails and the rail fasteners (not shown, but are under the rails), and 3) the wheel loads transmitted by the trains. The GEOTRACK model only considers vertical wheel loads.

Figure 2-3 shows the geometrical representation of the track structure in the GEOTRACK model. The roadbed is represented by five layers of finite thickness, the last layer being semi-infinite. The rails are assumed to be supported over eleven ties. The track section is assumed symmetric about the center tie and symmetry of loading on both rails is assumed. Thus, only one-quarter of the total track section, as shown in Fig. 2-3, need be specified.

The BURMISTER code, based on Burmister's three-dimensional elasticity solution of a multilayer system (Ref. 26), is employed in determining the stress, strain and displacement influence coefficients for the desired points of interest in the roadbed. Usually, points along the ties at the center of each tie segment, midway between ties (forming a grid as shown in Fig. 2-4), and at some depth locations directly under the surface points are taken as the desired points of interest. Each point of interest is identified by coordinates (r, θ, Z).

Each half-tie has been divided into five segments, with the tie-ballast contact area converted into a circular shape to be compatible with the Burmister solution. The influence coefficients are obtained by loading each of

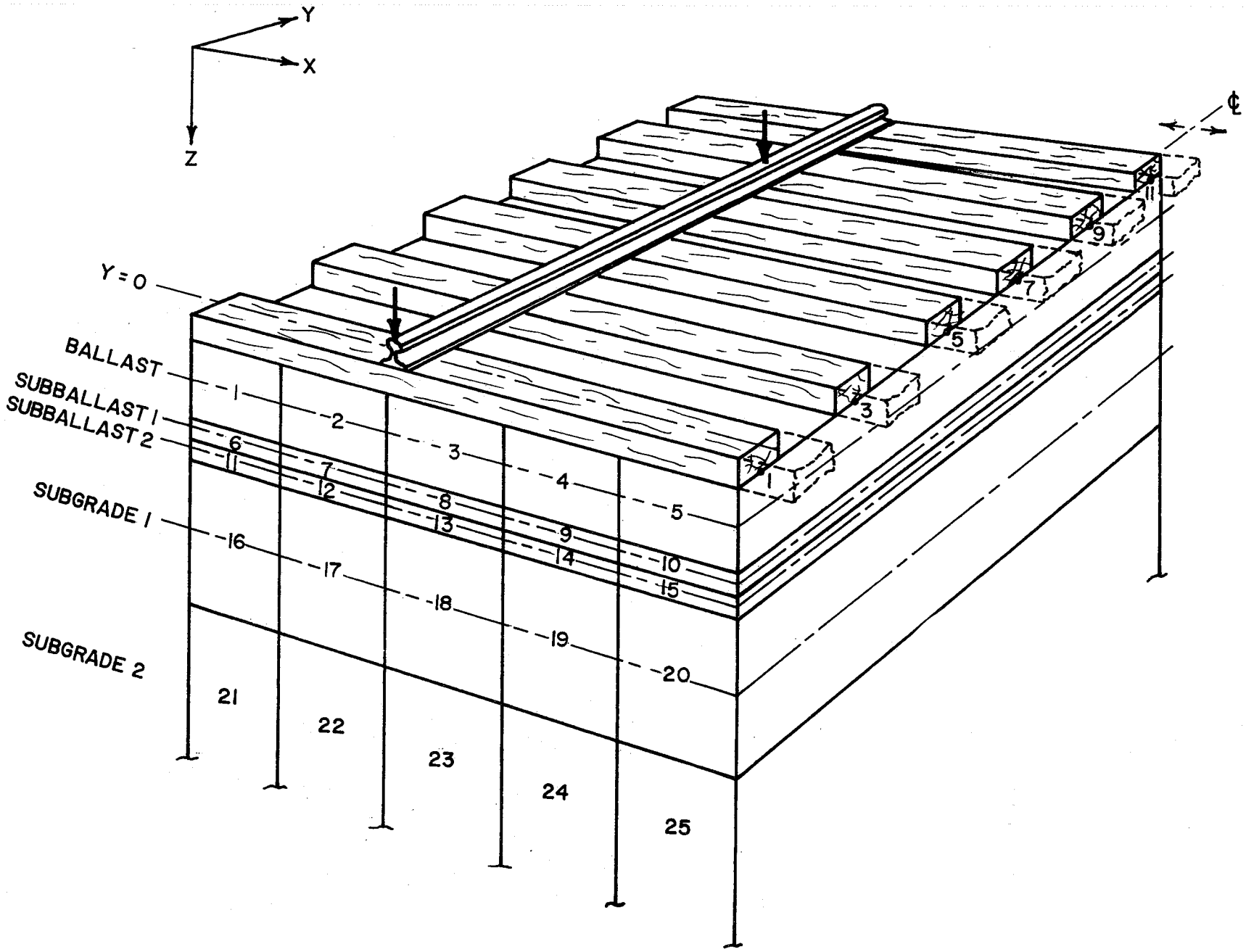

Fig. 2-3. Geometrical Representation of GEOTRACK Model

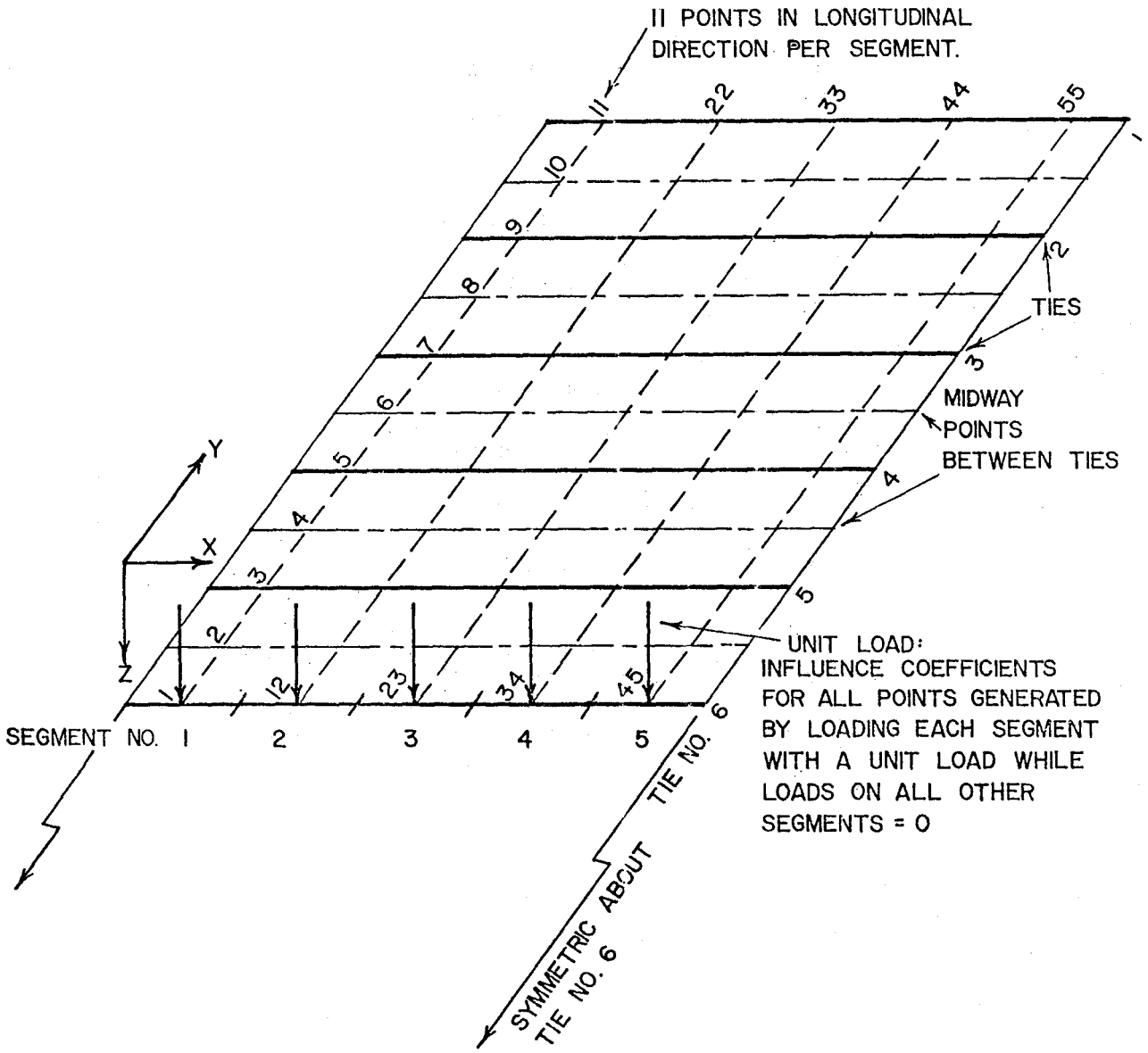

Fig. 2-4. Illustration of Supporting Ties, Loaded Segments, and Points of Interest

the equivalent circular areas of a tie segment with a unit load, with no load on the other segment areas. A study of Fig. 2-4 reveals the axisymmetric nature of the problem, that is, at a particular depth level in the roadbed, all points which are at the same relative radii locations to the loaded segment would have the same stress and displacement influence coefficients. Therefore, in the GEOTRACK model, the influence coefficients for loading on the 2nd to 5th tie segments are generated from those of the first segment.

The influence coefficients are first calculated in cylindrical coordinates and then transformed into cartesian coordinates for use with the LOAD and COMBINATION code.

The resilient moduli of the roadbed materials are made stress-dependent, and the stresses themselves are functions of the moduli. Thus an iterative procedure, which is one of the methods of approximating nonlinear material properties (Ref. 27), is employed in the GEOTRACK model. It consists of solving the same problem repeatedly under the axle load, choosing for successive solutions a value of resilient modulus for each layer corresponding to an average effective state of stress calculated for the layer in the preceding cycle. Thus in each iteration,

$$(E_r)_{i+1} = E_r\,(\sigma_{ij})_i \quad , \qquad (2\text{-}4)$$

where $(E_r)_{i+1}$ = new E_r for the $(i+1)^{th}$ iteration, and

$(\sigma_{ij})_i$ = stress state in the i^{th} iteration.

The iteration is continued until $(E_r)_{i+1} - (E_r)_i \leq \varepsilon$, where ε is the tolerance of convergence. The final stresses and displacements are those obtained in the $(i+1)^{th}$ iteration. In each iteration, the materials are treated as linearly elastic with E and ν replaced with the values consistent with the current state of stress in accordance with the nonlinear relation between modulus and stress state, Eq. 2-1.

The following procedures are carried out in the iterative scheme employed in the GEOTRACK model:

1. Previous study (Ref. 1) has shown that the incremental bulk stress, $\Delta\Theta$, caused by train loads does not vary appreciably across the tie, but there is a significant variation of $\Delta\Theta$ in the vertical direction. In order to account for variation of $\Delta\Theta$ as well as the material properties with depth, the roadbed system is divided into five layers, such as shown in Fig. 2-3. However, GEOTRACK can handle other layer divisions. For example, in this study the ballast has often been divided into two layers and the subballast reduced to one layer.
2. Stress states are computed at 55 locations on a horizontal plane corresponding to the center of each layer. These consist of 11 points in the longitudinal direction for each of five tie segments. The numerical designation of the 55 locations are as shown in Fig. 2-4. Each layer is considered to be composed of 5 "elements," one element under each tie segment extending in length along the longitudinal rail direction (Y-axis). Thus for each element, stress states are computed at 11 locations along its length. Numerical designation of the elements is as shown in Fig. 2-3.
3. Geostatic bulk stress is computed at the center of each layer as

$$\Theta_o = \bar{\sigma}_{vo} + 2K_o\bar{\sigma}_{vo} = (1 + 2K_o)\bar{\sigma}_{vo}, \qquad (2\text{-}5)$$

where Θ_o = geostatic bulk stress,

$\bar{\sigma}_{vo}$ = geostatic vertical effective stress, and

K_o = coefficient of lateral stress at rest.

4. The final bulk stress at each of the 11 longitudinal locations on each element is computed as

$$\Theta_f = \Theta_o + \Delta\Theta,$$

where Θ_f = final bulk stress, and

$\Delta\Theta$ = incremental bulk stress due to train loads = $\Delta\sigma_1 + \Delta\sigma_2 + \Delta\sigma_3 = \Delta\sigma_x + \Delta\sigma_y + \Delta\sigma_z$.

5. Several alternatives are available to determine an average value for the bulk stress in each layer used to calculate the resilient modulus. Adegoke (Ref. 2) used a weighted average using the rail-seat load under each tie as the weighting factor. Alva-Hurtado (Ref. 3) used the bulk stress at the middle of the layer in the plane of the load.

6. The representative modulus for each layer is obtained from $E_r = K_1\Theta^{K_2}$, using Θ from step 5. The parameters K_1, K_2 are different for each roadbed material.

For the track sections analyzed in this study, the resilient moduli have converged substantially at the end of three iterations. In the fourth iteration, the stress and displacement values are obtained at the interface locations or any other depth location rather than at the middle of the layer, the resilient moduli obtained in the third iteration being employed in the 4th and final iteration.

2.4 Model Validation

In this section, the GEOTRACK model is validated against the dynamic measurements for five FAST sections: 17E, 18A, 18B, 20B, and 20G. Table 2-1 summarizes the various track parameters associated with these sections, while Table 2-2 shows the resilient equations for the FAST roadbed materials.

Using these parameters, the GEOTRACK model was run for all the five sections for wheel loads of 2, 5, 8, 11.7, 14, 23.5, and 32.9 kips, respectively. Each run is for truck loading, i.e., response under the two adjacent axles of a truck with the wheel load on each axle as indicated. The moduli assumed for

the first iteration were 30, 20, 20, 10 and 5 ksi for the ballast, subballast 1, subballast 2, subgrade 1, and subgrade 2 layers, respectively. During construction, the upper 3 ft of the subgrade was compacted and thus was treated as a separate layer so that a higher value was assigned to this layer than to the lower section of subgrade.

GEOTRACK predicted values are compared to measured values in Figs. 2-5 through 2-12 as a function of wheel load. Except for ballast strains, the predicted values reasonably represent the measured values. The GEOTRACK model has predicted values of ballast strain for the wood tie sections which are an order of magnitude smaller than the measured values. Tie-seating phenomenon was suggested as a possible reason for the discrepancy (Ref. 2). However, the predicted ballast strains in the concrete tie section are close to the measured values. While the top strain coils were attached into recesses in the bottom of the wood ties, they were simply taped to the bottom of the concrete ties. The concrete tie being heavier than the wood tie will also help maintain a better contact between the top coil and the surface of the ballast. If the measured ballast strains were to be matched, a displacement profile as shown by the dashed line in Fig. 2-13 would be suggested. The displacement gradient indicated by this profile is definitely very unlikely. This evidence corroborates the existence of tie-seating effects in the ballast strain measurements. Thus, care should be taken to correct the measured dynamic ballast strains for tie-seating effects, before using the values in further analyses.

Figures 2-10 through 2-12 show that the multilayer model is predicting the same trends as observed for the 15 and 21-inch ballast depths. For example, multilayer theory shows that as the thickness ratio D_r increases for a fixed modular ratio, less stresses are transmitted to the underlying layers and therefore less strains and deformations. This is as observed in the 21-inch ballast section compared to the 15-inch ballast sections.

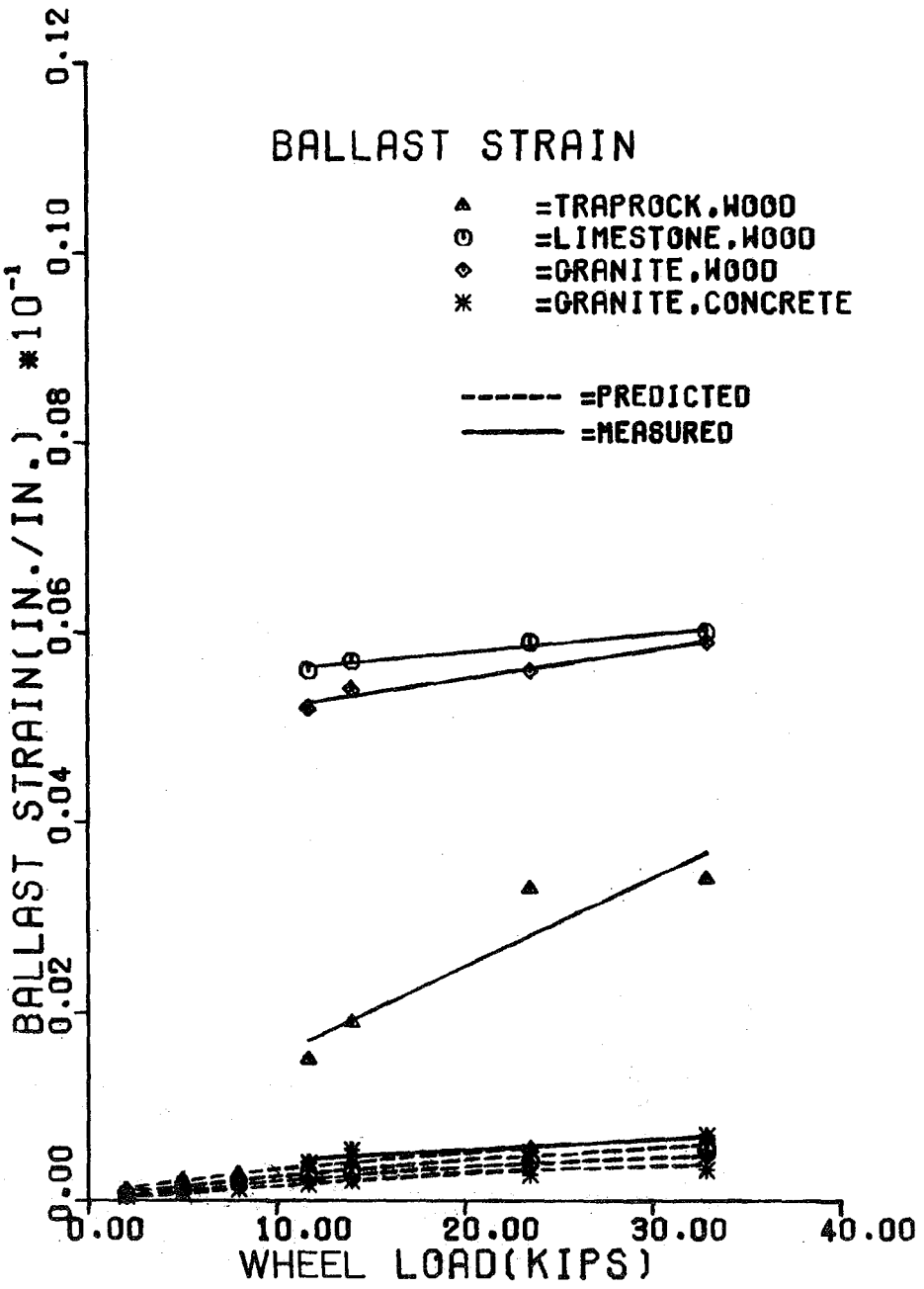

Fig. 2-5. Predicted Ballast Strains Compared to Measured Values in FAST Sections 20G, 20B, 18B and 17E

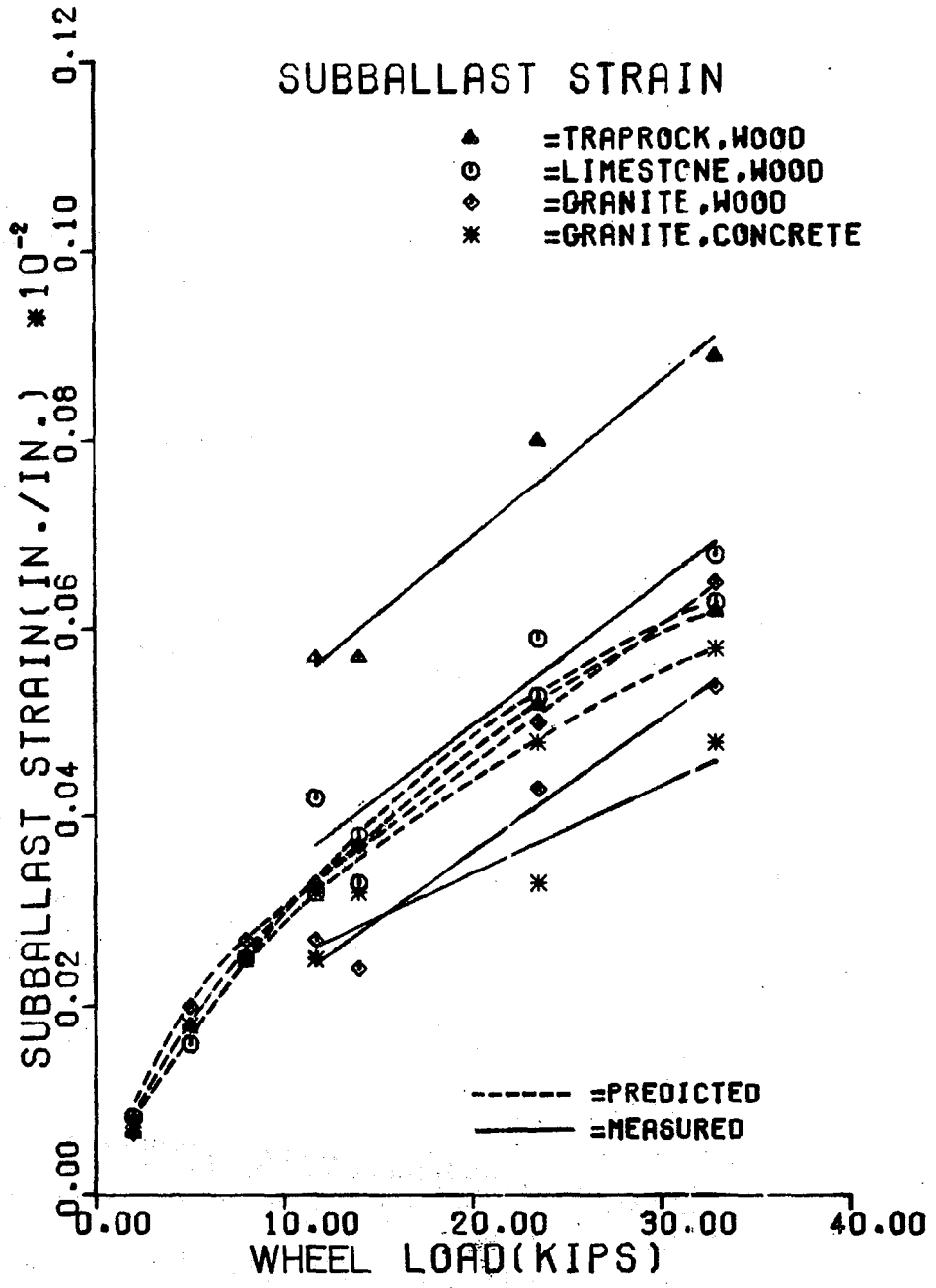

Fig. 2-6. Predicted Subballast Strains Compared to Measured Values in FAST Sections 20G, 20B, 18B and 17E

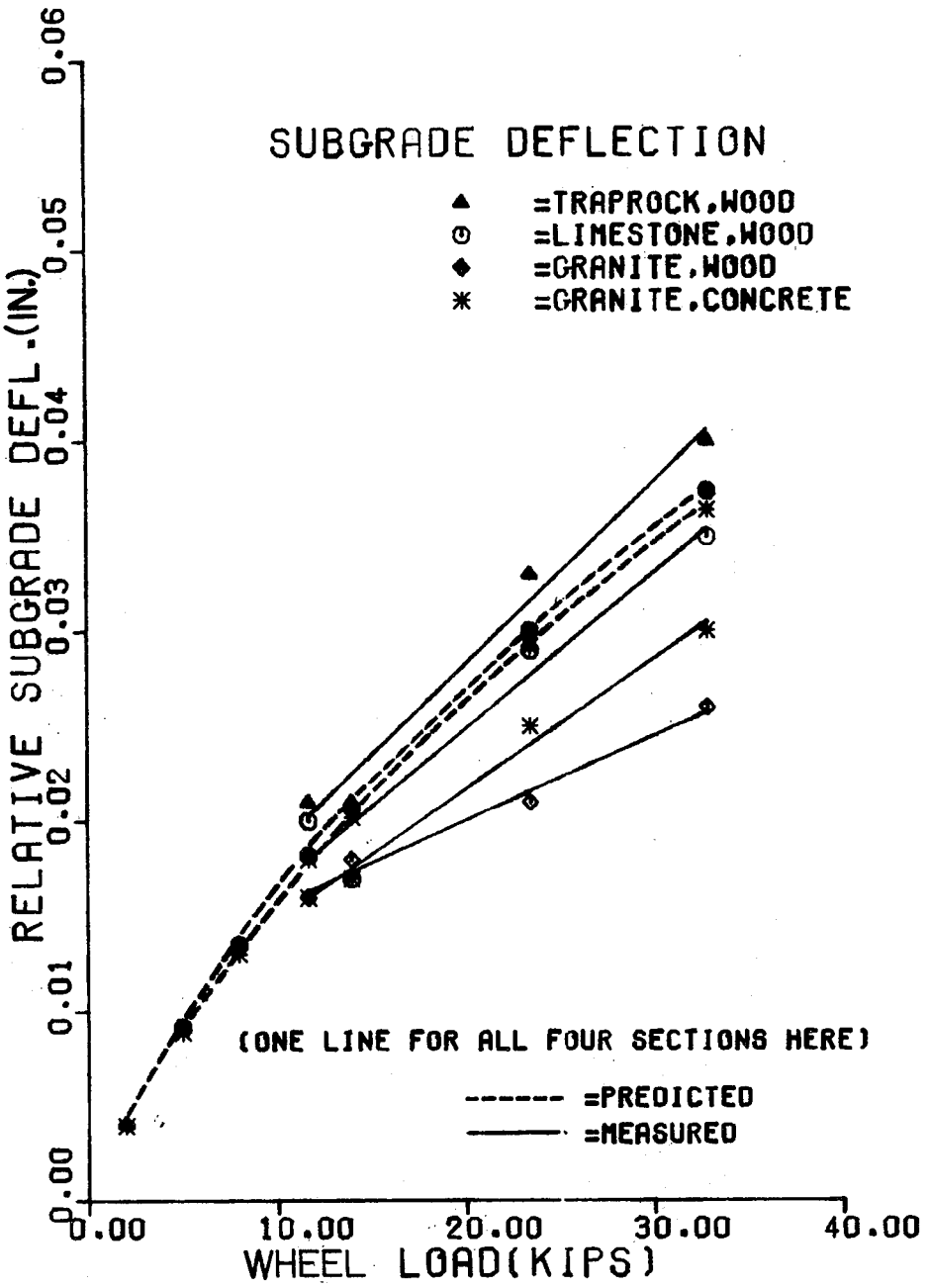

Fig. 2-7. Predicted Subgrade Deflections Compared to Measured Values in FAST Sections 20G, 20B, 18A and 17E

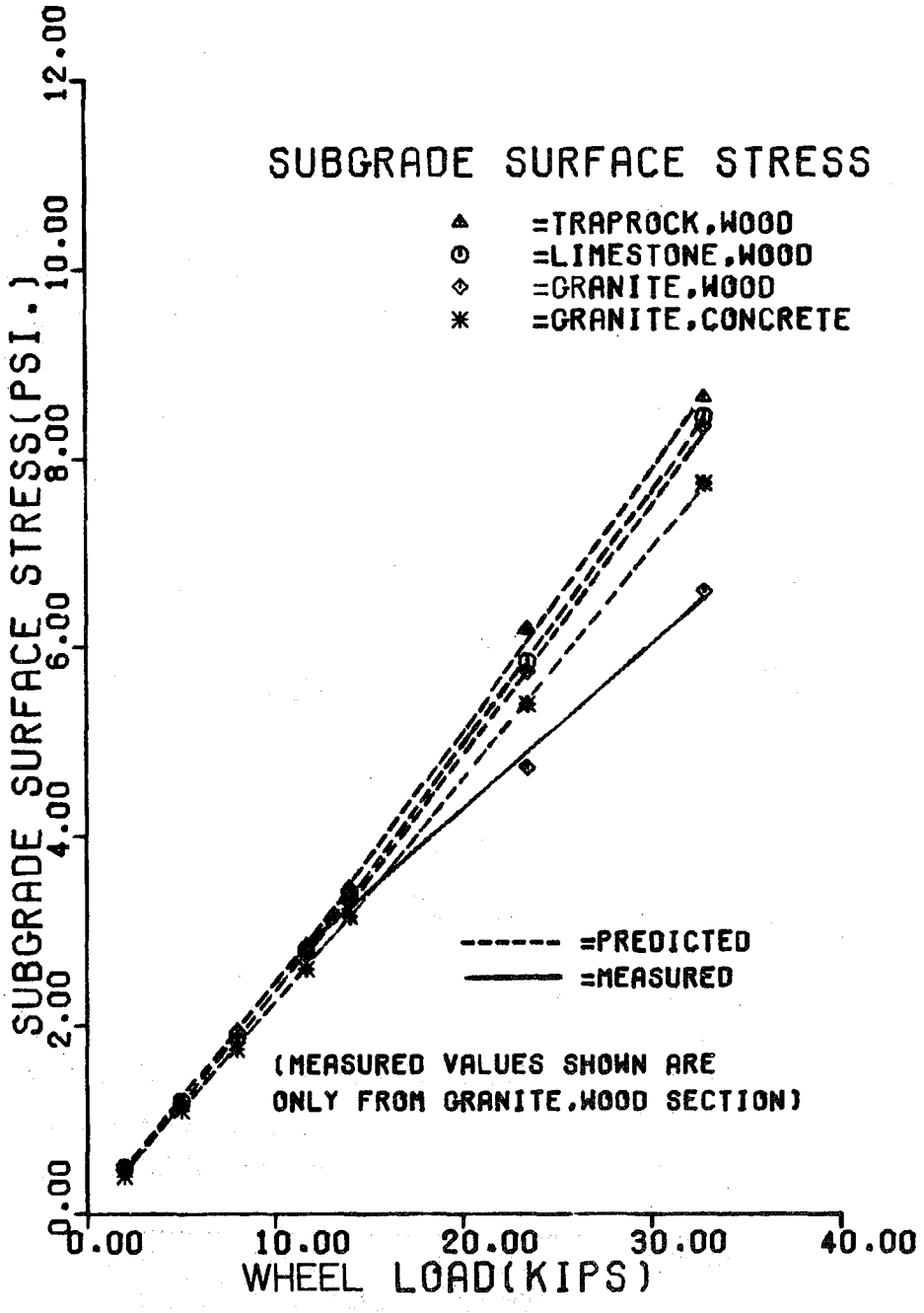

Fig. 2-8. Predicted Subgrade Stress Compared to Measured Values in FAST Sections 20G, 20B, 18A and 17E

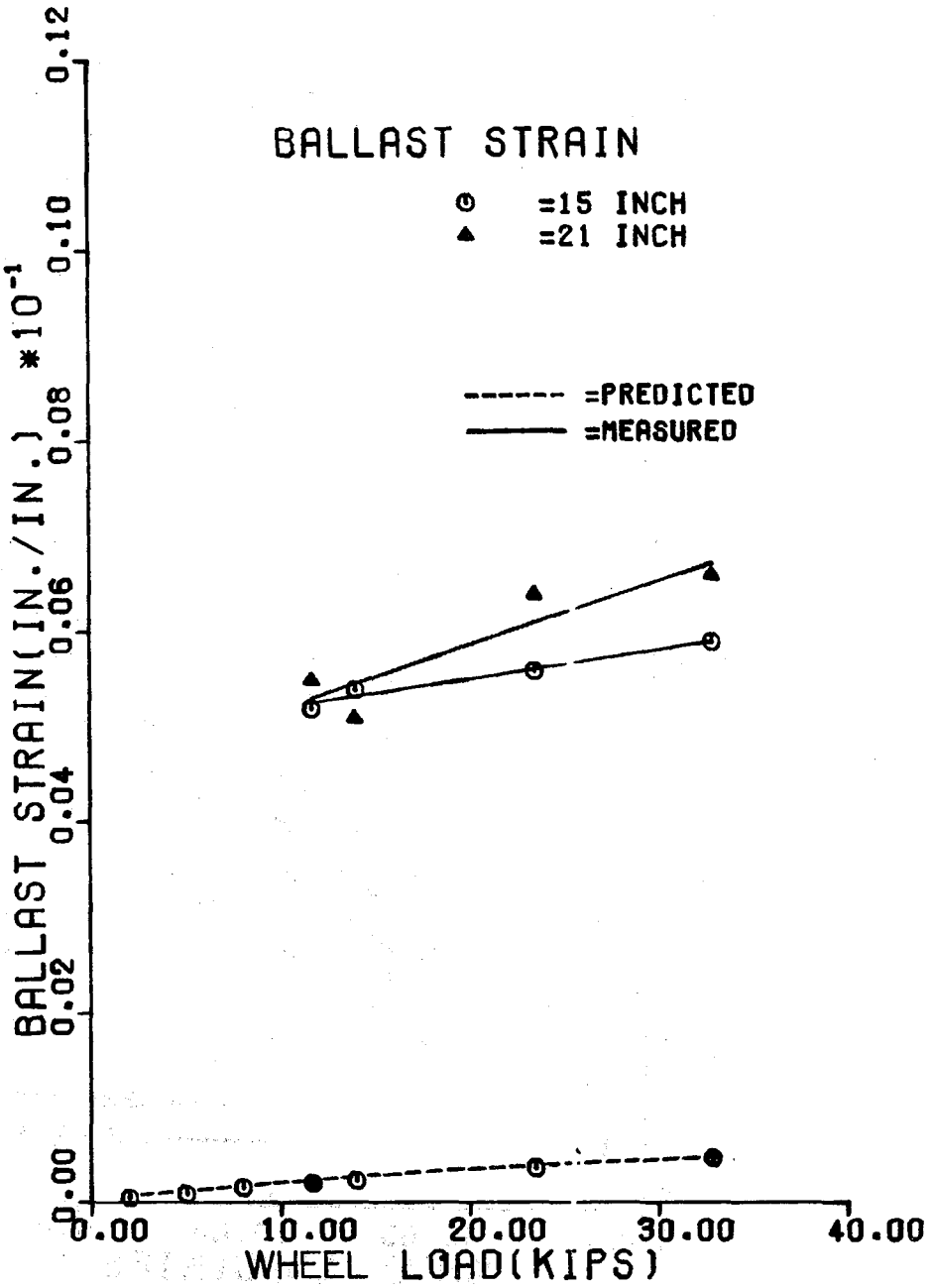

Fig. 2-9. Predicted Ballast Strains Compared to Measured Values in FAST Sections 18A and 18B

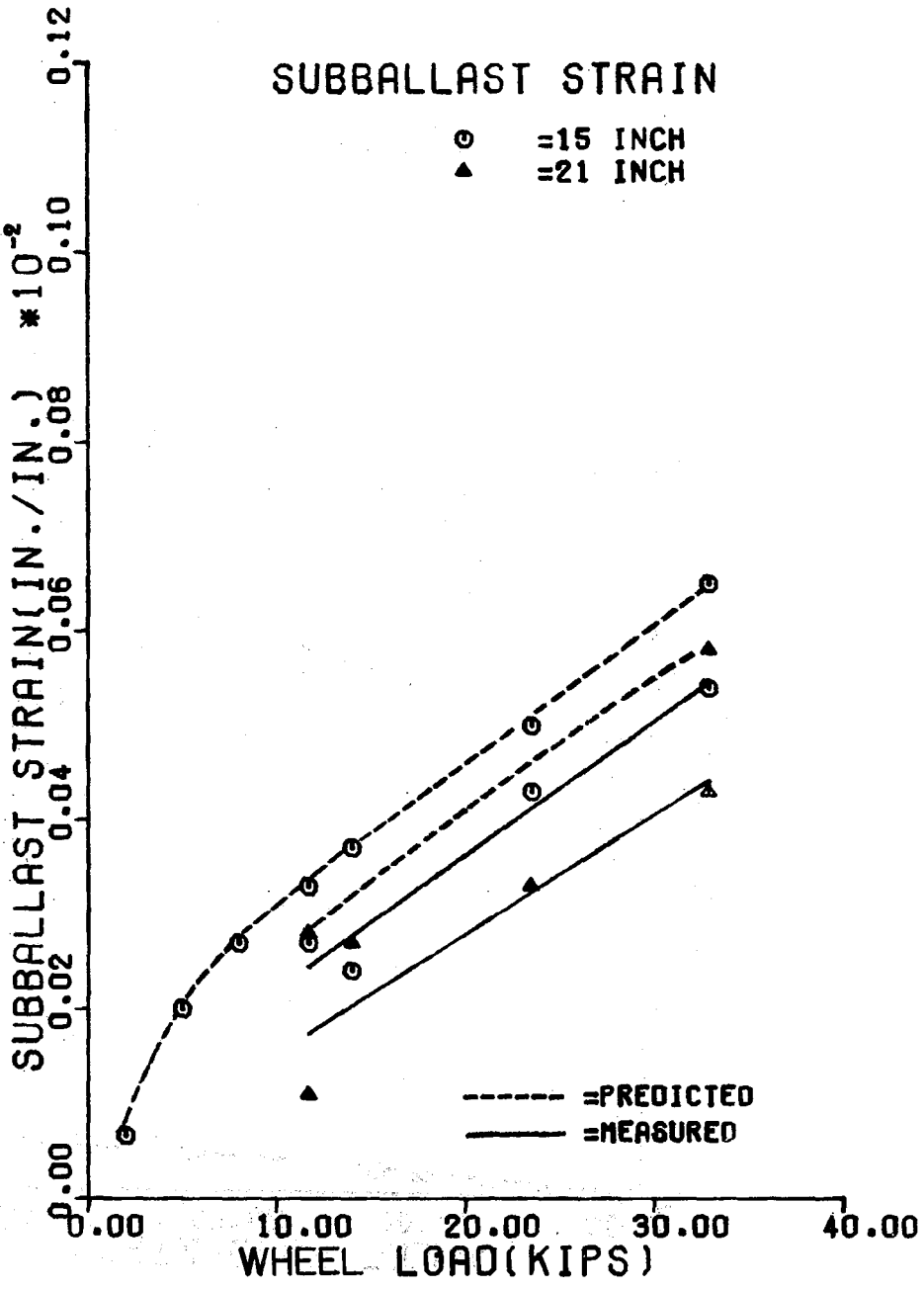

Fig. 2-10. Predicted Subballast Strains Compared to Measured Values in FAST Sections 18A and 18B

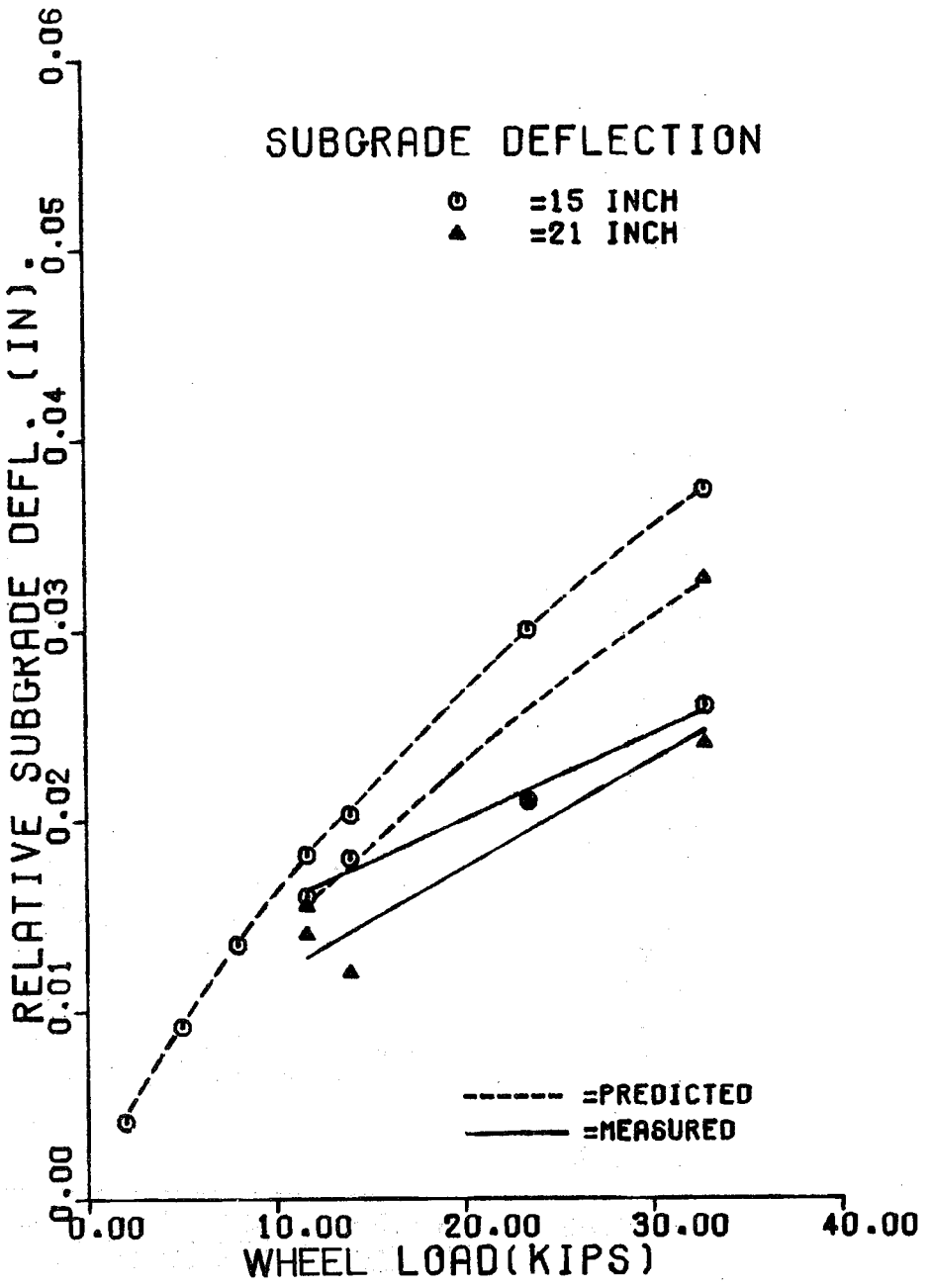

Fig. 2-11. Predicted Subgrade Deflections Compared to Measured Values in FAST Sections 18A and 18B

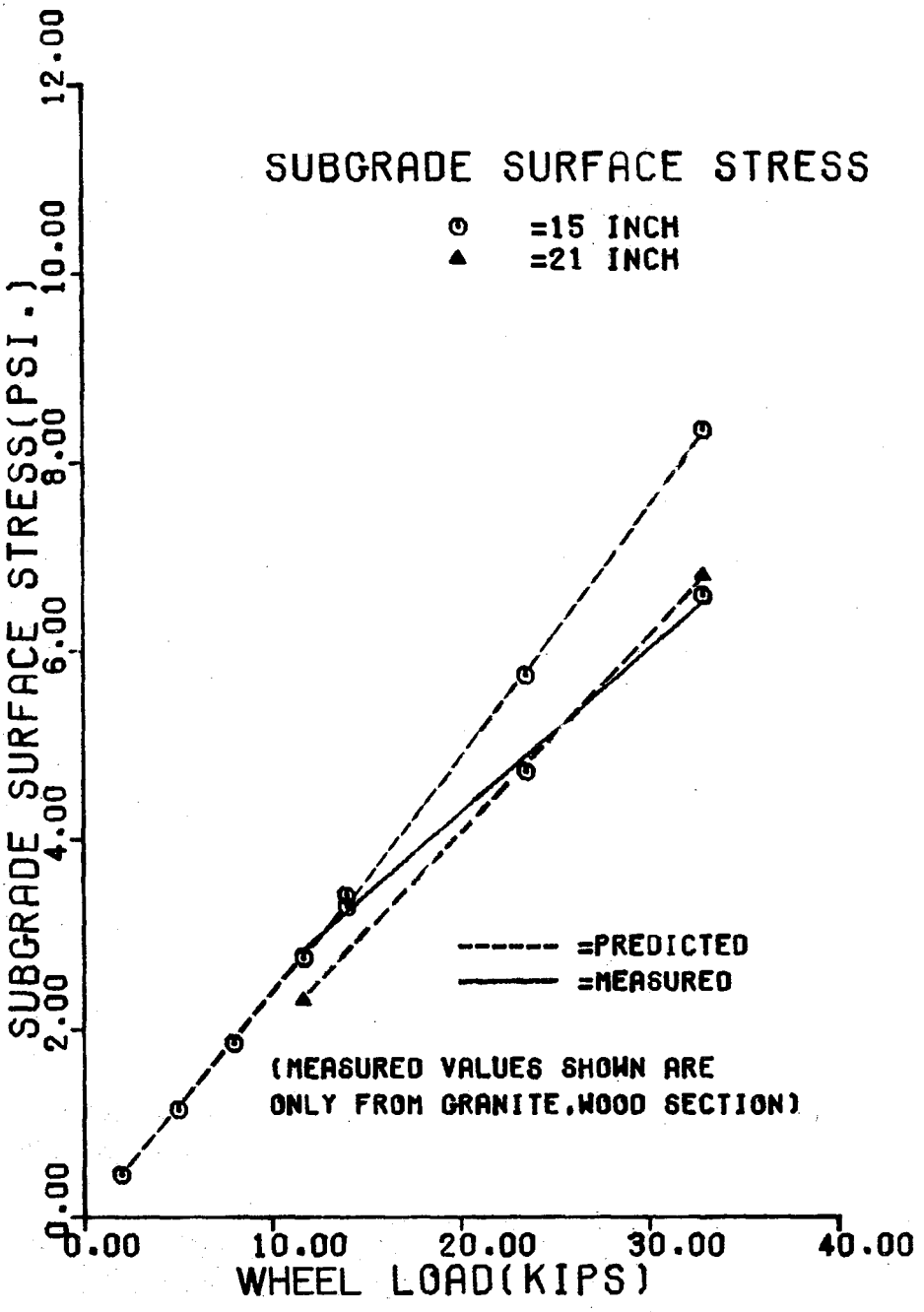

Fig. 2-12. Predicted Subgrade Stress Compared to Measured Values in FAST Sections 18A and 18B

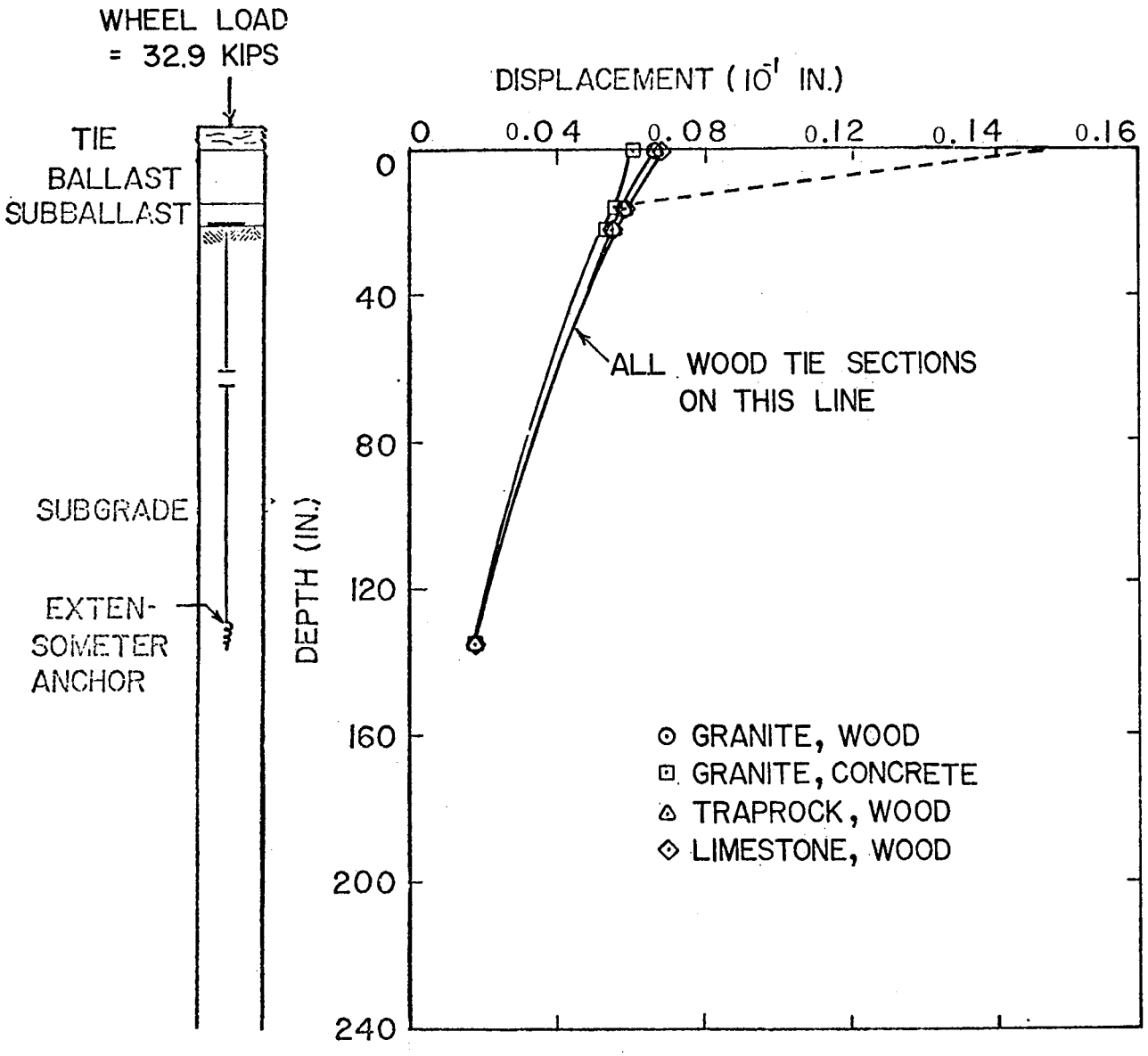

Fig. 2-13. Vertical Displacement Distribution with Depth Predicted by GEOTRACK

As a final comparison, PSA and ILLITRACK were run with the stress-dependent moduli obtained in the final iteration of GEOTRACK. These moduli values were 39, 13, 12, 8 and 13 ksi for ballast, subballast 1, subballast 2, subgrade 1, and subgrade 2, respectively.

Table 2-3 shows the comparative predictions. It can be seen from this table that GEOTRACK's predictions are the closest to the measured values.

Table 2-3. Comparison of GEOTRACK, PSA, and ILLITRACK Predictions with Measured Response at FAST Section 18B; Using Moduli Determined from Nonlinear GEOTRACK

	MEASURED		PREDICTED		
	3 MGT	75 MGT	GEOTRACK	PSA	ILLITRACK
Ballast strain (in./in.)	0.004	0.0056	0.00048	0.00064	0.00086
Subballast strain (in./in.)	0.0005	0.0005	0.00065	0.0009	0.0018
Subgrade surface deflection (in.)	--	--	0.0537	0.0623	0.115
Subgrade deflection at extensometer bottom anchor location (in.)	--	--	0.0163	0.0132	0.023
Subgrade surface deflection relative to extensometer bottom anchor (in.)	0.031	0.025	0.0374	0.049	0.092
Subgrade vertical stress (psi)	6.6	6.6	8.35	9.83	26.9

Load = 32.9 kips

CHAPTER 3. CYCLIC BEHAVIOR REVIEW

In general, types of loading can be broadly categorized as either monotonic or cyclic. Material behavior is completely different for these two loading conditions. Monotonic loading has been extensively investigated for many years and therefore is better understood. The type of loading influencing the behavior of the track system is cyclic. Unfortunately, there is no general constitutive law available to account for the effect of cyclic loading in ballast and roadbed materials.

An appreciable amount of data on cyclic (repeated) loading in granular materials has been generated from work in highway technology. Some of this available data will be summarized, and a section concerning ballast testing will also be presented. Finally, the application of this information to pavement deformation prediction will be described.

3.1 Resilient Behavior of Granular Materials

The typical behavior of a granular material, under moderate stress levels of repeated load, is that after the first few cycles, the material becomes "elastic" because the irrecoverable strain is small compared to the recoverable strain. However, the permanent strain can accumulate by a substantial amount after a large number of cycles.

To evaluate the resilient behavior of granular materials, several investigators (Refs. 7; 28-35) have used the conventional triaxial cell. The granular samples were subjected to repeated loading conditions having either a constant or a cyclic confining pressure.

The resilient response is usually characterized by a resilient modulus (E_r) and resilient Poisson's ratio (ν_r). The resilient modulus is defined as the repeated deviatoric stress divided by the recoverable portion of the axial

strain. The resilient Poisson's ratio is equal to the recoverable portion of the axial strain divided by the recoverable portion of the radial or lateral strain.

Values of the resilient modulus E_r at several stress states were obtained from laboratory testing. It was found that the resilient modulus is a function mainly of the state of stress. Two suggested predictive equations were presented in Chapter 2 to relate the modulus to the stress state. Results from Ref. 36 indicate that material type such as gravel or crushed stone is not a major factor affecting the resilient response of granular materials.

Stress-dependent properties of fine-grained soils typically found in track subgrades are considerably different from those of granular material used for ballast and subballast (Ref. 37). Generally, the resilient modulus of fine-grained soils decreases when the deviatoric stress is increased.

Several researchers, namely Hicks (Ref. 31), Allen (Ref. 32), and Brown (Ref. 35), have installed devices directly on the samples that can measure the resilient radial or lateral strain. From repeated loading testing with constant confining pressure, Hicks modeled the resilient Poisson's ratio as a function of the principal stress ratio (σ_1/σ_3) and experimentally determined constants of the form

$$\nu_r = A_o + A_1\left(\frac{\sigma_1}{\sigma_3}\right) + A_2\left(\frac{\sigma_1}{\sigma_3}\right)^2 + A_3\left(\frac{\sigma_1}{\sigma_3}\right)^3$$

Allen performed repeated load testing with variation of confining pressure independently of the deviatoric stress. Figure 3-1 presents the difference in resilient Poisson's ratio for the two different conditions: constant and variable confining pressure. Figure 3-2 portrays the different stress paths corresponding to these conditions. The stress path AB will represent a cyclic test in which both the confining pressure as well as the deviatoric stress are cycled, representative of the actual field stress conditions. Stress paths CB

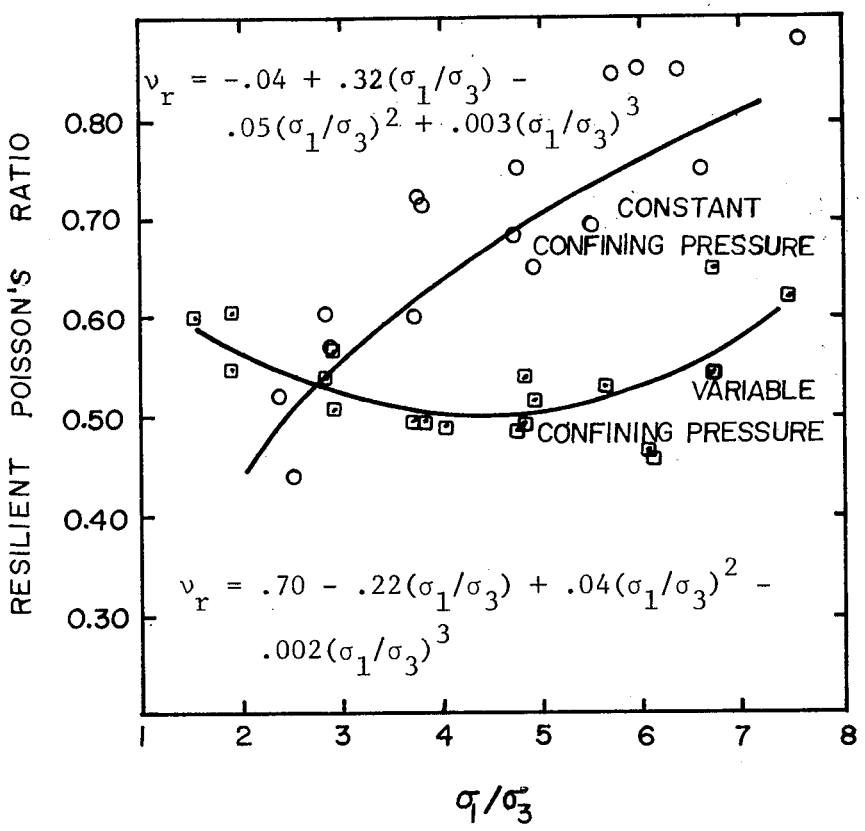

Fig. 3-1. Differences in Resilient Poisson's Ratio for Constant and Variable Confining Pressure (Ref. 32)

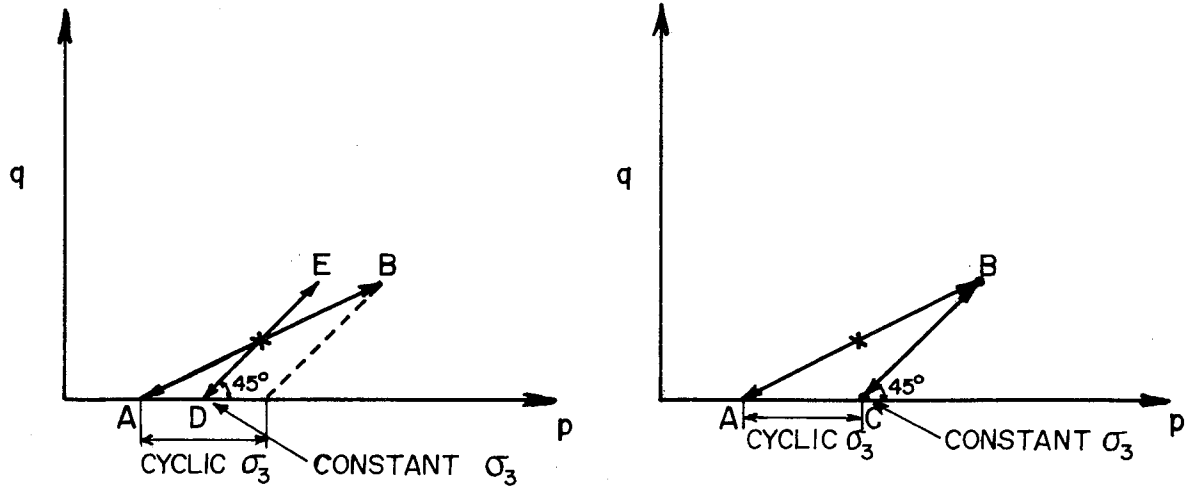

a) Stress Path DE with Constant σ_3 Equal to Mean Cyclic Value

b) Stress Path CB with Constant σ_3 Equal to Peak Cyclic Value

Fig. 3-2. Different Stress Paths in Triaxial Compression Testing to Simulate Field Stress Path AB with Varying Confining Pressure

and DE will represent equivalent constant confining pressure tests in which either the peak cyclic value is matched (CB) or the mean cyclic value is matched (DE).

The shape of the curve for ν_r in the variable confining pressure tests is flat and would indicate that in field conditions this parameter would vary only slightly. The explanation given for the higher Poisson's ratio in the constant confining pressure tests was that a portion of the lateral deformations observed were due to nonuniform states of stress and strain within the specimen.

Brown and Hyde (Ref. 38) believed that the difference in the values of the resilient Poisson's ratio was because the two tests had different stress paths, as can be seen in Fig. 3-2. They claimed that Allen was comparing the variable confining pressure tests with the tests from stress path CB. According to Brown and Hyde, if both types of tests are interpreted in terms of volumetric strain (V_r) and shear strain (γ_r), both tests are compatible, as can be seen in Fig. 3-3.

Procedures for evaluating the resilient properties of granular materials, mainly for highway pavement design purposes, have been developed since the early fifties (Ref. 7). Important work on repeated load testing of granular materials, mostly applied to highway design, has been presented by Dunlap (Ref. 39), Seed, et al. (Ref. 40), and Thompson (Ref. 41). More recent summaries of laboratory testing on resilient properties of granular materials are given by Hicks (Ref. 31), Allen (Ref. 32), and Knutson (Ref. 14).

All the previous studies of resilient behavior have shown that the most significant factor affecting the resilient modulus is the stress state. Several investigators have used either the confining pressure or the bulk stress as a parameter. Knutson (Ref. 14) indicated that the use of the bulk stress

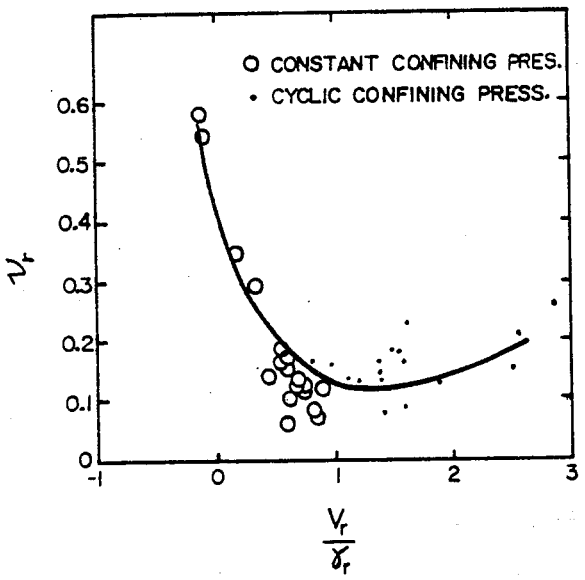

Fig. 3-3. Poisson's Ratio as a Function of Volumetric to Shear Strain Ratio for Constant and Cyclic Confining Pressures (Ref. 38)

gave better correlation coefficients and reduced scatter.

Most of the investigations of resilient behavior have been accomplished by triaxial repeated load testing using constant confining pressures. Allen (Ref. 32) and Brown and Hyde (Ref. 38) used cyclic confining pressure as well as cyclic deviator stress. Allen and Thompson (Ref. 42) concluded that although the constant confining pressure tests overestimated the resilient modulus, the use of the constant confining pressure triaxial test was justified as a means of characterizing the resilient response of granular materials. They concluded this because the error was not great and the testing equipment was simpler.

Hicks (Ref. 31) and Allen (Ref. 32) indicated that a reasonable estimate of the resilient response can be obtained after approximately 100 load cycles, this response being representative of the response after several thousand stress repetitions. They indicated that it was important, however, not to overstress the material. Furthermore, these researchers established that one specimen can be used to measure the resilient response over the entire range of stress levels and that the sequence of stress application had no significant effect on the results.

Kalcheff and Hicks (Ref. 43) reported that the number of stress repetitions and stress sequence had little effect on the resilience of granular materials. These researchers recommended that the resilient response of granular materials be determined after 150 to 200 load repetitions as a reasonable indication of resilient properties for a material subjected to a complex stress history.

Morgan (Ref. 33) and Brown (Ref. 35) indicated that the resilient modulus increased with the number of cycles, but reached equilibrium values after approximately 10,000 cycles of deviator stress. Boyce, Brown and Pell (Ref. 44)

indicated that the resilient modulus is subjected to stress history effects, particularly if the material has developed permanent strain. These effects can be reduced by using only a few cycles and avoiding high stress ratios.

Hicks and Monismith (Ref. 22) observed no influence on the resilient modulus for load durations in the range of 0.1 to 0.25 seconds. Seed, et al. (Ref. 40) demonstrated that by decreasing the stress duration from 20 minutes to 1/3 second, the resilient modulus increased by about 18 percent. Allen (Ref. 32) concluded that the resilient response of well-graded granular materials is independent of stress pulse duration.

Kalcheff and Hicks (Ref. 43) reported that there was no evidence of a change in resilient behavior with changes in load duration or frequency. Boyce, Brown and Pell (Ref. 44) found that frequencies between 0.2 to 20 Hz had little or no effect on resilient strains.

From tests conducted on well-graded crushed gravel and crushed rock, Hicks and Monismith (Ref. 22) concluded that resilient modulus at a given stress increased with increasing particle angularity or surface roughness. Haynes and Yoder (Ref. 30) observed higher resilient modulus values for gravel specimens than for crushed stone when both were compacted to the same relative density. Allen (Ref. 32) found that the effects of material type on the resilient parameters are slight compared with the effects of changes in the state of stress. Allen conducted repeated load testing on crushed stone, gravel and a blend of the two. In general, the crushed stone yielded slightly higher values of E_r than the gravel. The modulus of the blend material was normally between those of the other materials.

Hicks (Ref. 31) observed decreases in the resilient moduli of well-graded materials as the fines content (percent passing number 200 sieve) was increased.

Barksdale (Ref. 28) tested various soil-aggregate blends and concluded that

a 20% soil/80% aggregate blend exhibited higher values of resilient modulus at low stresses than a 40% soil/60% aggregate blend specimen. At higher stress levels, the situation was reversed. Haynes and Yoder (Ref. 30) observed little change in resilient modulus values of well-graded aggregates for changes in the percent of fines ranging from 6.2 to 11.5 percent.

Hicks (Ref. 31) concluded that for a given stress condition, the resilient modulus increased with an increase in density. Poisson's ratio, however, was only slightly influenced by density.

Allen (Ref. 32) investigated the variation of the resilient parameters with density for crushed stone, gravel and a blend of both. Generally, the resilient modulus increased as density increased. The Poisson's ratio showed no consistent variation with density changes.

Hicks (Ref. 31) indicated that for sands and gravels at different degrees of saturation, the resilient modulus decreased as the degree of saturation increased, so long as comparisons were made on the basis of total confining pressures. Comparisons on the basis of effective stresses indicated that the resilient moduli for 100 percent saturated samples differed only slightly from those for dry samples.

3.2 Permanent Deformation Behavior

As presented in the resilient behavior section, the deformations of granular material under each load application of stresses below failure are almost completely recoverable. However, the relatively small inelastic strains that occur in each cycle accumulate to significant levels upon repeated applications of such stress. The accumulation of deformation upon repetition of stresses is called the permanent deformation behavior.

The permanent deformation behavior of granular materials, and in particular ballast, under the application of repetitive loading had been studied both in

the laboratory (Refs. 12, 13, 14, 29, 45 and 46) and in the field (Refs. 2, 6). Both types of studies indicated that the response under each load is elastic, but with number of load applications and traffic, there is an accumulation of permanent strains and deformations.

There is not a great amount of information available on the factors influencing the permanent deformation behavior of granular materials in the triaxial test, but most of the factors affecting the resilient behavior will probably affect the permanent deformation behavior in a similar manner.

Knutson (Ref. 14) concluded that an increase in stress ratio (repeated deviator divided by confining pressure) resulted in additional permanent deformation for ballast samples. However, stress ratio by itself cannot be used to predict adequately the permanent deformation behavior of ballast materials. For a given stress ratio, for instance four, the development of permanent deformation with number of cycles will be different for two different confining pressures in the triaxial test. The lower confining pressure, for instance σ_3 = 5 psi, produces much lower permanent deformation than the higher confining pressure, for instance 15 psi. Knutson (Ref. 14) indicated that the stress level effects were difficult to discern because both the deviator stress and the confining pressure, and not merely the ratio of the two, must be considered.

Barksdale (Ref. 28) concluded that the permanent deformation decreased significantly as the confining pressure increased for a given deviator stress. The rate of accumulation of permanent deformation at low repeated deviator stress is proportional to the number of load applications, but at deviator stresses above a critical value, the rate of permanent deformation accumulation increased with increasing number of load applications.

Brown and Hyde (Ref. 38) and Knutson (Ref. 14) have shown that unlike the resilient behavior, the permanent deformation behavior is dependent on the load

application sequence or stress history. The total permanent deformation was less when a specimen was subjected to gradually increasing stress levels than when the highest stress level was applied first. A typical result of this type of behavior is given in Fig. 3-4 (Ref. 38).

Knutson (Ref. 14) presented the concepts of Lade and Duncan (Ref. 47) that offer a reasonable explanation for the stress history effects on the permanent deformation behavior of sands. Their theory indicates that elastic and permanent strain develop simultaneously upon loading. The elastic strain is determined primarily by the elastic deformation of individual particles, but permanent strain results from sliding between particles. The stress changes on a specimen can therefore be of these types: primary loading, unloading, and reloading. According to elasto-plastic theory, only primary loading (when stress level is increased beyond the previous maximum) will cause large permanent strains.

Field evidence of the importance of the primary loading on the permanent deformation of ballast has been presented by ORE (Ref. 45). They concluded that "smaller loads cause negligible settlement, and that a small number of large dynamic loads determine the deterioration of the track level, rather than the general level of the axle loads."

Allen (Ref. 32) found that an increase in density resulted in a decrease of permanent deformation and that crushed material experienced less permanent deformation than gravel. ORE (Ref. 45) indicated that permanent deformation is proportional to the initial porosity and is thus inversely proportional to initial density. Knutson (Ref. 14), in performing repeated load testing on different ballast materials, concluded that no other specimen parameter is as important in influencing the permanent deformation behavior than the degree of compaction. Figure 3-5 presents the effect of density on the permanent strain

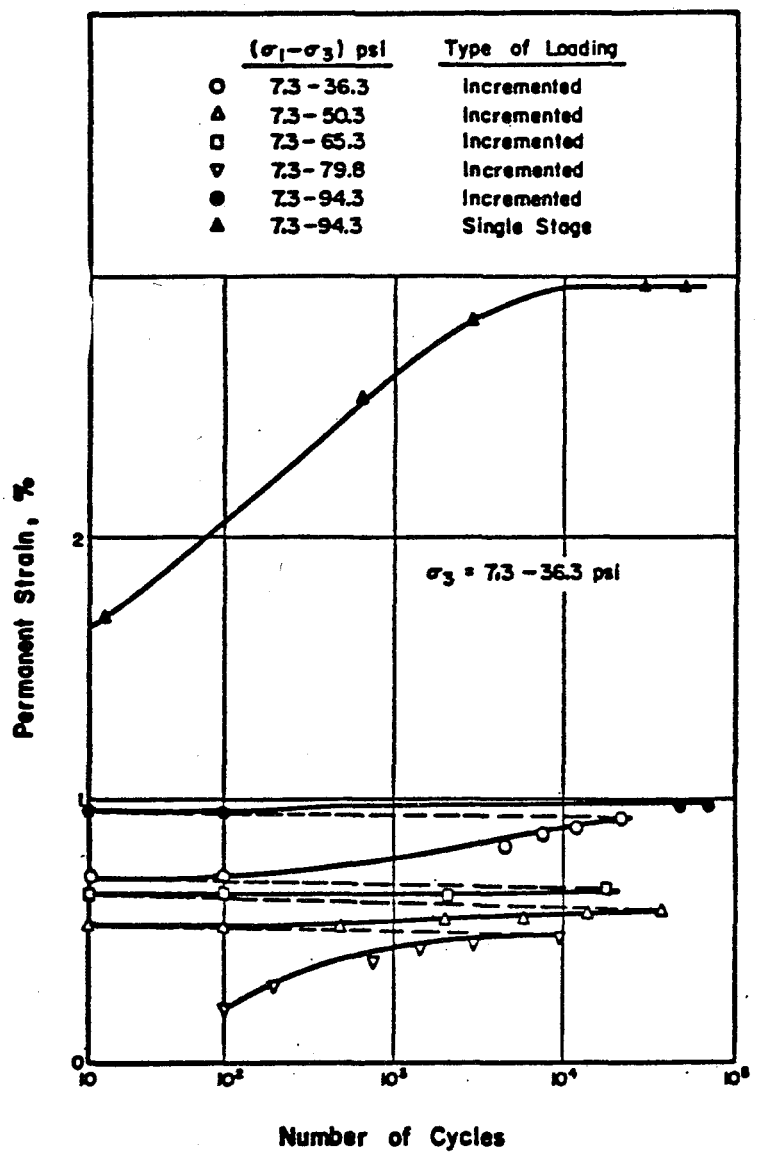

Fig. 3-4. Effect of Stress Sequence on Permanent Strain Response (Ref. 38)

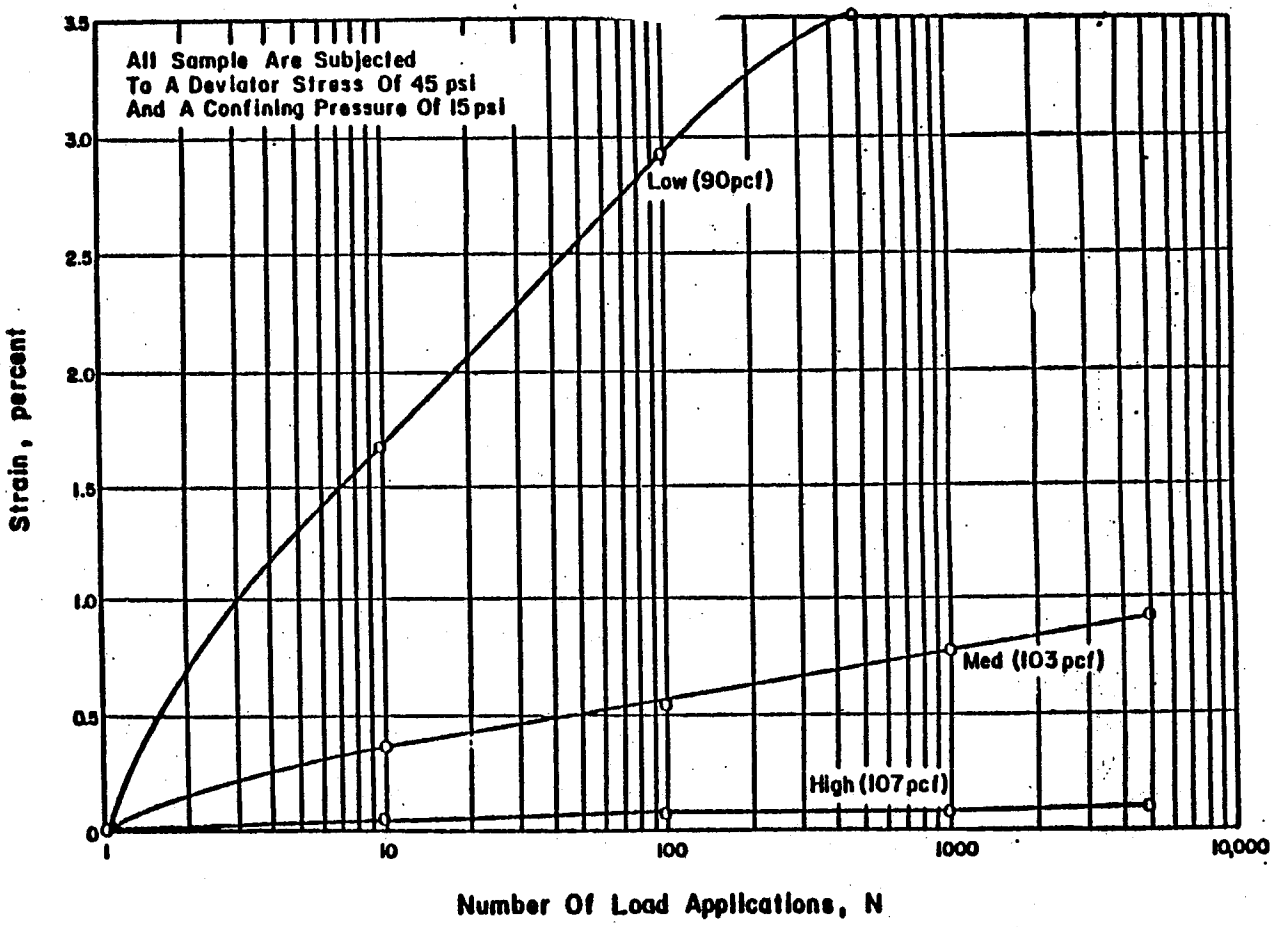

Fig. 3-5. Effect of Density on Permanent Deformation Response of Limestone Ballast (Ref. 14)

of a limestone ballast.

Knutson (Ref. 14) found no significant differences in the permanent deformation behavior of three granular materials: limestone, basalt and gravel. The effects of material properties such as particle index and flakiness index were not consistent and therefore no conclusions were drawn with respect to those properties. He also reported the effect of gradation on permanent deformation behavior. In general, the AREA number 4 gradation tended to resist permanent deformation less than did the number 5 or the "well-graded" materials.

3.3 Ballast Cyclic Testing

Previous work related to ballast cyclic testing is scarce. Some published information about ballast cyclic testing is given in Refs. 13, 14, 45, 46, and 48. The main emphasis of this section will be given to the permanent deformation behavior.

Raymond and Williams (Ref. 48), based on Olowokere (Ref. 13), presented typical stress-strain-volume change relationships with number of cycles for triaxial compression repeated load testing of dolomite ballast. An example of the material response is given in Fig. 2-2. A large axial strain was observed at the end of the first cycle. After the first cycle, the amount of strain occurring in each successive cycle tended to decrease. The width of the loading-unloading loop is also greatest in the first cycle and decreases with subsequent cycles until the loading curves eventually coincide with the corresponding unloading curve.

Figure 3-6 from Olowokere (Ref. 13) presents plots of permanent axial and volumetric strains with the logarithm of the number of cycles. The plots approximate straight line relationships, although there is evidence that the curves were flattening to a stable condition after 100,000 cycles. There are

three tests presented in Fig. 3-6 representing stress difference factors of 0.25, 0.50 and 0.75. The stress difference factor is defined as the ratio of deviatoric stress applied in repeated loading to the deviatoric stress at failure. Among the conclusions by Olowokere were:

1. For a given material and a given density, increasing the stress difference factor will result in increased permanent deformations.
2. For a given stress difference factor and same material and density, the permanent deformation increases with increasing confining pressure.
3. A large deformation is produced by the first load application. This deformation is comparable to static loading, that is, a function of the confining pressure and deviatoric stress applied.
4. The rate of permanent deformation accumulation decreases with the number of cycles.
5. The volumetric permanent strain increases gradually and steadily with increasing number of load cycles.

The work of Olowokere was extended by Raymond and Williams (Ref. 48) to include extension tests. However, only one density was used in both types of tests.

Knutson (Ref. 14) presented results of the permanent deformation behavior with number of cycles of loading for a variety of ballast material. Typical behavior has been presented in Fig. 3-5. The most important factors influencing the permanent deformation behavior of ballast were postulated to be: the number of load repetitions, the degree of compaction, and the stress level. It is important to point out that in this work, the importance of the deformation after the first cycle was not stressed. In fact, in Fig. 3-5 the permanent deformation after the first cycle is given as zero.

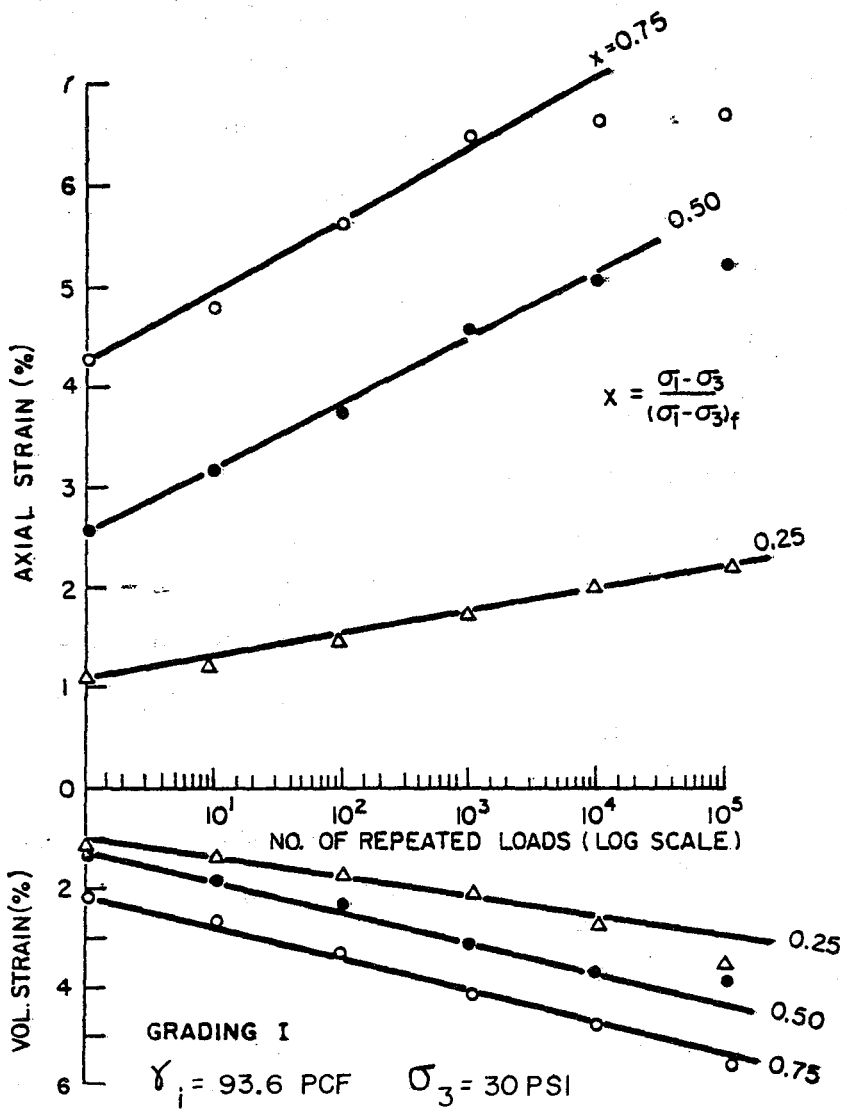

Fig. 3-6. Strain Response as a Function of Repeated Triaxial Loading of Coteau Dolomite Ballast (Ref. 13)

The Office of Research and Experiments (ORE) of the International Union of Railways (Ref. 45) undertook studies both in the laboratory and in the field to determine the behavior of the ballast layer in the track foundation under the action of repetitive loads. Laboratory repeated load tests were made on Derbyshire limestone and Meldon stone ballasts. Different densities were tested. The results indicated that under controlled stress conditions, the ballast permanent strain can be predicted by the equation:

$$\varepsilon_N = 0.082\ (100n - 38.2)(\sigma_1-\sigma_3)^2(1 + 0.2 \log N)\ ,$$

where ε_N = permanent strain after N loading cycles,

n = initial porosity of the sample,

$\sigma_1-\sigma_3$ = deviator stress, and

N = number of repeated loading cycles.

The main points that arose from the predictive equation were that:

1. The development of the permanent deformation of the ballast (deformation/load cycle) reduced considerably as the number of cycles increased.
2. The first load application produced a very large permanent deformation. The deformations produced by subsequent loading can be related to that produced at the first loading by:

   $\varepsilon_N = \varepsilon_1(1 + 0.2 \log N)$.

   This relationship was independent of initial porosity, stress levels, or material type (Figs. 3-7 and 3-8).
3. The permanent deformation was very dependent on the initial compaction of the ballast.
4. The permanent deformation was proportional to the square of the applied deviatoric stress.

Shenton (Ref. 46) continued the laboratory testing undertaken by ORE mainly

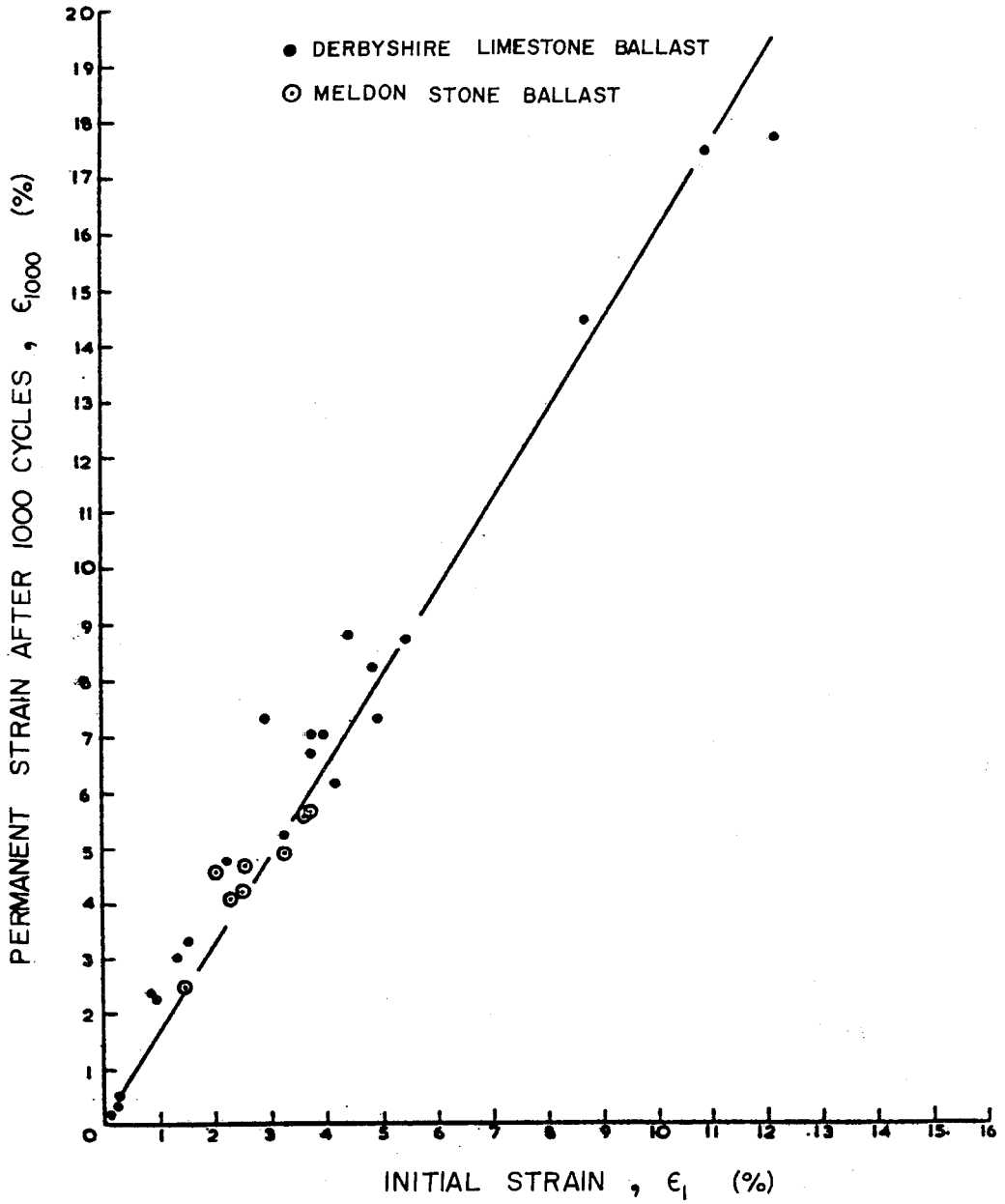

Fig. 3-7. Relationship Between Permanent Strains After First and Tenth Load Cycles for Range of Ballast Stresses and Gradings (Ref. 45)

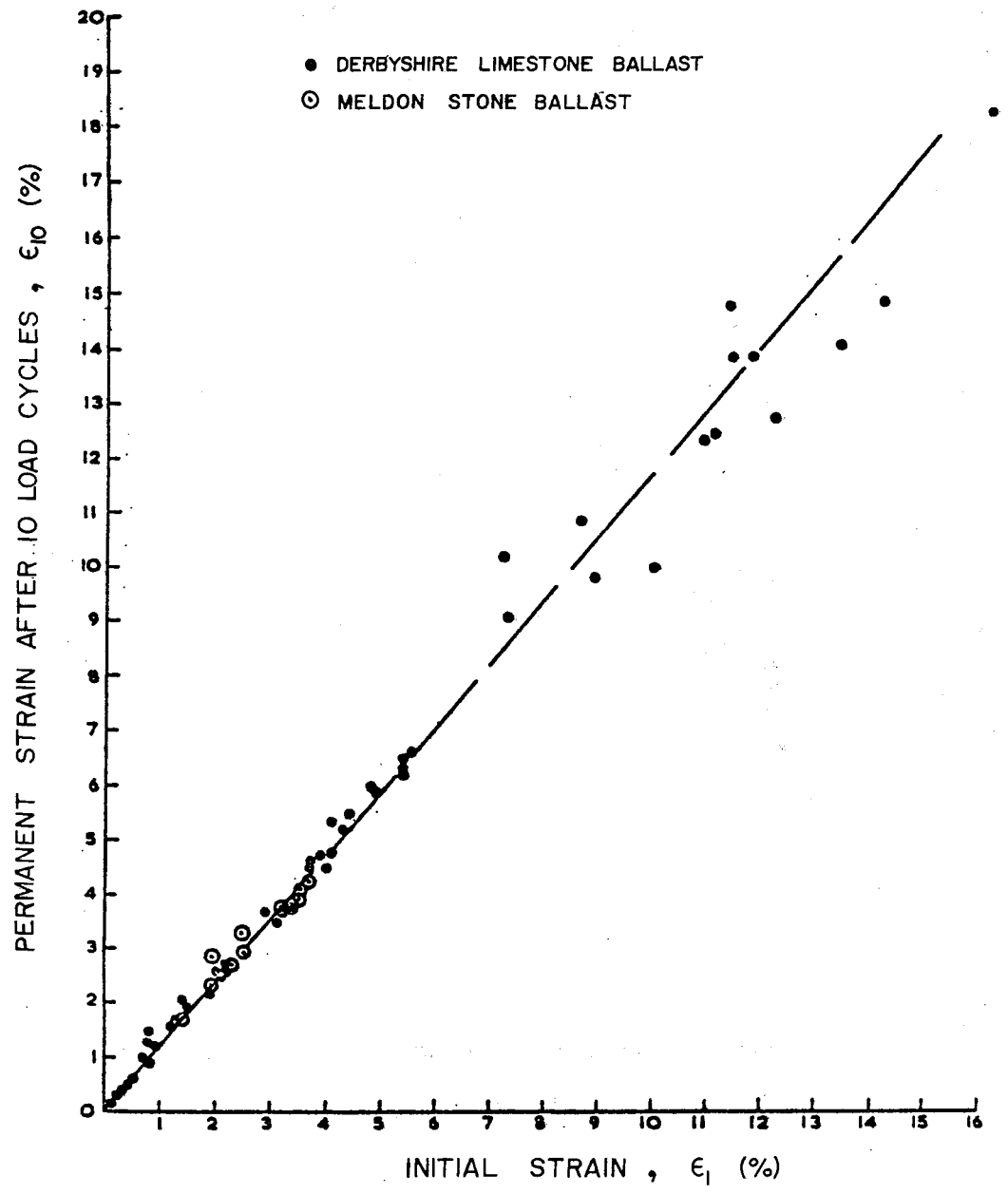

Fig. 3-8. Relationship Between Permanent Strains after First and Thousandth Load Cycles for Range of Ballast Stresses and Gradings (Ref. 45)

to determine and qualify the effects of changes in the applied loading pattern. He made the following conclusions:

1. The first load cycle produced a large permanent strain followed by a period where the permanent strain is proportional to the log of the number of cycles. This is the same as in Ref. 45.
2. There is a large variation in ballast strains even when the ballast samples are identically prepared and subjected to the same stresses.
3. The permanent strain is proportional to the axial stress raised to an exponent within the range of 1 to 3.
4. The permanent strain is determined mainly by the largest load when two load levels are applied.
5. The permanent strain is reduced if full load removal is not allowed between load cycles.
6. The same relationship as ORE of permanent deformation at cycle N with permanent deformation at cycle 1 was obtained, that is, $\varepsilon_N = \varepsilon_1(1 + 0.2 \log N)$ for Ballidon limestone tested at three different densities (Fig. 3-9).

Hargis (Ref. 29) studied the permanent deformation behavior of a limestone gravel subjected to repetitive loading. From the data, he developed a regression model to predict permanent deformations with the application of loads. The independent variables were the number of cycles of loading, N, and the ratio of cyclic deviator stress to maximum static deviator stress, R. The regression model was of the form:

$$\log \varepsilon_{vp} = -1.8688 + 0.1666 \log N + 2.4048R,$$

where ε_{vp} = the predicted vertical permanent strain in percent.

Brown (Ref. 35) conducted a series of laboratory repeated triaxial tests on a crushed granite with a 0.2-in. maximum particle size. He found that under

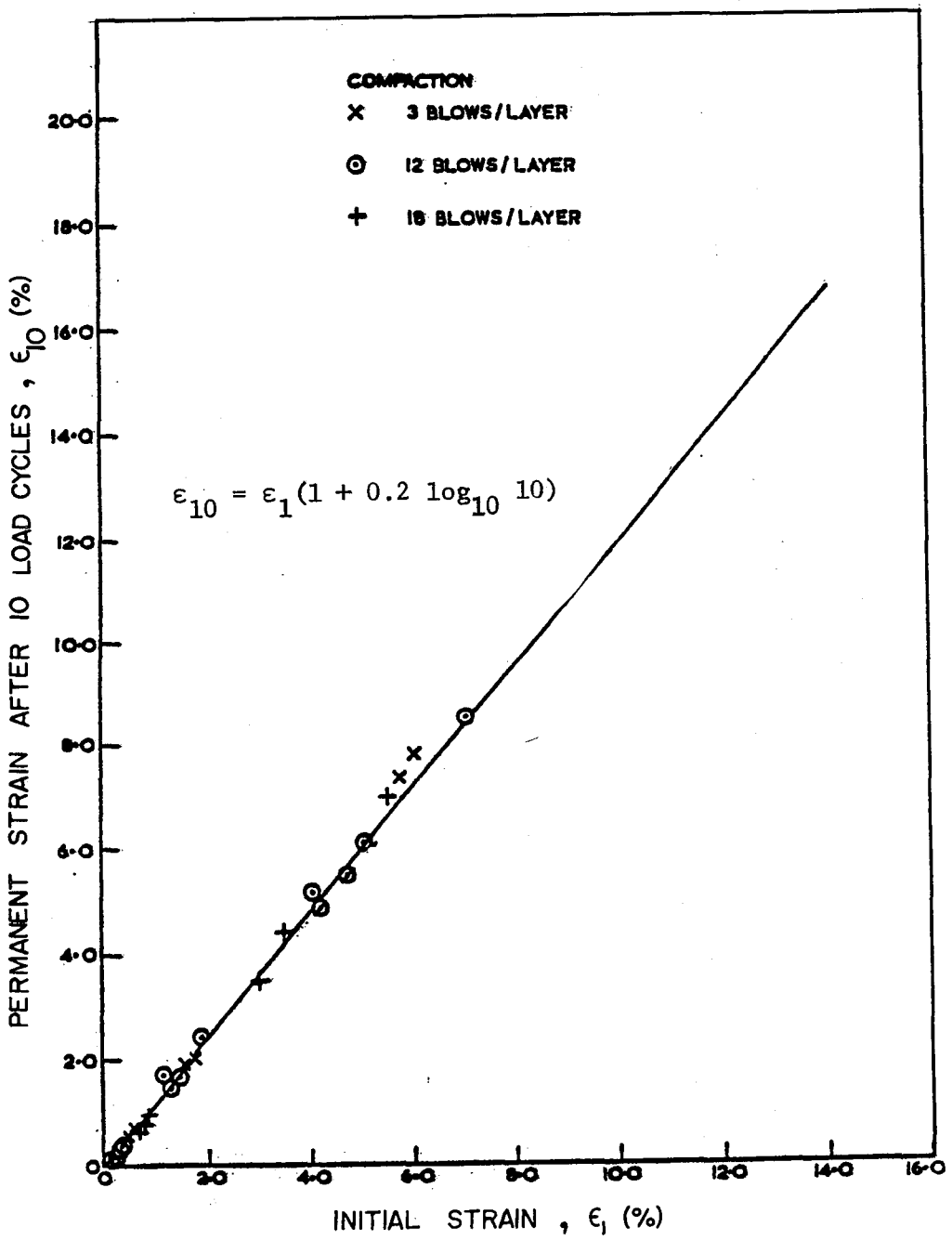

Fig. 3-9. Relationship Between Permanent Strains after First and Tenth Load Cycles for Different Degrees of Compaction of Ballidon Limestone (Ref. 46)

drained conditions, the permanent strain reached equilibrium values after approximately 10,000 cycles of deviatoric stress. The permanent strain at equilibrium was related to the applied stresses by:

$$\varepsilon_{vp} = 0.01\ (q/\sigma_3),$$

where q was the deviator stress and σ_3 was the confining pressure.

In a recent extension of Brown's work at Nottingham, Hyde (Ref. 49) investigated the influence of loading sequence and that of applying cyclic confining pressure to the same granular material. The limited study of loading sequence showed that while the resilient modulus was unaffected by this, the permanent deformation behavior was significantly affected. The permanent strain which built up after successive applications of about 100,000 cycles of gradually increasing level was less than half of the value resulting when the highest stress level was applied constantly.

3.4 Pavement Approach to Deformation Prediction

Pavement research towards the prediction of elastic and inelastic deformation (rutting) has been underway for several years. A state-of-the-art report by the Transportation Research Board (Ref. 50) was entirely dedicated to this problem. Also, Monismith (Ref. 51) and Monismith and Finn (Ref. 52) have presented a state-of-the-art paper on this subject.

According to Monismith and Finn (Ref. 52), there are two design approaches available based on rutting from repeated traffic loading. One of the approaches involves limiting the vertical compressive strain at the subgrade surface to some tolerable amount associated with a specific number of load repetitions, i.e., Shell criteria (Ref. 53). The other approach involves prediction of the actual amount of deformation which might occur in the pavement system using material characterization data developed in the laboratory together with an analysis procedure used to represent the pavement structure. The procedures for

the estimation of the amount of rutting in pavements from repeated traffic loading use linear or nonlinear elastic layered systems to represent the pavement structure, employing materials characterization from repeated load triaxial compression tests. To use the aforementioned approach, relationships between permanent strain and applied stress must be available for each of the pavement components.

The method as adapted by Barksdale (Ref. 28) is a simplified engineering approach that consists of subdividing each layer of the pavement structure into sublayers and, by use of linear or nonlinear elastic layered theory, determine the major principal stress σ_1 and average confining pressure σ_3 at the center of each sublayer beneath the wheel load (Fig. 3-10). Because of the location under the center of the load, the principal stresses are in the vertical and horizontal planes; therefore, this situation can be simulated in the laboratory by the triaxial test.

The permanent strains can be calculated at the center of each sublayer by using the relationship between permanent strain and applied stress from laboratory results for the desired number of load applications. The total permanent deformation is then obtained by summing up all of the products of the average permanent strain occurring at the center of each layer and the corresponding sublayer thickness. This step can be mathematically expressed as

$$\delta^P_{total} = \sum_{i=1}^{n} (\varepsilon_i^P h_i),$$

where δ^P_{total} = total permanent deformation beneath the wheel load,

ε_i^P = average permanent strain in the i^{th} sublayer,

h_i = thickness of the i^{th} sublayer, and

n = total number of sublayers.

The values of permanent strain ε_i^P are obtained from laboratory tests for a given state of stress at various number of load repetitions.

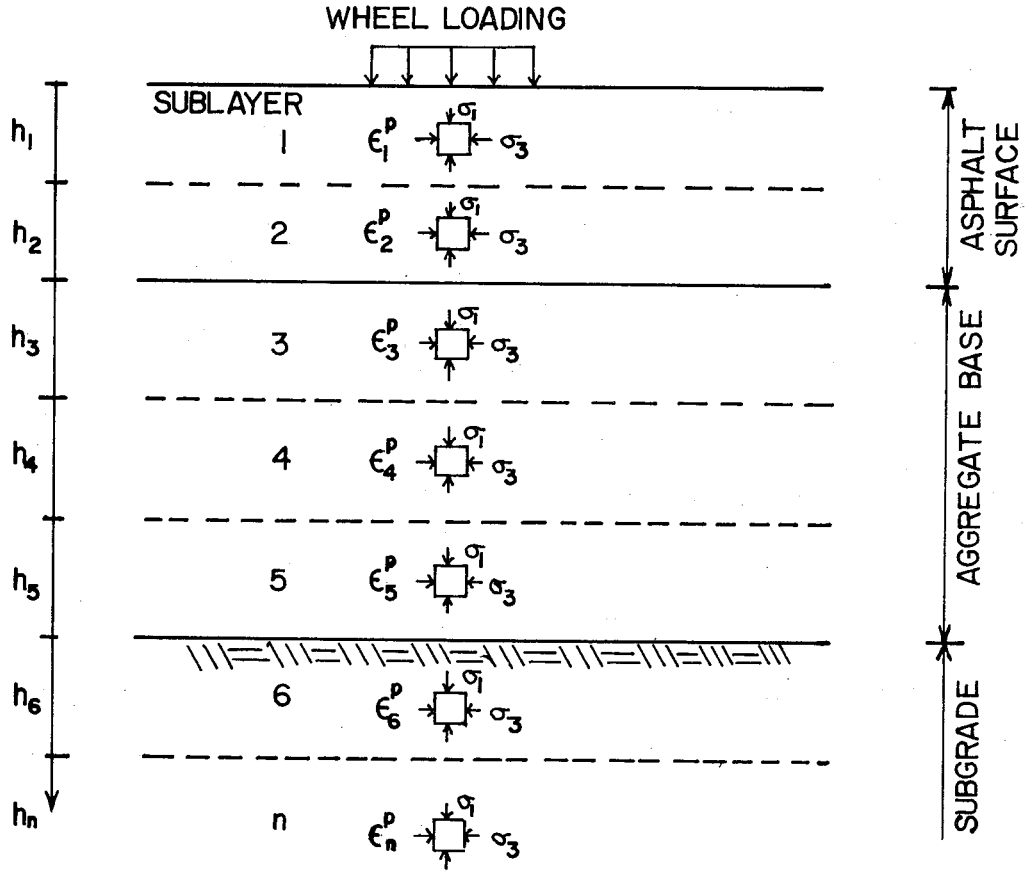

Fig. 3-10. Idealization of Layered Pavement Structure for Calculating Permanent Deformation (Ref. 28)

Barksdale (Ref. 28) proposed a method to relate the permanent axial strain caused by repeated loading to the state of stress in the triaxial test, based on a modification of the hyperbolic model of Kondner (Ref. 16) and Duncan and Chang (Ref. 17). The strain after 100,000 cycles of well-graded materials can be predicted by

$$\varepsilon_{vp} = \frac{(\sigma_1 - \sigma_3)/E_i}{1 - \left[\frac{(\sigma_1-\sigma_3)(1-\sin\phi)R_f}{2(c\cos\phi + \sigma_3 \sin\phi)}\right]}$$

where ε_{vp} = permanent axial strain,

$\sigma_1 - \sigma_3$ = deviator stress,

σ_3 = confining pressure,

E_i = initial tangent modulus equal to $K\sigma_3^n$, where K and n are experimentally determined constants,

c, ϕ = Mohr-Coulomb parameters, cohesion and friction angle, and

R_f = a ratio of the stress difference at failure to the stress difference where the stress-strain curve approaches infinite strain, i.e., $(\sigma_1 - \sigma_3)_f/(\sigma_1 - \sigma_3)_{ult}$.

Figure 3-11 (Ref. 12) shows the agreement between the measured and the calculated values of permanent strain.

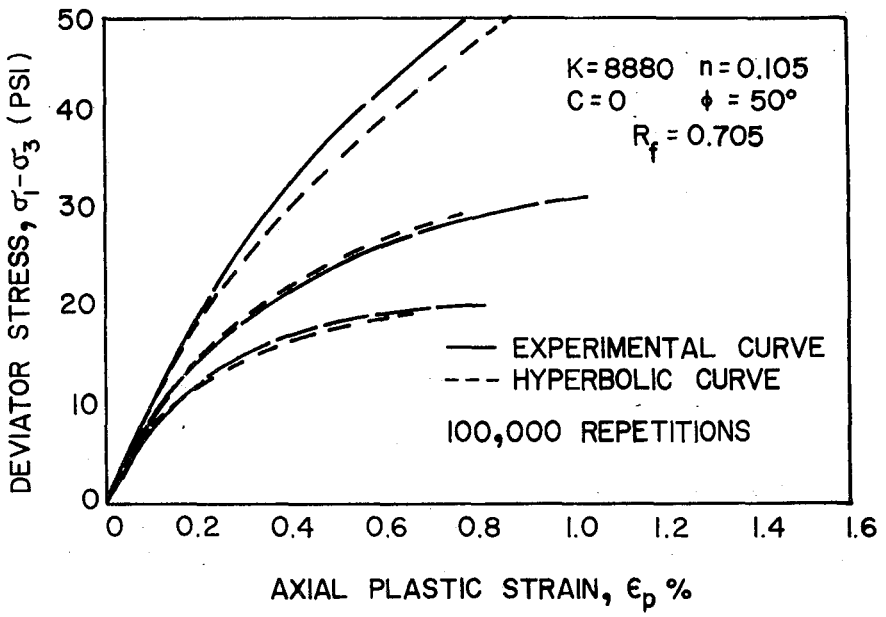

Fig. 3-11. Hyperbolic Fits to Experimental Plastic Strain Curves (Ref. 12)

CHAPTER 4. STRESS PATH DETERMINATION

This chapter presents the method used for determining the stress paths in the roadbed materials which define the stress states for the laboratory property tests. The computer model GEOTRACK was employed to estimate the stress distribution in the roadbed materials caused by train loading. From these incremental stresses and the geostatic stresses, the octahedral normal and shear stresses for both the loaded and unloaded track conditions were calculated for different points in the roadbed. The octahedral stresses were then converted to equivalent stresses for the repeated-load triaxial test which was used to measure the elastic moduli and permanent strain characteristics of the roadbed materials.

The approach will be illustrated using numerical results from FAST section 18B. Reference 3 gives the results for FAST sections 18A and 17E. The geometry and initial properties for section 18B are shown in Fig. 4-1. The rail and tie properties are given in Table 2-1. The resilient moduli shown in Fig. 4-1 are the values used for the first iteration. The resilient moduli for the subsequent iterations are calculated from the equations in Table 2-2 based on the bulk stress at the middle of each layer where the load is acting (Y = 0 in.). The wheel load employed was 32.9 kips. The solutions presented are for a single axle only.

4.1 GEOTRACK Results

The variation of incremental stresses with depth is shown in Fig. 4-2 for the point along the tie which is directly underneath the load. This is typical of the stress distribution at other point locations along the tie. Some observations that can be drawn from Fig. 4-2 are:

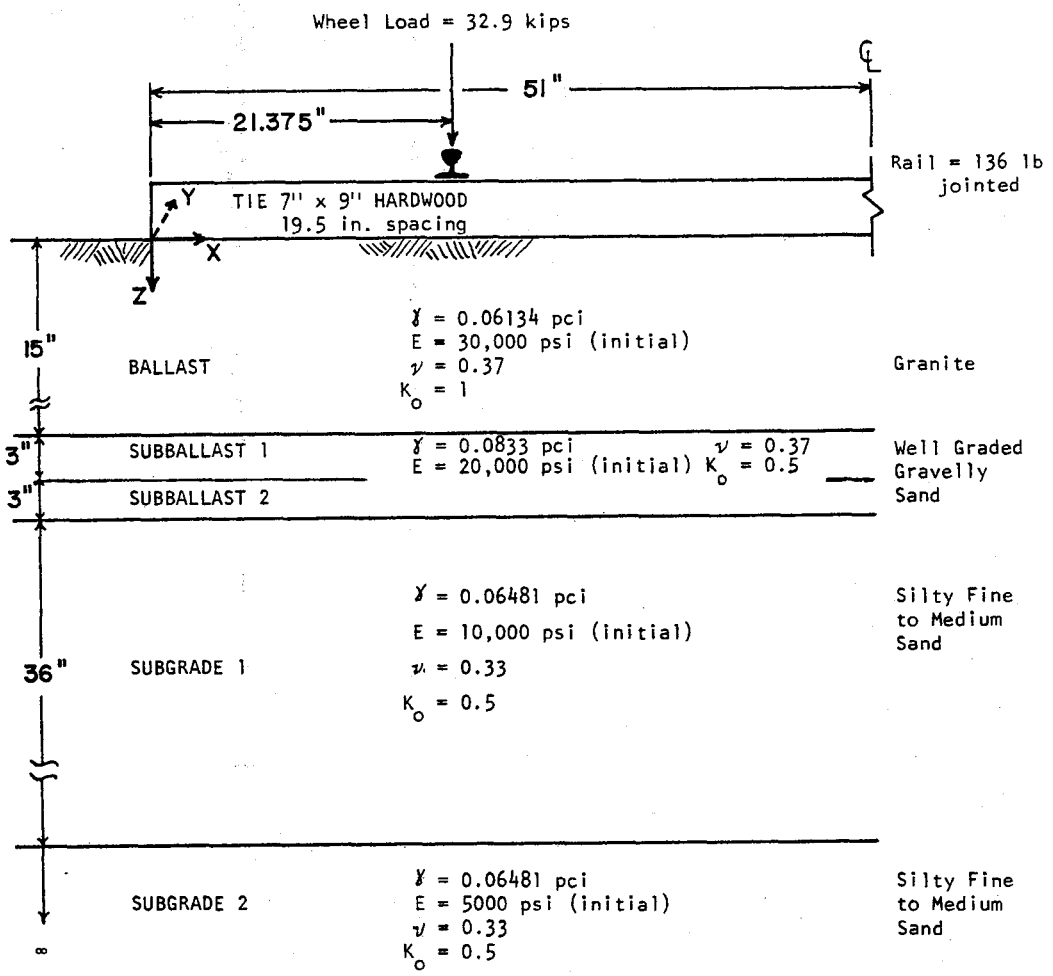

CHOSEN POINTS GEOTRACK ANALYSIS

X = 5.1, 15.3, 25.5, 35.7, and 45.9 in.

Z = 0, 3.8, 7.5, 11.3, 14.9, 16.5, 19.5, 21.1, 39.0, 57.1, 80, 120, and 240 in.

Fig. 4-1. Geometry and Initial Properties for FAST Section 18B

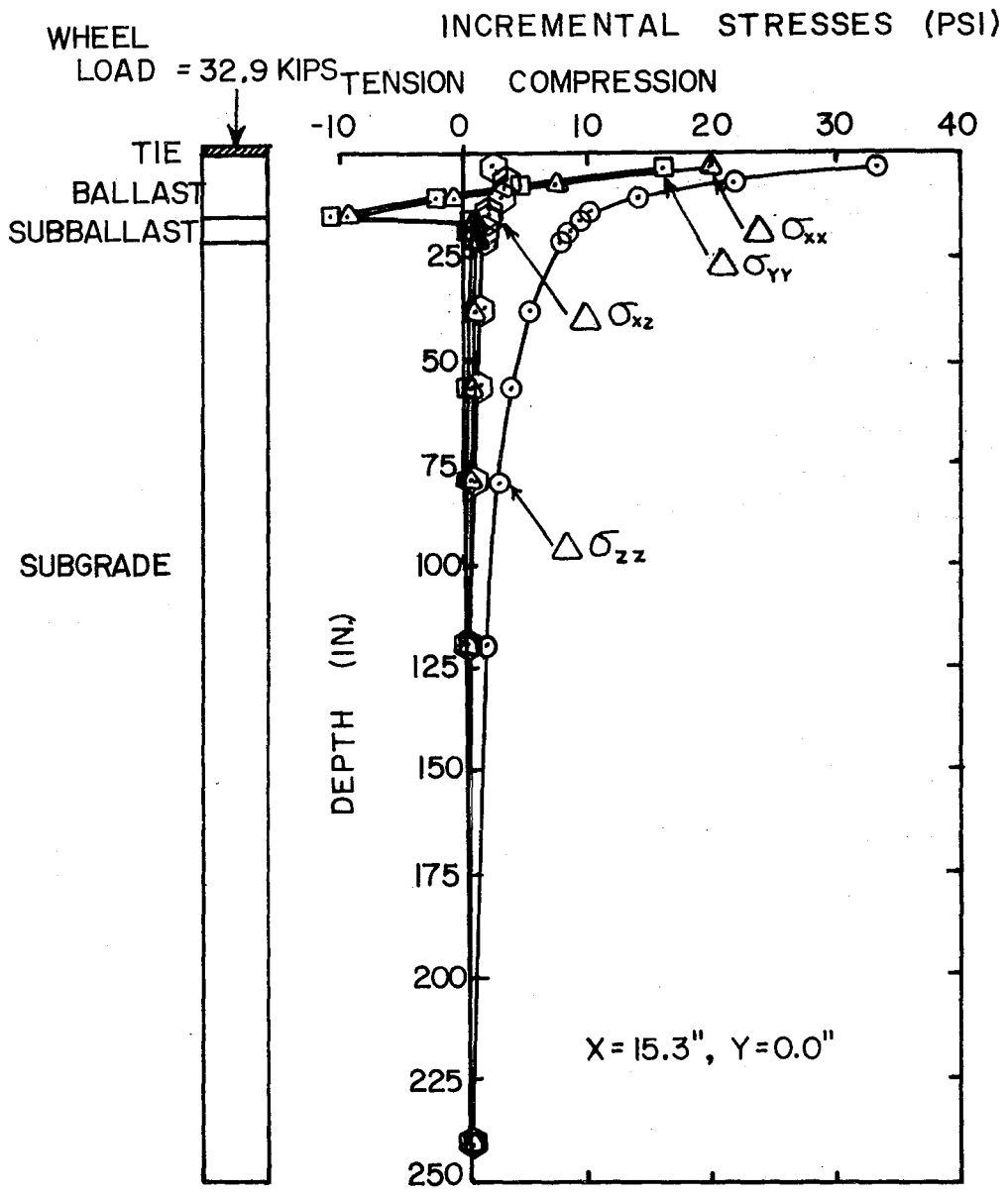

Fig. 4-2. Variation of Incremental Stresses with Depth below the Wheel Load Computed from GEOTRACK for Section 18B

1. The reinforcing and load spreading characteristics of layered systems can be appreciated. This fact is demonstrated by the normal stress gradients, in particular in the ballast layer.
2. Because of symmetry conditions, the only non-zero shear stress present in the plane of the load is $\Delta\sigma_{xz}$. The value of the shear stress increases to a maximum value near the mid-depth of the ballast layer, reduces to a lower value at the first interface, and becomes negligible in the subgrade.
3. Tensile stresses are developed at the bottom of the ballast in the transverse and longitudinal directions. However, it should be pointed out that the incremental vertical stress always remains compressive. The tensile stresses reach a value of approximately 10 psi at the first interface.

The variation of the incremental stresses across the tie for the ballast layer are presented in Figs. 4-3 through 4-6. The values of the incremental vertical stresses in the ballast near the surface are higher under the load than in the middle of the tie, but with depth these stresses become smaller and more uniform along the tie. As was pointed out before, at the ballast-subballast interface, tension develops for the transverse and longitudinal stress, the tension being higher under the load. The incremental shear stress changes in sign across the tie, being zero right underneath the load and at the axis of symmetry about the center of the tie. The maximum incremental shear stresses are at the ballast midlayer. It can be noticed that the level of incremental shear stress is not too high, 6.5 psi being the maximum.

Because the GEOTRACK model calculates only the incremental stresses imposed by the passing trains, a calculation of the geostatic stresses was added in order to combine them with the incremental stresses and hence determine the total

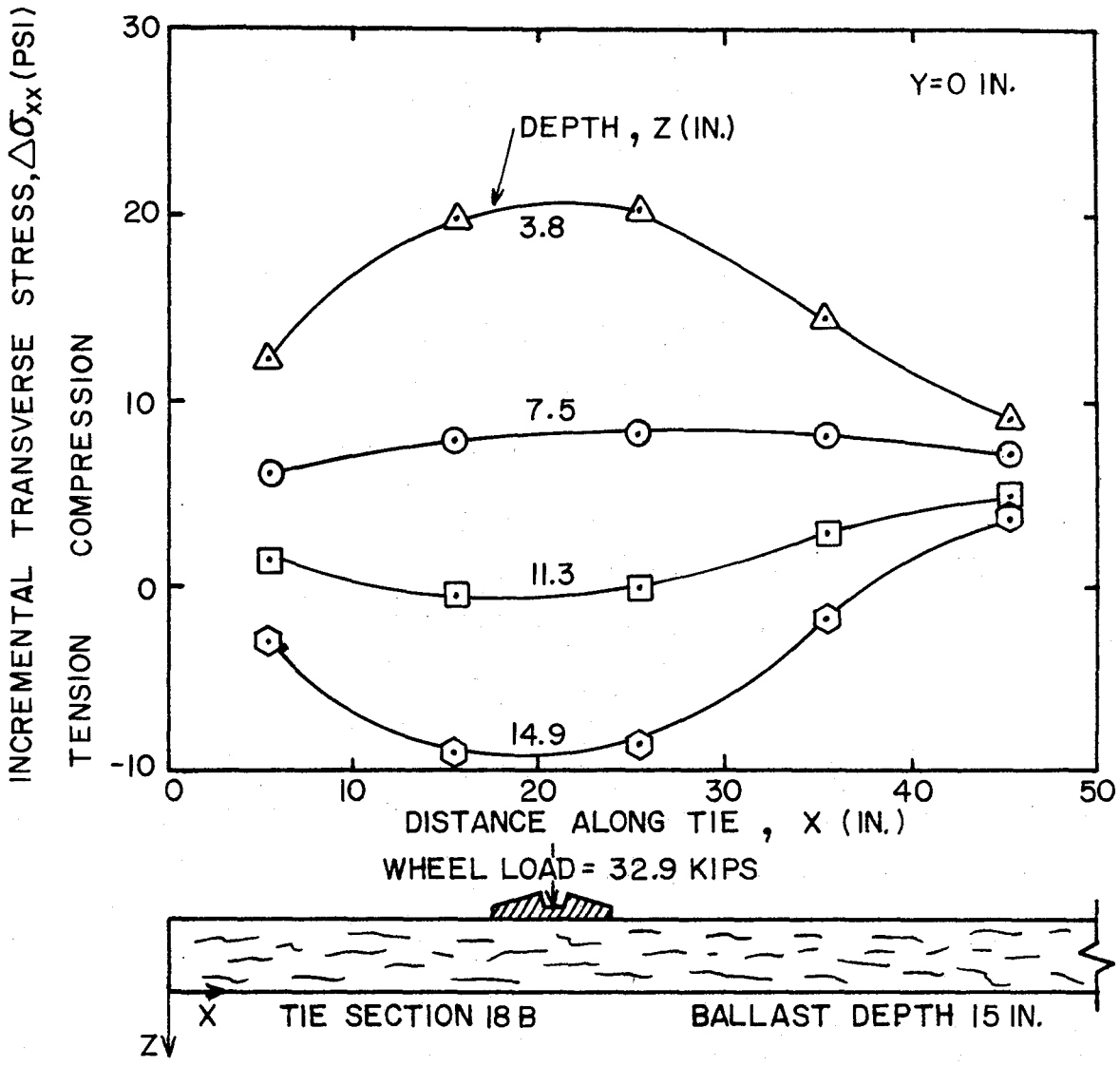

Fig. 4-3. Incremental Transverse Stress from GEOTRACK Under Center of Tie for Section 18B in Ballast Layer

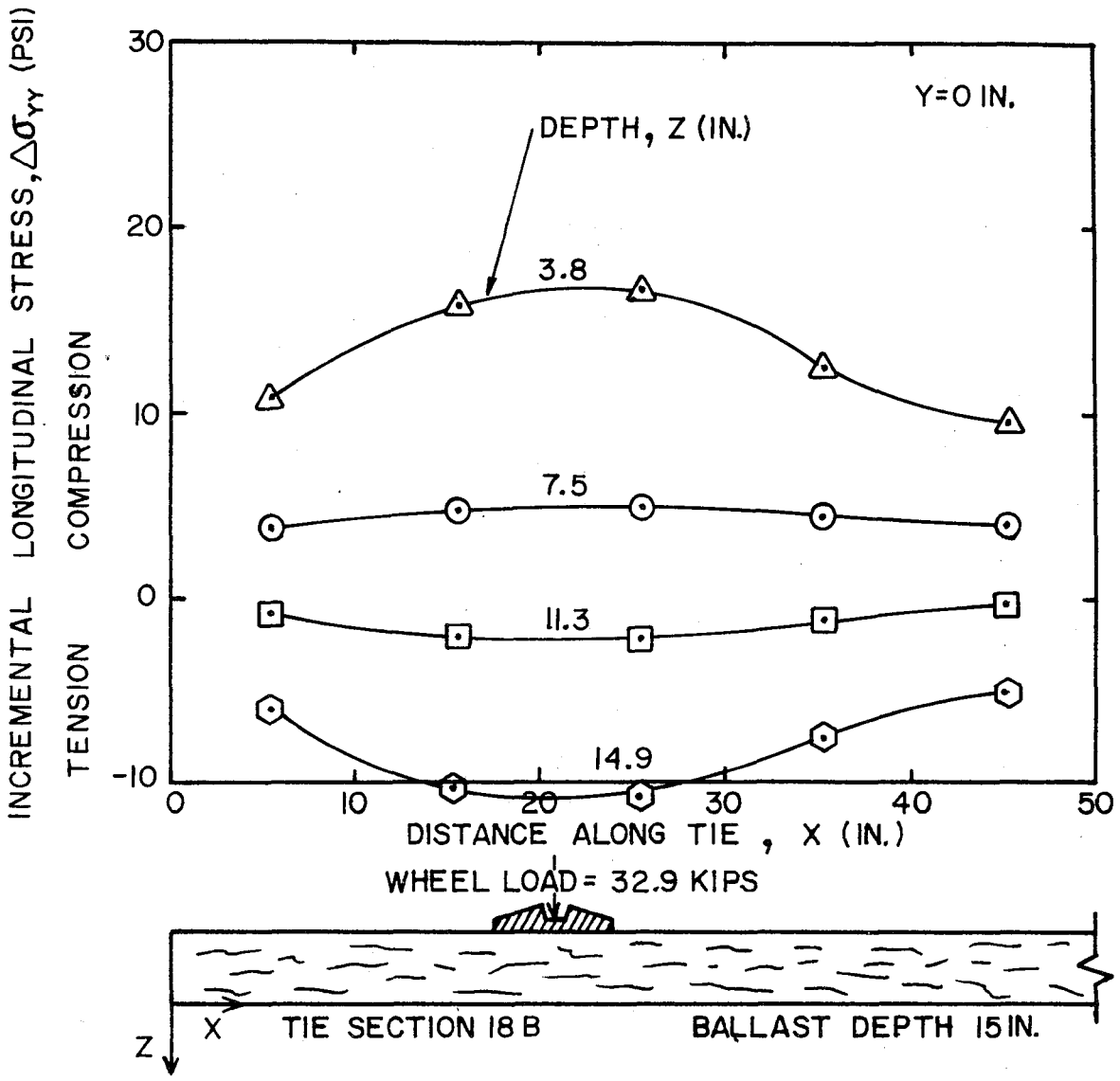

Fig. 4-4. Incremental Longitudinal Stress from GEOTRACK Under Center of Tie for Section 18B in Ballast Layer

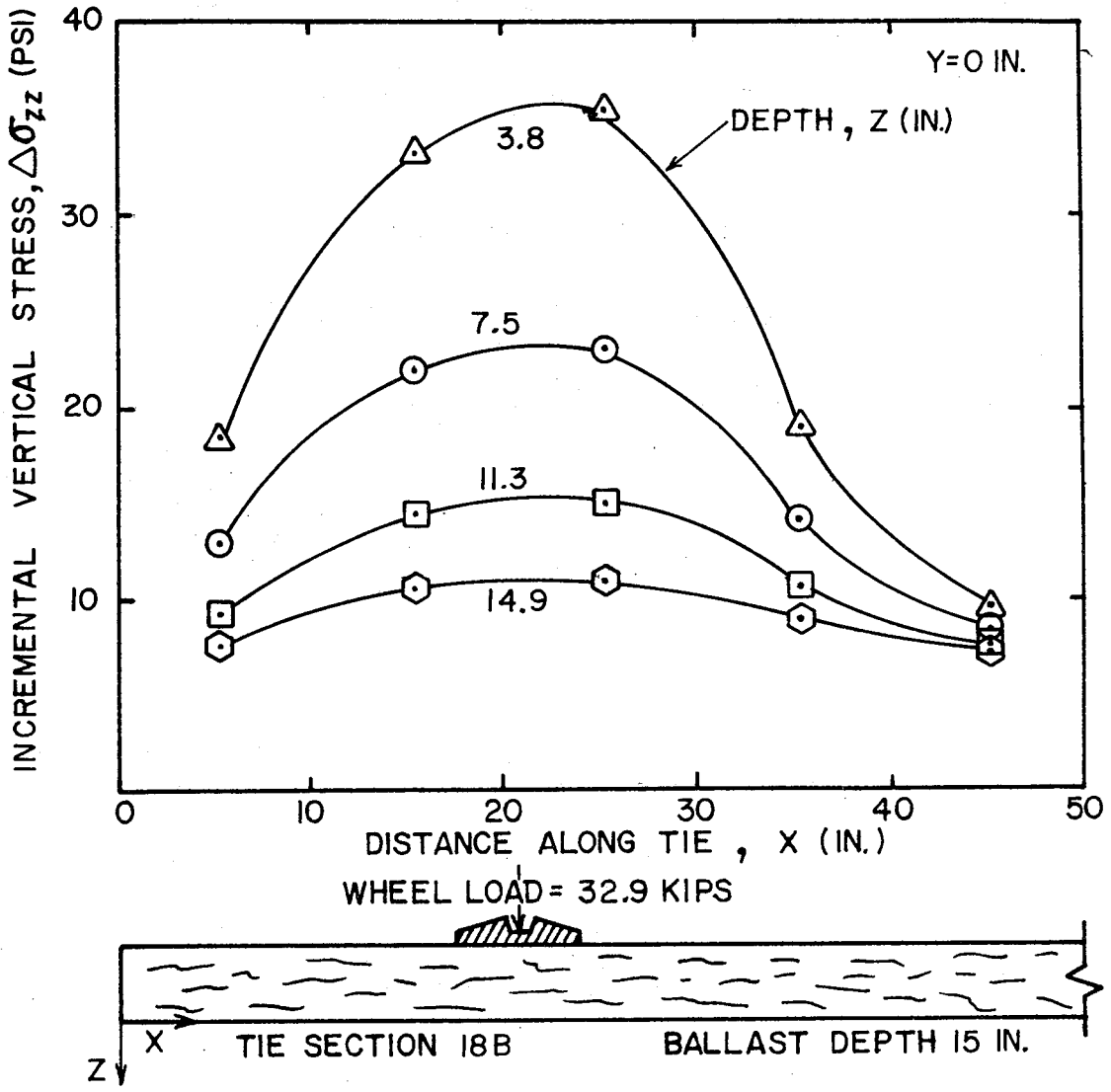

Fig. 4-5. Incremental Vertical Stress from GEOTRACK Under Center of Tie for Section 18B in Ballast Layer

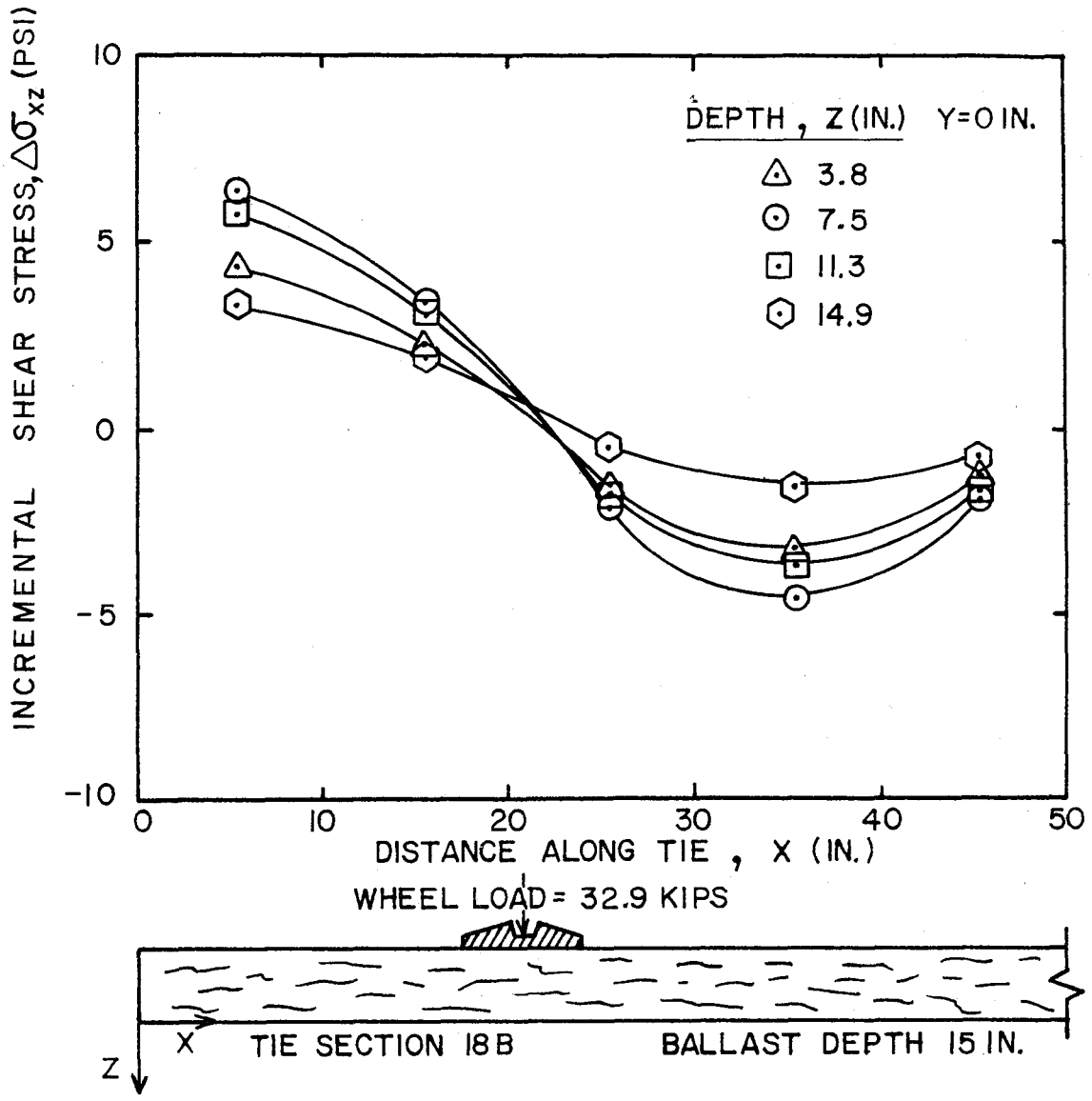

Fig. 4-6. Incremental Shear Stress from GEOTRACK Under Center of Tie for Section 18B in Ballast Layer

stresses. The values of K_o and γ used for the geostatic stresses are given in Fig. 4-1. Twelve different points at varying depths (Z direction) in the roadbed were chosen under each of the five different divisions beneath half the tie to determine the stresses. Octahedral stresses were used to account for the three-dimensionality of the problem and to obtain an easier physical interpretation of the three-dimensional system by considering the applied stresses to be divided into those causing volume change and those causing shear distortion. In addition, this allows easier conversion of the field stresses into equivalent laboratory cyclic triaxial stress states.

The total field octahedral normal stress (σ_{oct_f}) and total field octahedral shear stress (τ_{oct_f}) are determined from the total principal stresses by the expressions

$$\sigma_{oct_f} = \frac{\sigma_{1f} + \sigma_{2f} + \sigma_{3f}}{3} ,$$

and

$$\tau_{oct_f} = 1/3 \sqrt{(\sigma_{1f}-\sigma_{2f})^2 + (\sigma_{2f}-\sigma_{3f})^2 + (\sigma_{3f}-\sigma_{1f})^2} ,$$

where σ_{1f}, σ_{2f} and σ_{3f} are the three total principal stresses from the field.

Figure 4-7 presents the variation of total principal stresses with depth directly beneath the wheel load. This figure differs from Fig. 4-2 by the addition of the geostatic stresses. At this particular location, near the position of the load, there is not a large rotation of principal stress directions. Also, the values of σ_{2f} and σ_{3f} are close to each other, this case being nearly an axisymmetrical condition.

The variation of total σ_{oct_f} across the tie in the ballast layer for the Y = 0 plane is shown in Fig. 4-8, and with depth beneath the load in Fig. 4-9. In the ballast near the surface, the values of σ_{oct_f} are higher under the rail

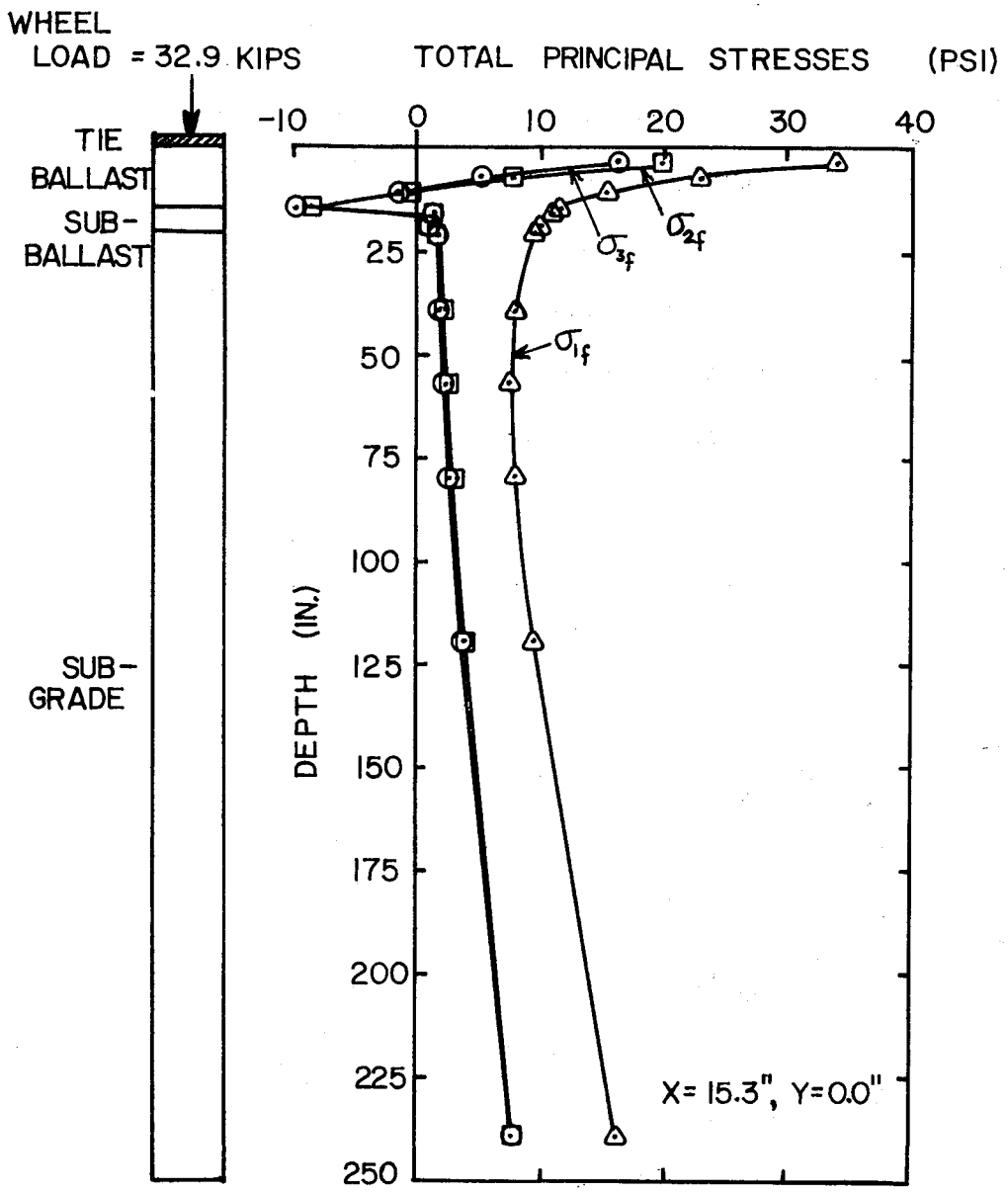

Fig. 4-7. Variation of Total Principal Stresses with Depth below Wheel Load from GEOTRACK for Section 18B

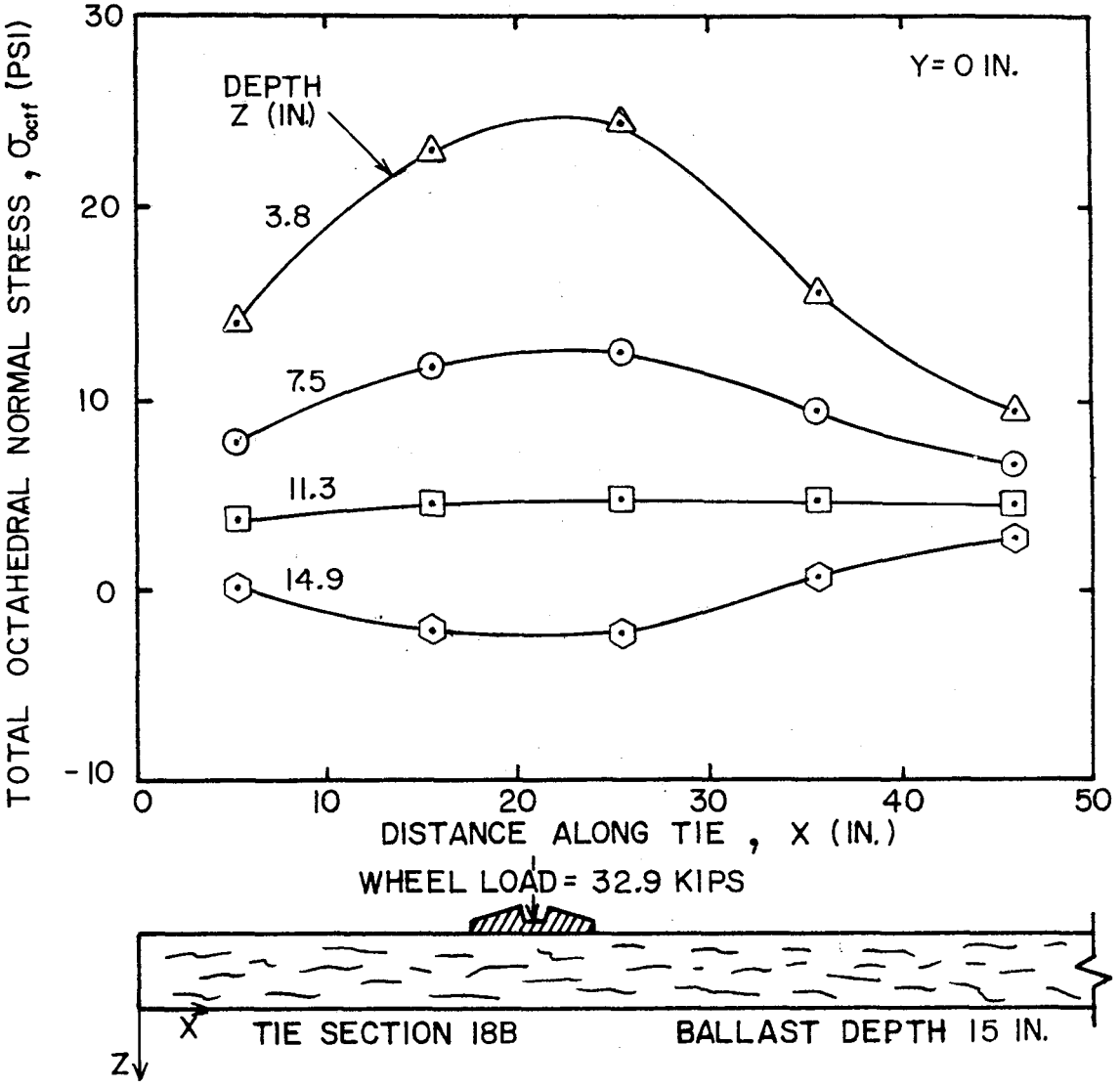

Fig. 4-8. Total Octahedral Normal Stress Under Center of Tie from GEOTRACK for Section 18B in Ballast Layer

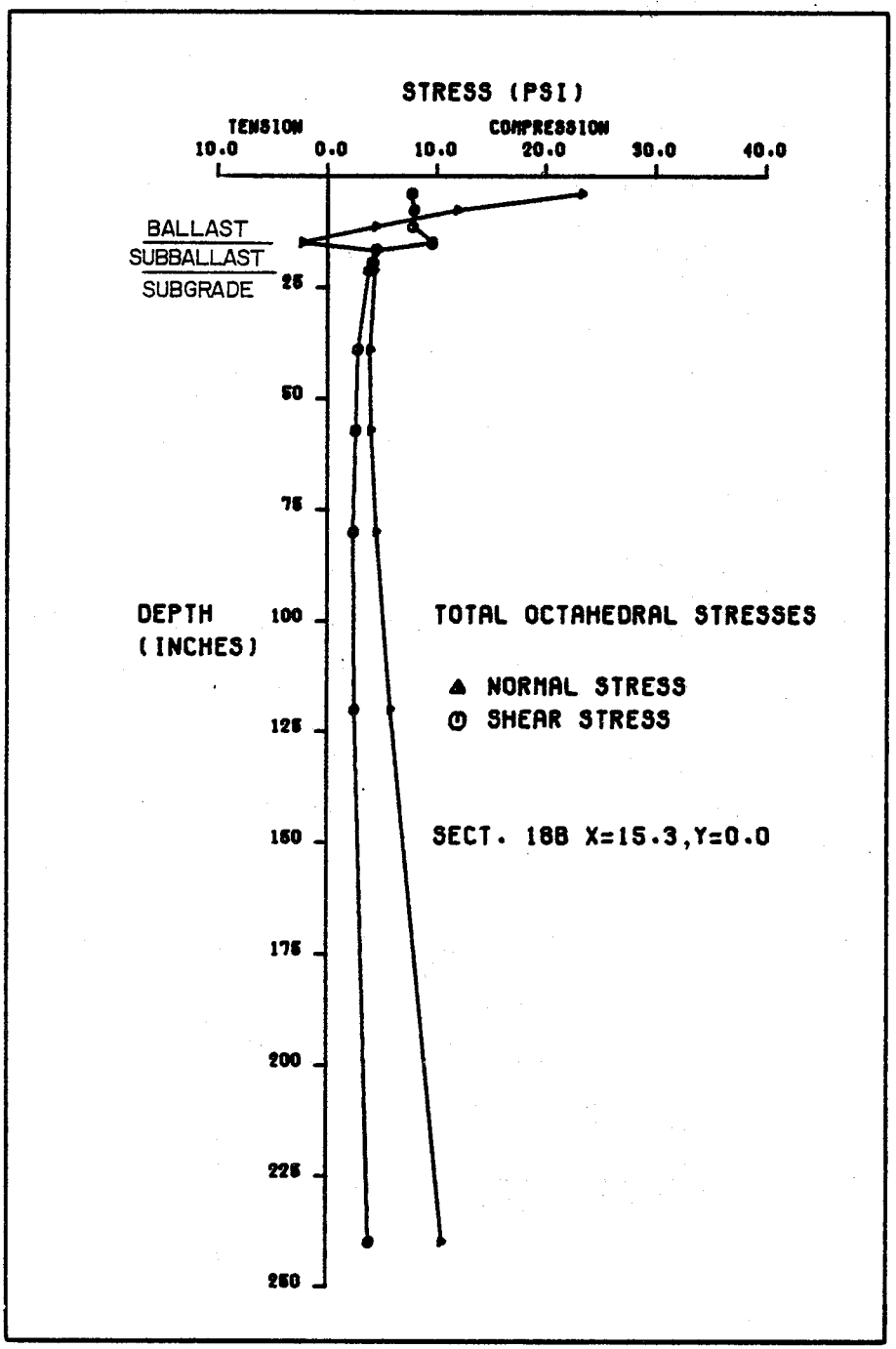

Fig. 4-9. Distribution with Depth Below Wheel Load of Total Octahedral Stresses for Section 18B

than in the middle of the tie, but with depth the stresses become smaller and more uniform along the tie, for example in the subballast and subgrade. Another interesting result is the development of tensile incremental octahedral normal stresses in the bottom of the ballast layer. As was previously mentioned, the incremental vertical stress transmitted by the wheel load is always compressive, but the longitudinal and transverse incremental stresses become tensile in the elastic multi-layer model. The same fact has been previously noted by Brown (Ref. 54) and others when using the multi-layer theory in asphaltic pavements.

The variation of the total τ_{oct_f} across the tie in the ballast layer for the Y = 0 plane is presented in Fig. 4-10, and with depth beneath the load in Fig. 4-9. A rapid decrease of the total octahedral shear stress is noticed at the interface between the ballast and the subballast. It can also be noticed that the magnitude of octahedral shear stress is small, 10 psi being the maximum with the Y = 0 plane. As in the case of normal stresses, the maximum shear stress occurs under the load, and with depth the distribution tends to be more uniform across the tie. It should be pointed out that the higher values of the octahedral stresses at the first interface (Z = 14.9 in.) are produced by the development of tensile normal stresses.

The variations of total octahedral normal and shear stresses across the tie in the ballast layer for the concrete tie section are shown in Figs. 4-11 and 4-12. These distributions are quite different from those of wood ties shown in Figs. 4-8 and 4-10. The concrete tie distribution approximates the behavior of a rigid footing supported by an elastic foundation. The maximum stresses are found at the tie ends and they decrease to a minimum value at the tie center. On the other hand, in the case of the wooden ties, the stress distribution is similar to that of a flexible footing supported by an elastic

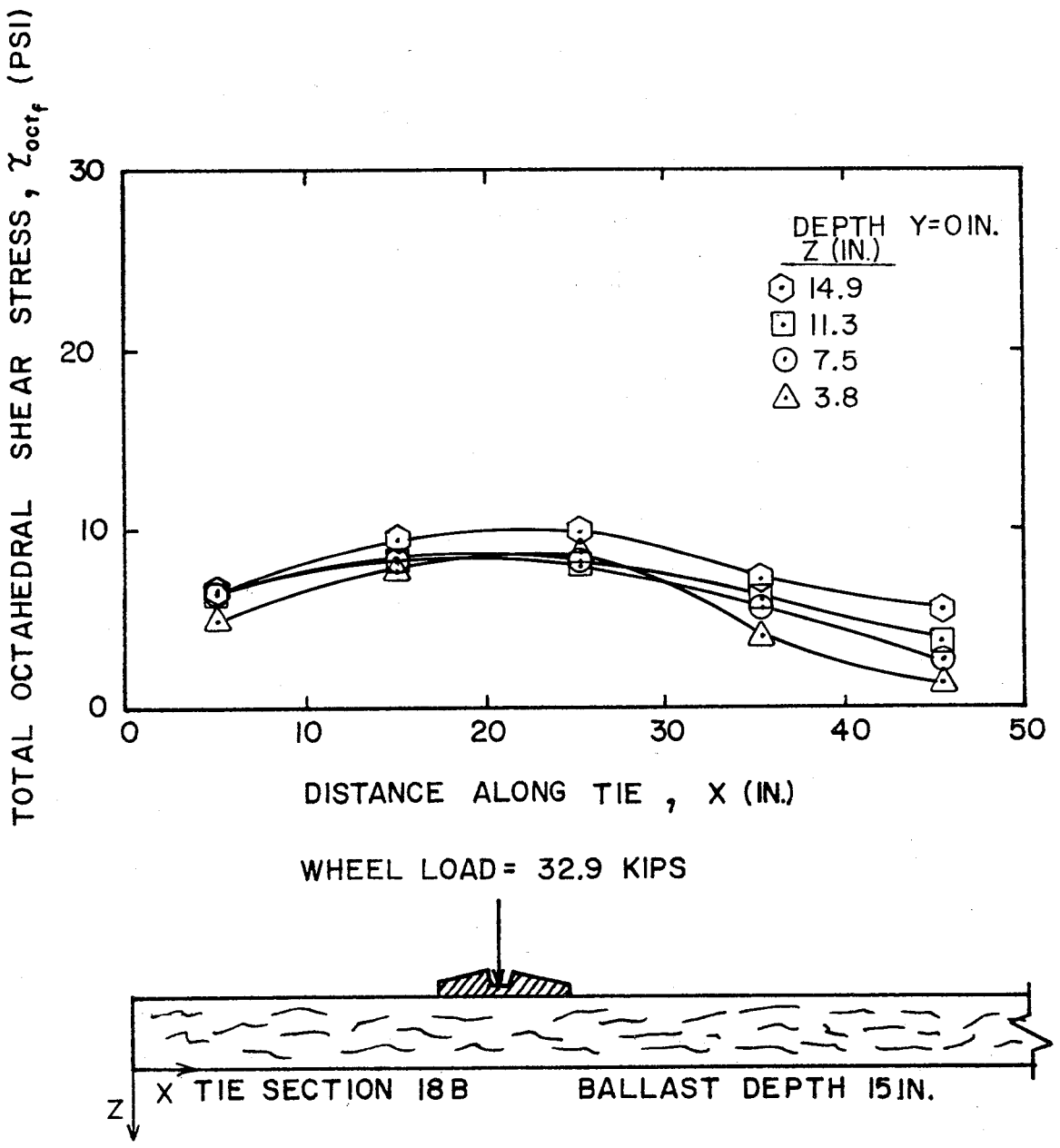

Fig. 4-10. Total Octahedral Shear Stress from GEOTRACK Under Center of Tie for Section 18B in Ballast Layer

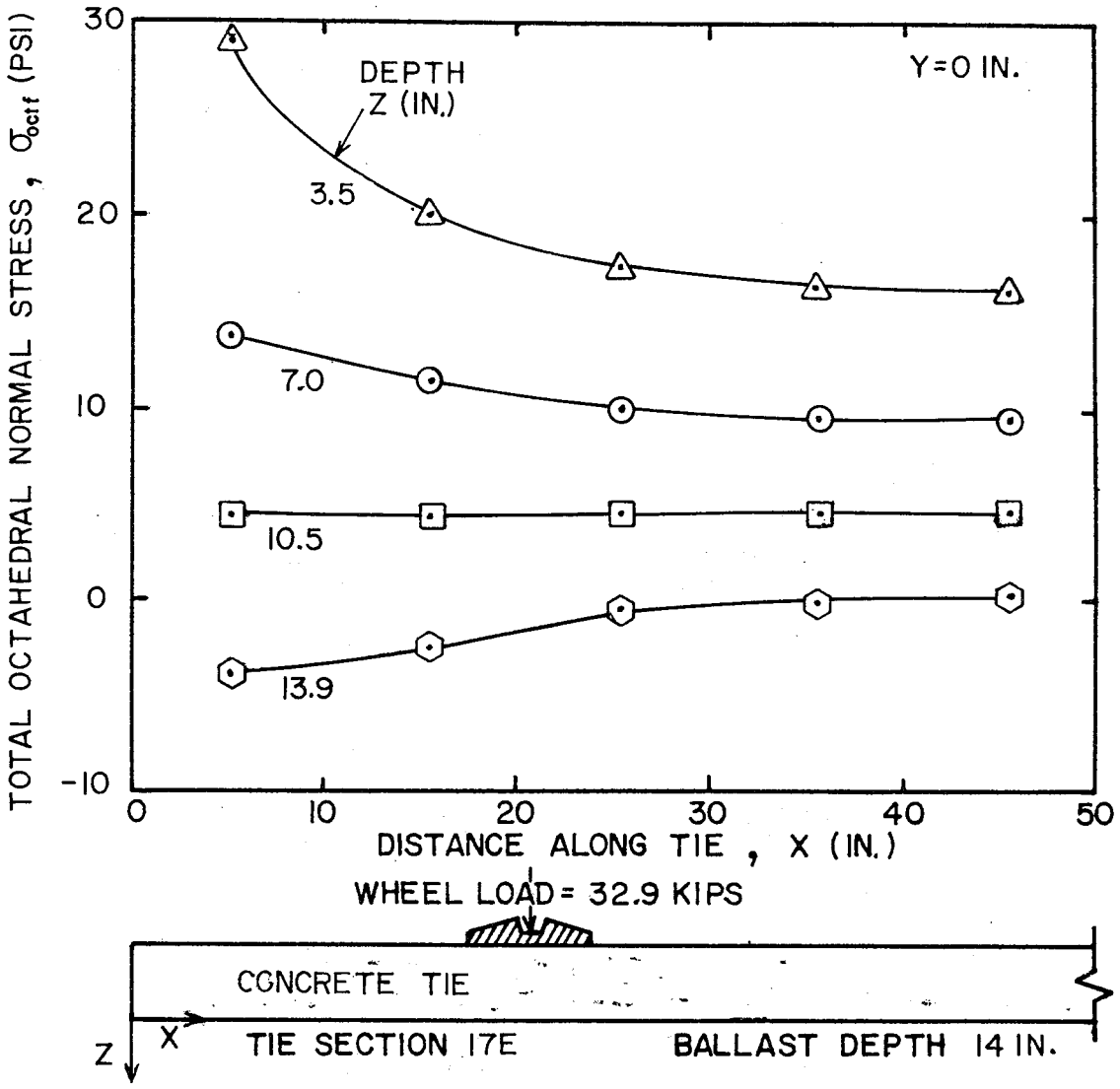

Fig. 4-11. Total Octahedral Normal Stress from GEOTRACK Under Center of Tie for Section 17E in Ballast Layer

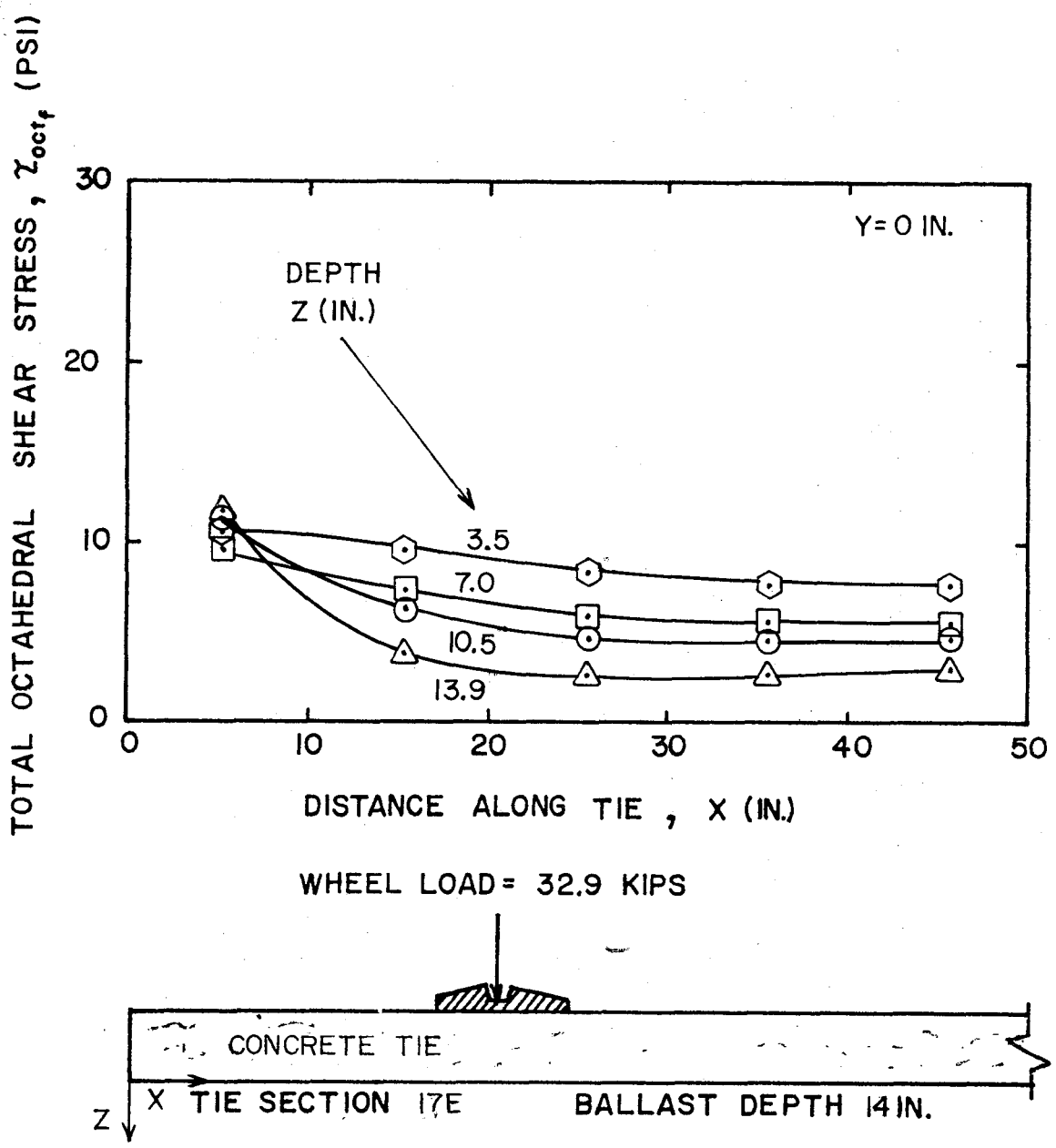

Fig. 4-12. Total Octahedral Shear Stress from GEOTRACK Under Center of Tie for Section 17E in Ballast Layer

foundation. In this case, the maximum stress is found beneath the load point at the rail and decreases towards the ends and center of the tie.

4.2 Cyclic Triaxial Test Stress Paths

The stress paths produced in the field with the imposition of wheel loads were simulated in the laboratory by means of cyclic (repeated load) compression triaxial tests. The test facility used permitted varying only the axial load (deviatoric stress), while maintaining the cell pressure constant. The triaxial stress states for the laboratory tests were based on the field octahedral stresses predicted with the GEOTRACK model described in the previous section. The manner in which the field stresses are converted to constant confining pressure triaxial stress paths will be presented in this section.

The conventional triaxial compression test consists of using a cylindrical sample with a hydrostatic confining pressure σ_3 and applying a deviatoric stress $\sigma_1 - \sigma_3$ to the sample by increasing the axial stress. The octahedral stresses in the triaxial test when the deviatoric stress is applied are defined by

$$\sigma_{oct_t} = \frac{\sigma_1 + 2\sigma_3}{3} \quad ,$$

and

$$\tau_{oct_t} = \frac{\sqrt{2}}{3}(\sigma_1 - \sigma_3) \quad .$$

The triaxial test has an axisymmetrical stress state because the confining pressure σ_3 acts in all horizontal directions. Furthermore, for the usual triaxial test, the only stress change that occurs is in the axial stress σ_1, in which case the triaxial test is also considered uniaxial.

The total stresses in the field consist of the stresses from train loading

predicted from GEOTRACK and the geostatic stresses. From these, the octahedral stresses σ_{oct_f} and τ_{oct_f} were determined. If these octahedral stresses from field conditions (σ_{oct_f} and τ_{oct_f}) are equated to the expression for octahedral stresses for the axisymmetric triaxial condition, values of σ_1 and σ_3 can be determined for the triaxial test which represent the field stress path as closely as possible.

Figure 4-13 compares, in the p-q stress plot, the different stress paths that can be studied with this approach. Point A represents the geostatic stress state in the field without train loads. This stress state is assumed to be hydrostatic. Point B is the equivalent axisymmetric stress state that considers geostatic plus incremental stresses produced by the train loading. Thus stress path AB is the cyclic state to which the roadbed elements will be subjected with moving wheel loads. This stress path generally will have an inclination different than 45^{o}, which is the stress path for a conventional, constant-confining-pressure triaxial compression test.

Figure 4-13 presents two ways by which the constant σ_3 triaxial tests can be employed to simulate the axisymmetric, but not constant, σ_3 field stress path AB. These are stress paths CB and DE, both having constant σ_3. The stress path CB consists of matching the maximum normal and shear stresses. The specimen will be given an initial confining pressure equal to that at point C. While the confining pressure is held constant, σ_1 is increased until point B is reached. On the other hand, the stress path DE will match the average field stress which is half-way between A and B. This is accomplished by applying the constant confining pressure σ_3, represented by point D, calculated by matching the stress states at point F. While this confining pressure is held constant, σ_1 is increased until stress state E is reached. Stress path DE is a straight line

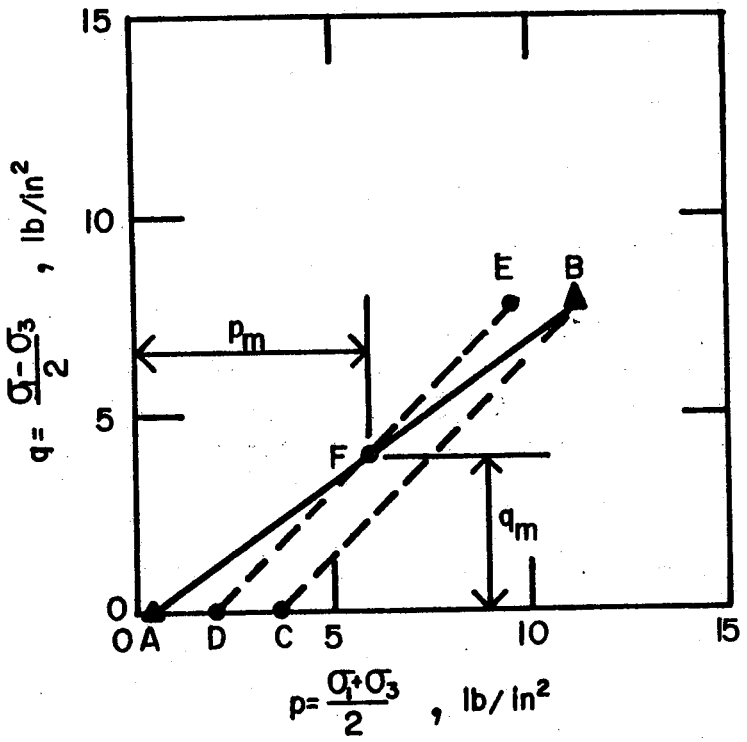

Fig. 4-13. Equivalent Stress Paths for Roadbed Materials

inclined at 45^{o} and passing through point F.

Figure 4-14 shows the equivalent triaxial stress distributions with depth for FAST section 18B for point B on stress path CB. The development of a tensile zone at the bottom of the ballast layer has created a situation that cannot be simulated in the laboratory because the confining pressure (σ_3) would have to be tensile. However, this tension zone is small compared to the larger compression zone in the ballast layer. This problem has been by-passed by using the middle of the ballast layer to represent the ballast stress path. Figure 4-15 portrays the stress paths CB and DE for points in the middle of the ballast layer, approximately underneath the load for section 18B.

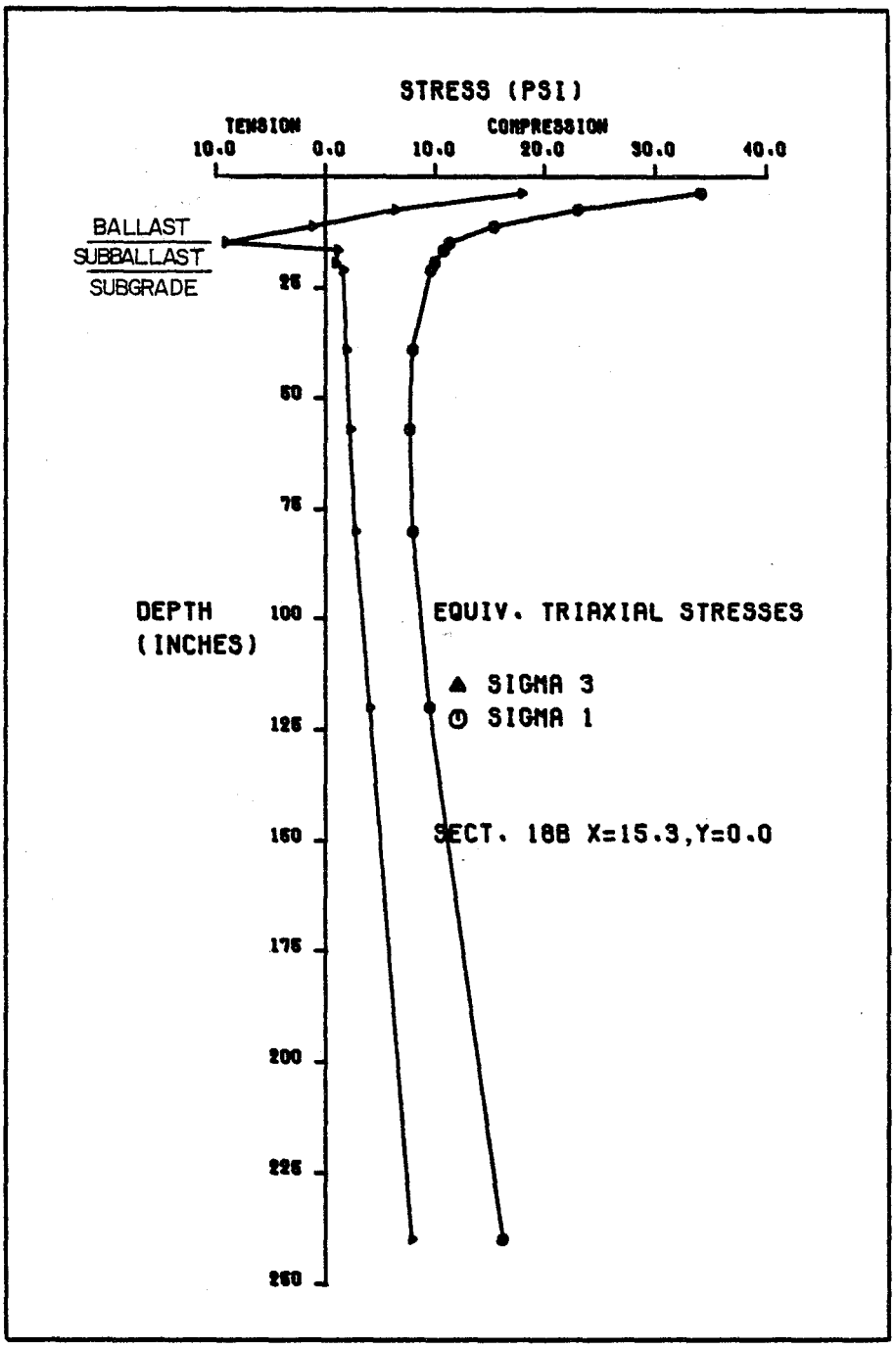

Fig. 4-14. Distribution with Depth Below Wheel Load of Triaxial Stresses for Section 18B using Equivalent Stress Path CB

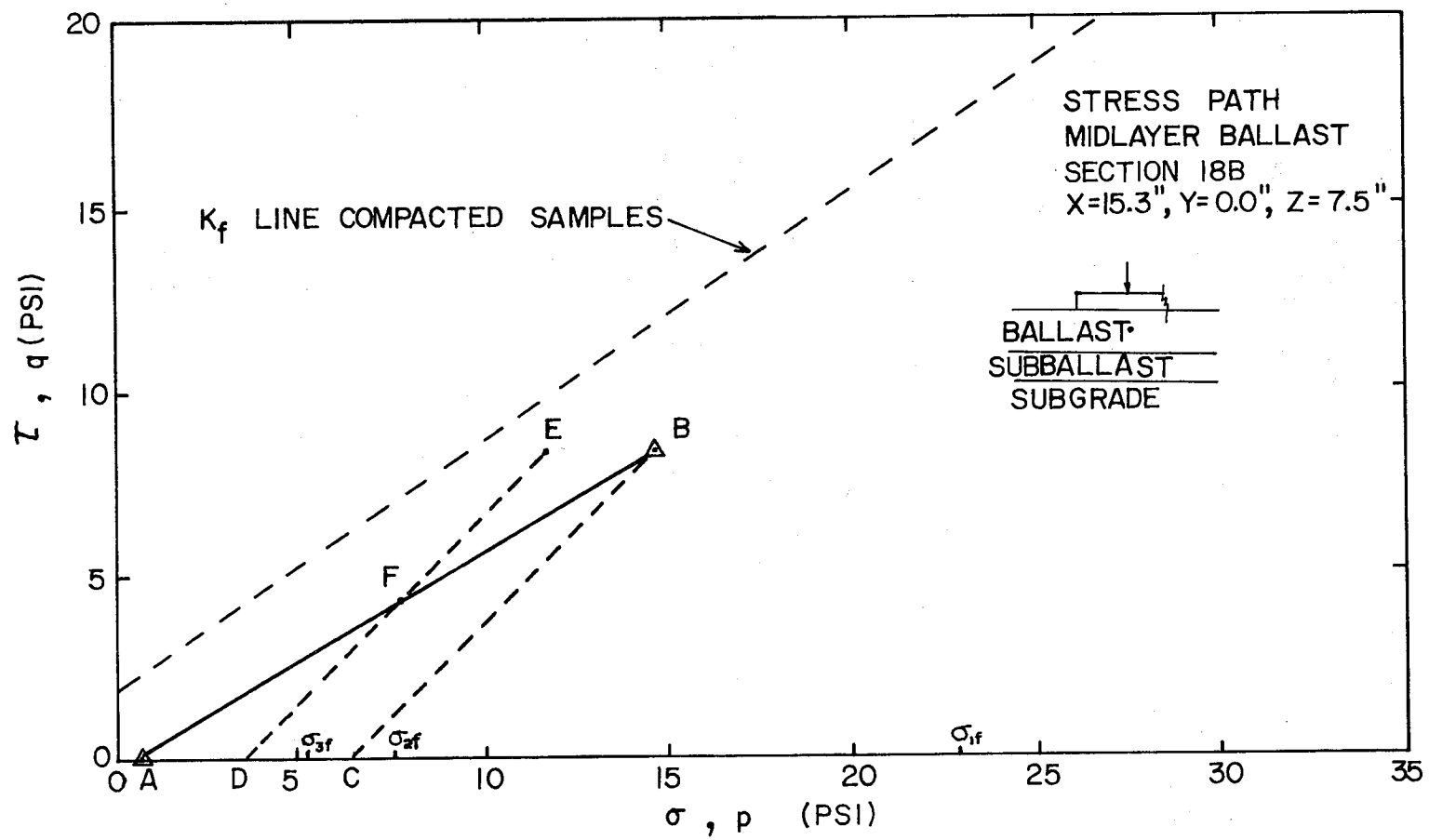

Fig. 4-15. Stress Paths for Middle of Ballast in Section 18B

CHAPTER 5. OBSERVED TRACK RESIDUAL DEFORMATION

This chapter presents the permanent strains and deformations accumulated with traffic in the granite ballast sections of the FAST track located in Pueblo, Colorado. Three sections (17E, 18A and 18B) were instrumented with this ballast to represent wooden and concrete ties, tangent tracks and ballast depths from 14 to 21 inches (Table 2-1). The data presented are restricted to vertical strains and deformations under the rail, and traffic up to 50 MGT (million gross tons). Only granite test sections are considered because the laboratory testing was limited in the second year to granite ballast samples. However, in the future the study will be extended to the limestone and traprock ballast sections of FAST.

For each FAST section, several different tie locations were instrumented. The average values are taken as representative of the entire section. Details of the entire instrumentation plan and all of the measurements are given in Ref. 6. The information is summarized in Refs. 2, 3 and 4.

5.1 Test Conditions

The instrumentation for the FAST track section in Pueblo (Fig. 5-1) includes soil strain gages installed in the ballast and subballast layers to measure vertical and/or horizontal strains, and vertical extensometers in the subgrade to measure vertical deformation of the subgrade surface relative to a reference anchor ten feet below the subgrade surface.

The ballast is a crushed granite material from Wyoming. This ballast, with particle sizes ranging from about 0.2 to 1.5 in., is finer than the AREA No. 4 gradation.

The subballast is a well-graded gravelly sand. It is designated SW in the

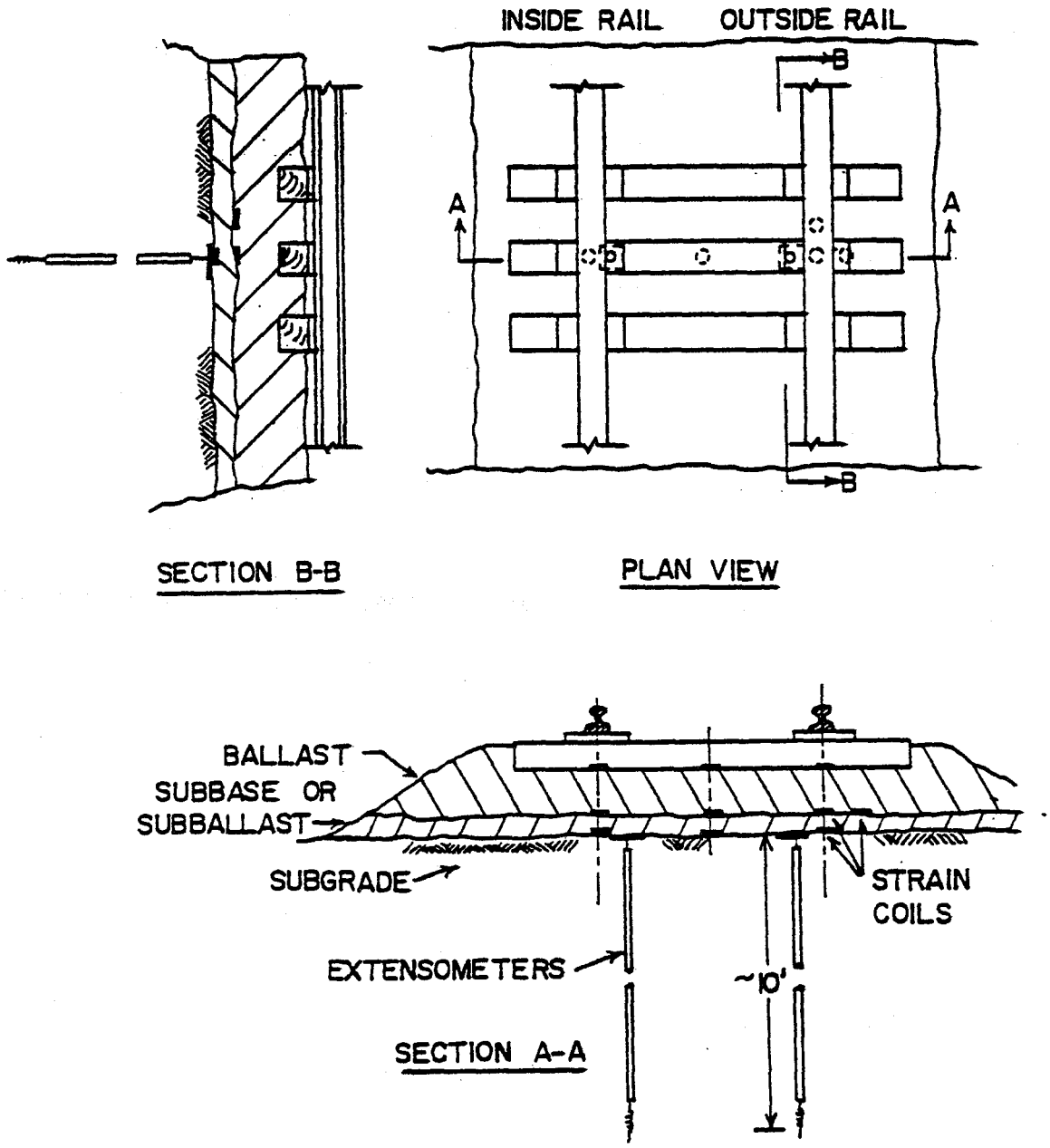

Fig. 5-1. Illustration of Strain Gage and Extensometer Layout

USCS system or A-1 in the AASHTO system. The subballast was compacted with a vibratory roller prior to track construction. Inspection records indicated that compaction exceeded 90% AASHTO T-99 at water contents of 6 to 12%. At the time of instrument installation, the moisture content ranged from 3 to 5%. Laboratory compaction tests performed on the subballast material from three different locations at FAST give maximum dry densities ranging from 115.8 pcf to 119.5 pcf.

The subgrade material is generally classified as a silty to very silty, fine to medium sand, in some areas becoming a sandy silt. The principal designation in the USCS system is SM, and in the AASHTO system is A-1 to A-4. No distinct subgrade layer boundaries were evident from the borings; however, visual observations made during drilling of the extensometer holes suggested a general tendency for increasing silt content with depth. The subgrade material also generally decreased in moisture content from 6 to 12% in the top 4 ft to 1 to 5% in the next 6 ft. The compaction specification for the construction of the first 3 ft of the subgrade was 90% of the AASHTO Test T-99, method C.

5.2 Measured Residual Deformations

The average values for vertical ballast strains were calculated by combining the inside and outside rail measurements. Measured values were disregarded only when the coefficient of variations calculated were excessively high (greater than 100%) and the field records indicated instrument malfunctioning. The mean and coefficient of variation values from the statistical analysis are presented in Ref. 3. The average coefficient of variation of strain in the ballast layer for section 17E was 17%, for section 18A was 32%, and for section 18B was 23%. The number of measured values was 4 for section 17E, 3 for section

18A and 8 for section 18B.

Figures 5-2 to 5-4 present the mean values and ranges of ballast residual strains for sections 17E, 18A and 18B, respectively, as a function of million gross tons (MGT) of traffic. The values of ballast strain under the rails follow the same general trend in all three sections, that is, the strains accumulate with traffic. The ballast strains increase more rapidly during the early stages of loading. Approximately 50% of the strain at 50 MGT is reached as early as 5 MGT of traffic. The rate of increase in strain diminishes after 5 MGT and seems to have a constant value afterwards.

The measured values of vertical strains in the ballast at the center of the tie have not been analyzed, nor the measured longitudinal or transverse strains in the ballast.

The ballast residual strains in section 17E (concrete) seem to be higher than the ones in section 18B (hardwood) for the same ballast depth of 15 in. The values presented for section 18A (21 inches of ballast) are higher than those in section 18B, but lower than those in section 17E. However, the measured ballast strain values for section 18A are for the upper middle ballast layer only, because the strain sensors did not span the entire layer thickness. Also, the tie spacing in section 17E is 24 in., compared to 19.5 in. in sections 18A and 18B. Finally, the tie stiffness for the concrete and wooden ties should also be taken into account in comparing the data in the roadbed materials.

The average values for vertical subballast strains were also calculated by combining the inside and outside rail measurements. For sections 17E and 18B, the strain values are for the whole subballast depth, but the section 18A strains are calculated using the upper subballast and the lower portion of the ballast layer.

The average coefficient of variation for subballast strains for section 17E

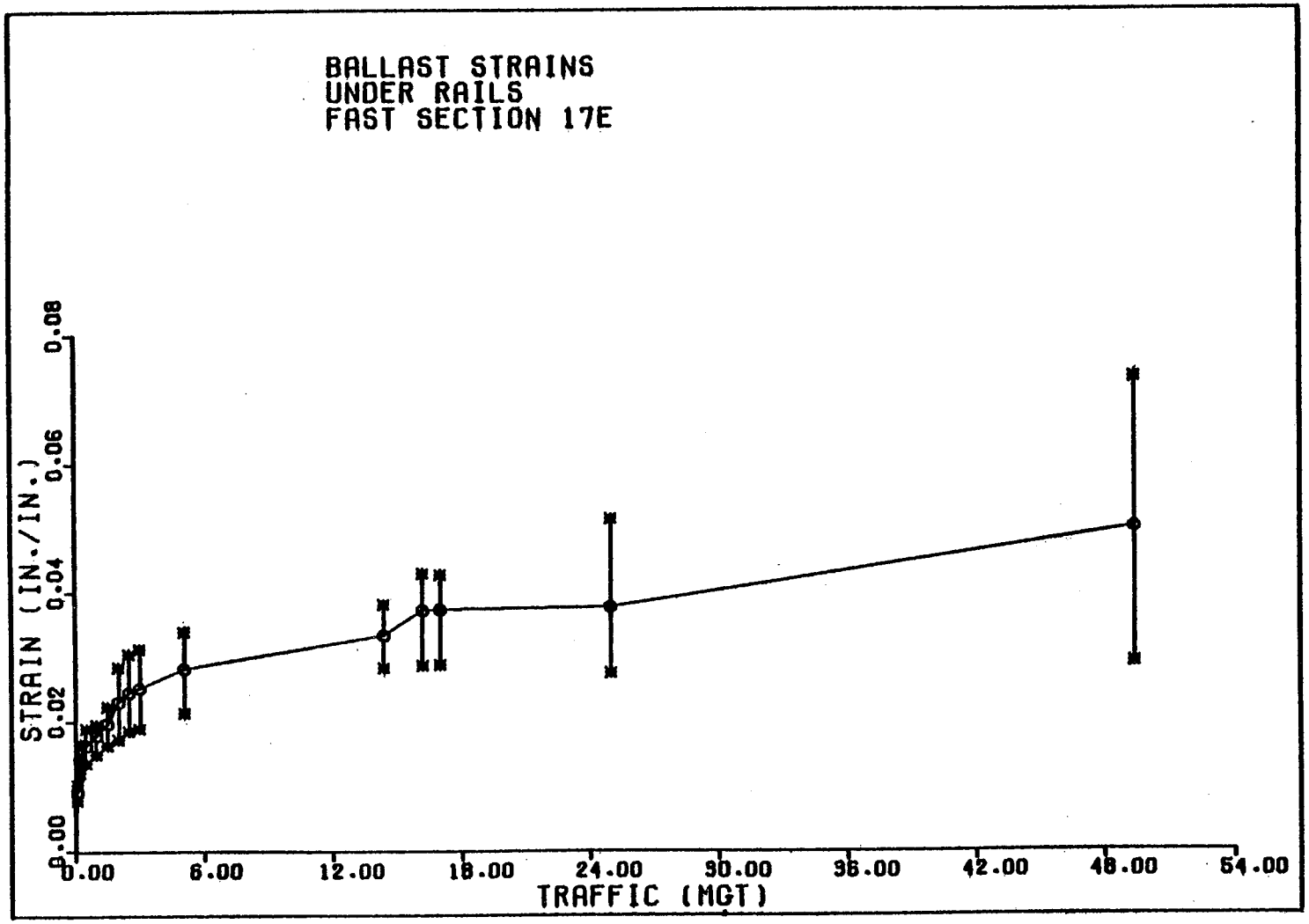

Fig. 5-2. Ballast Strains Accumulating with Traffic in FAST Section 17E

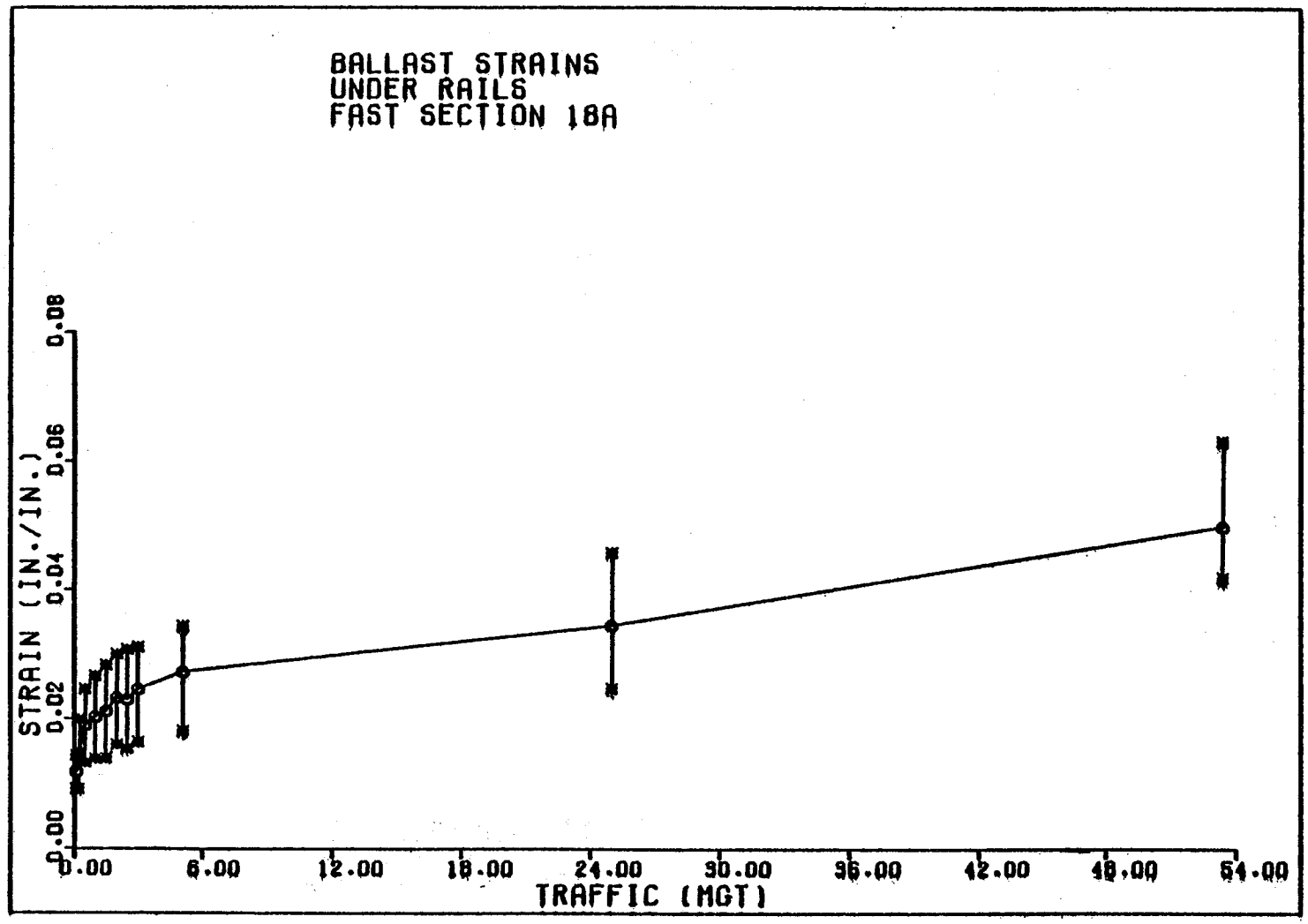

Fig. 5-3. Ballast Strains Accumulating with Traffic in FAST Section 18A

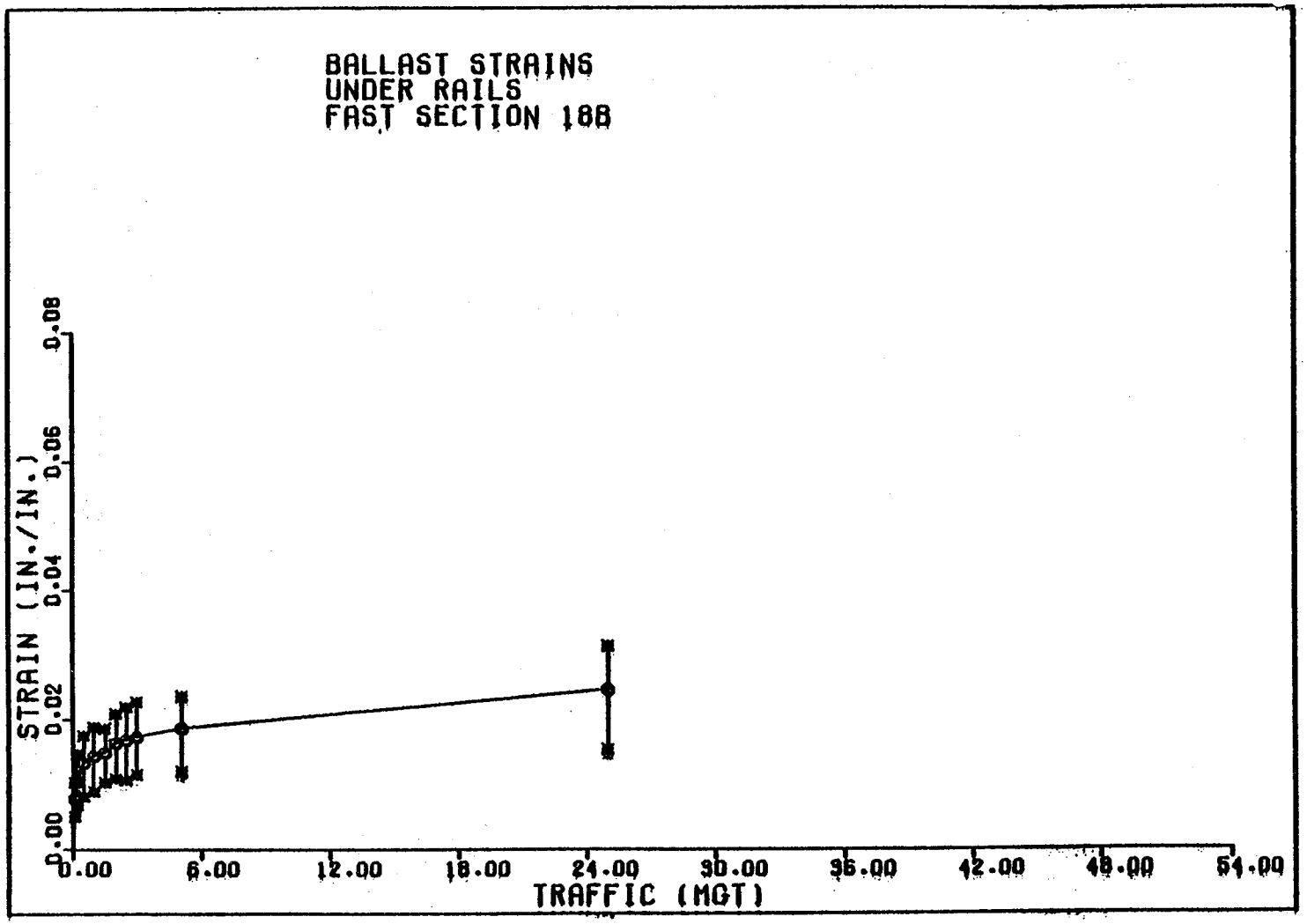

Fig. 5-4. Ballast Strains Accumulating with Traffic in FAST Section 18B

was 18%, for section 18A was 25%, and for section 18B was 34%. The number of measured values were 3 for section 17E and 18A and 4 for section 18B.

Figures 5-5 to 5-7 present mean values and ranges of subballast residual strains for sections 17E, 18A and 18B, respectively. All three sections follow the same general trend of strain accumulation with traffic. The subballast strains under the rail increase more rapidly during the initial stages of loading with 50% of the strain occurring as early as 1 MGT. For subsequent loading, the rate of increase is approximately constant, this rate being lower than in the case of ballast strains.

It should be noted that the order of magnitude for the subballast strains under the rails in the three cases is very similar. Furthermore, the slopes of the curves are also very similar. The subballast strains in section 18B are the highest, but sections 17E and 18A are of the same magnitude. Again, it should be pointed out that the values for section 18A include some ballast strain due to the location of the coil sensor in this section.

The average coefficient of variation for subgrade deformation for section 17E was 29%, for section 18A was 76.5%, and for section 18B was 29%. Four values were considered in most of the cases. The coefficient of variation is double for section 18A, probably due to instrumentation problems in section 18A.

Figures 5-8 to 5-10 present the average values and ranges of subgrade deformations with traffic for sections 17E, 18A and 18B, respectively. The trend of permanent deformation of the subgrade with traffic is different from ballast and subballast strains. The subgrade deformations continue to grow after 50 MGT, in contrast to the levelling off of the ballast and subballast strains.

The subgrade deformation in section 17E (concrete tie) with traffic seems to be higher than in section 18B (hardwood tie), even though both sections have the same ballast depth of 15 in. Section 18A (ballast depth of 21 in.) has a

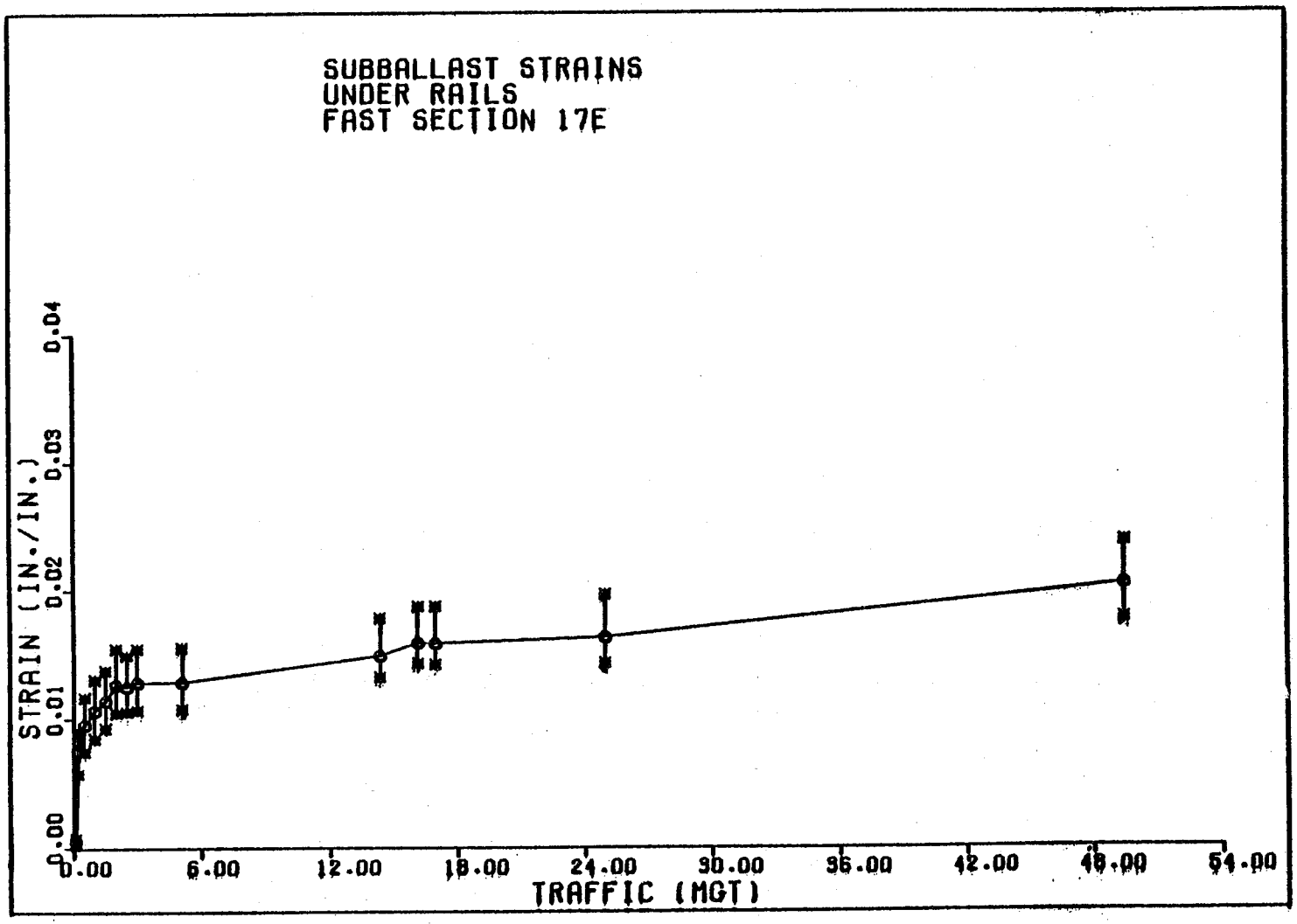

Fig. 5- 5. Subballast Strains Accumulating with Traffic in FAST Section 17E

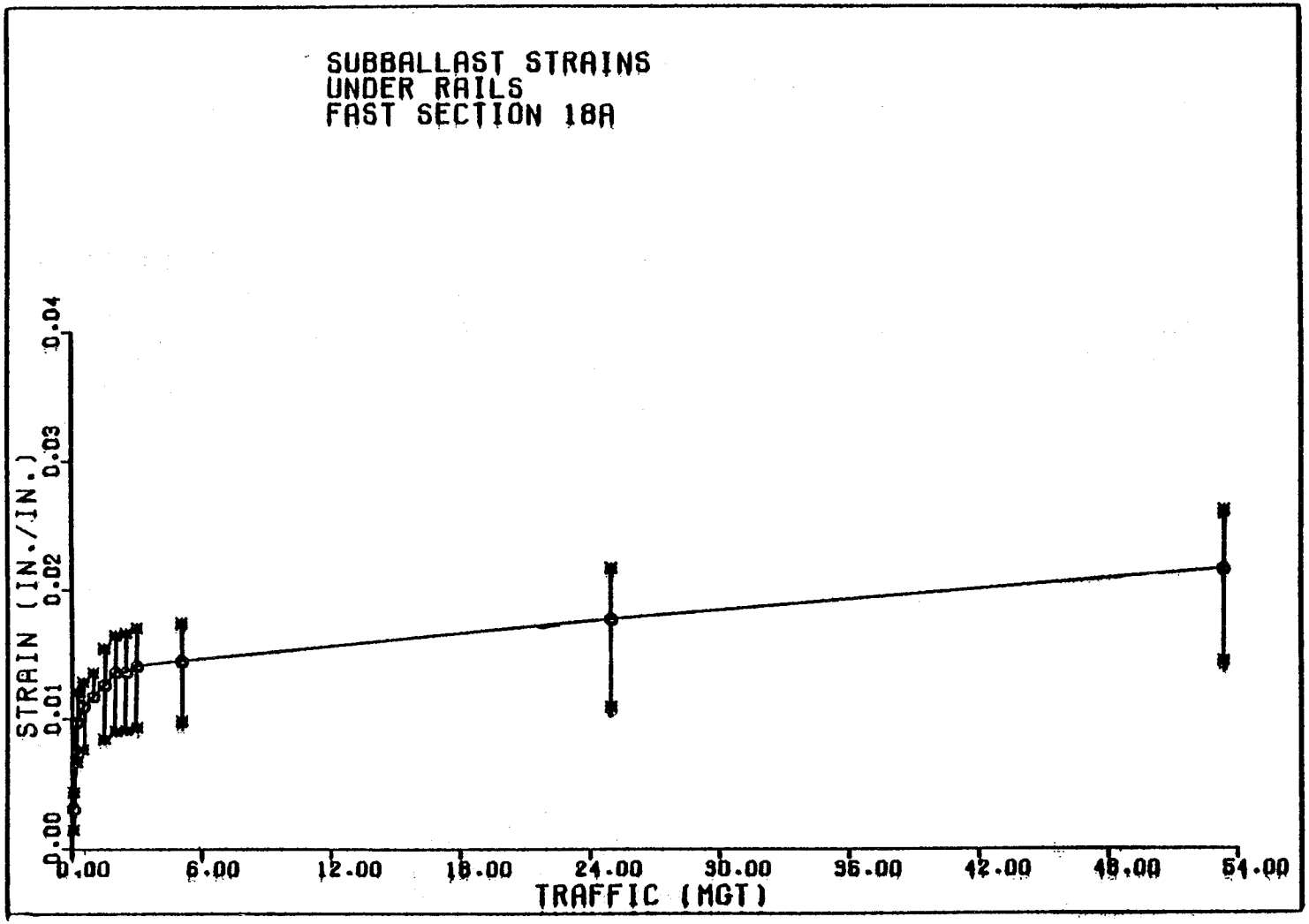

Fig. 5-6. Subballast Strains Accumulating with Traffic in FAST Section 18A

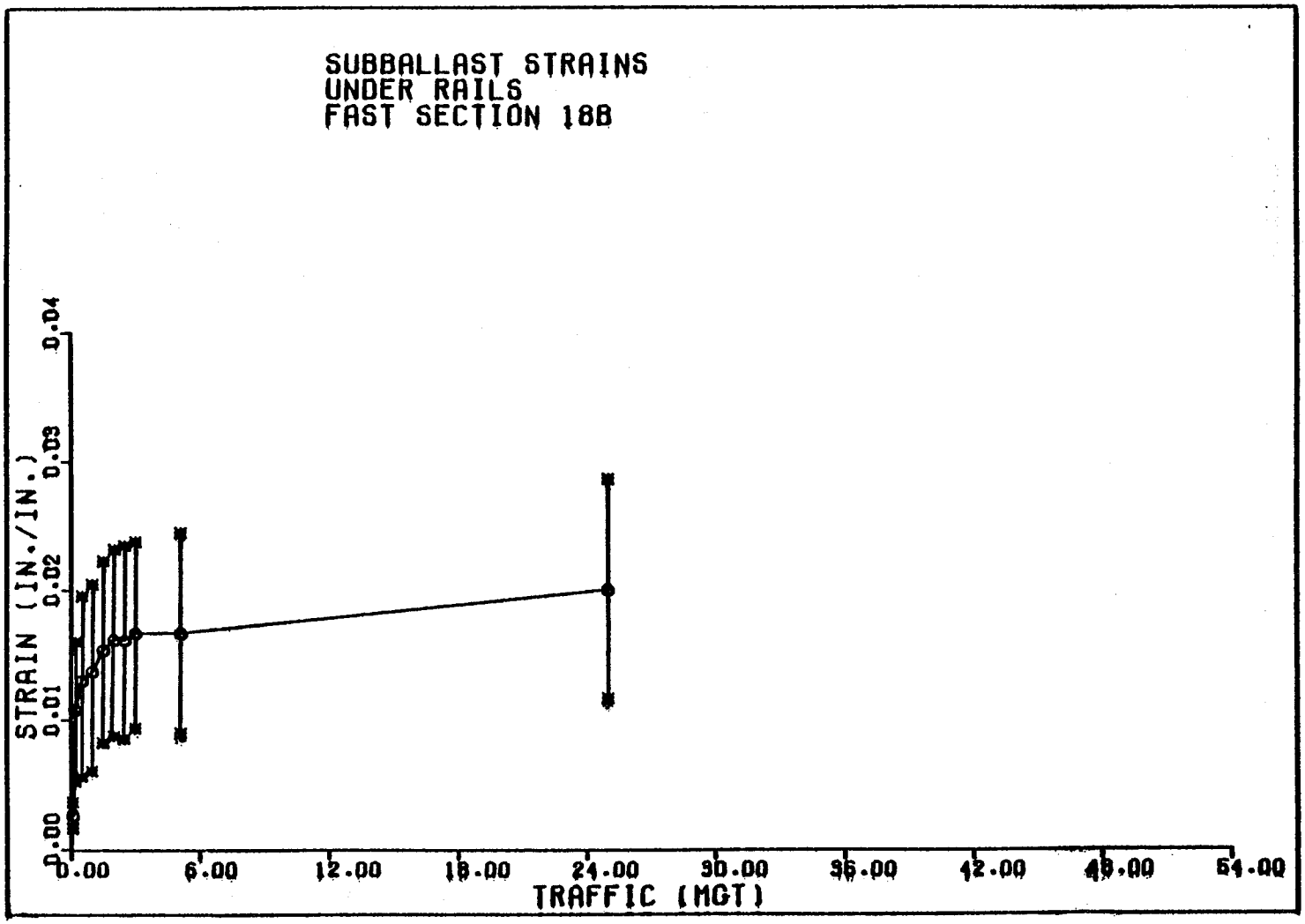

Fig. 5-7 . Subballast Strains Accumulating with Traffic in FAST Section 18B

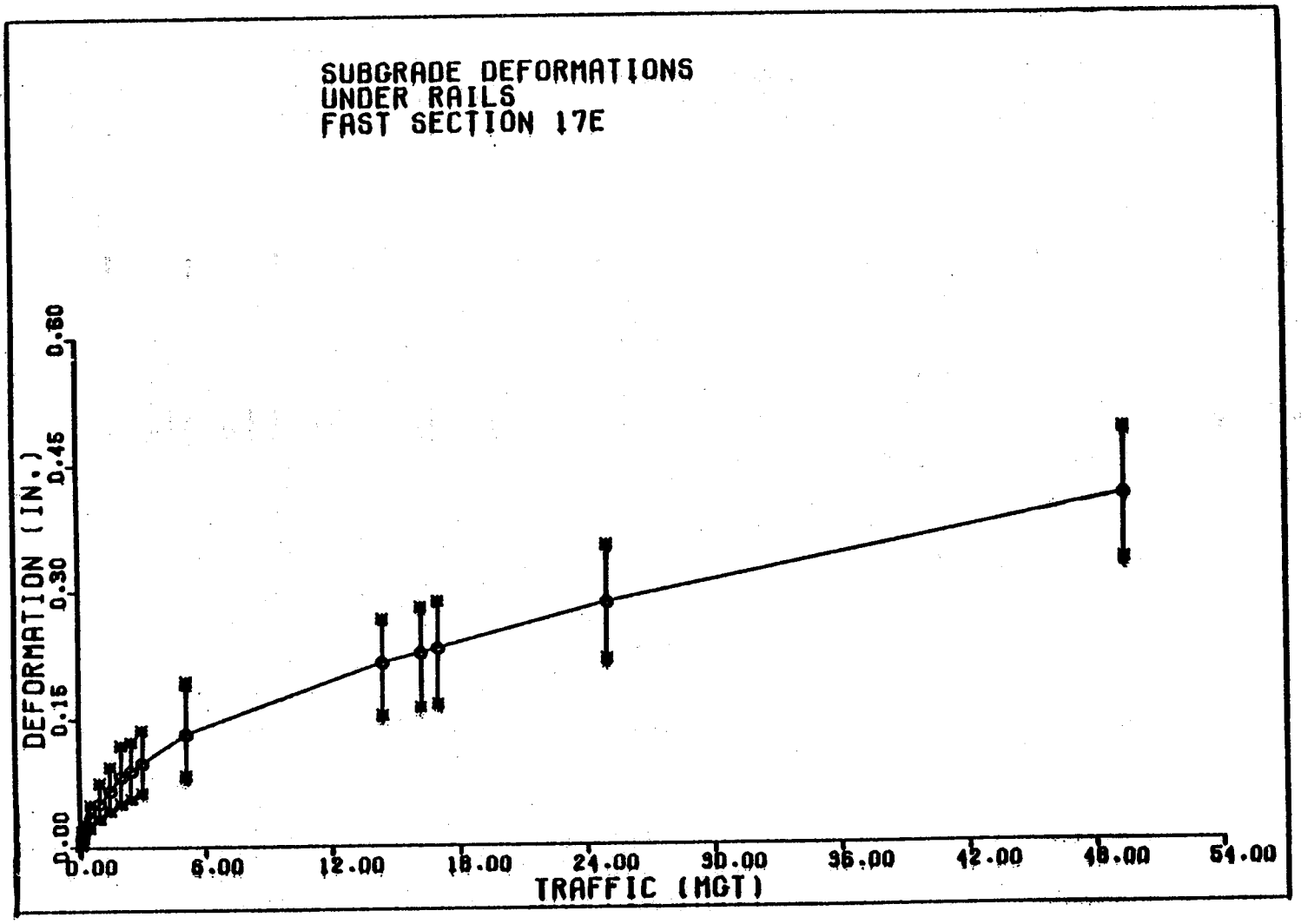

Fig. 5-8 . Subgrade Deformations Accumulating with Traffic in FAST Section 17E

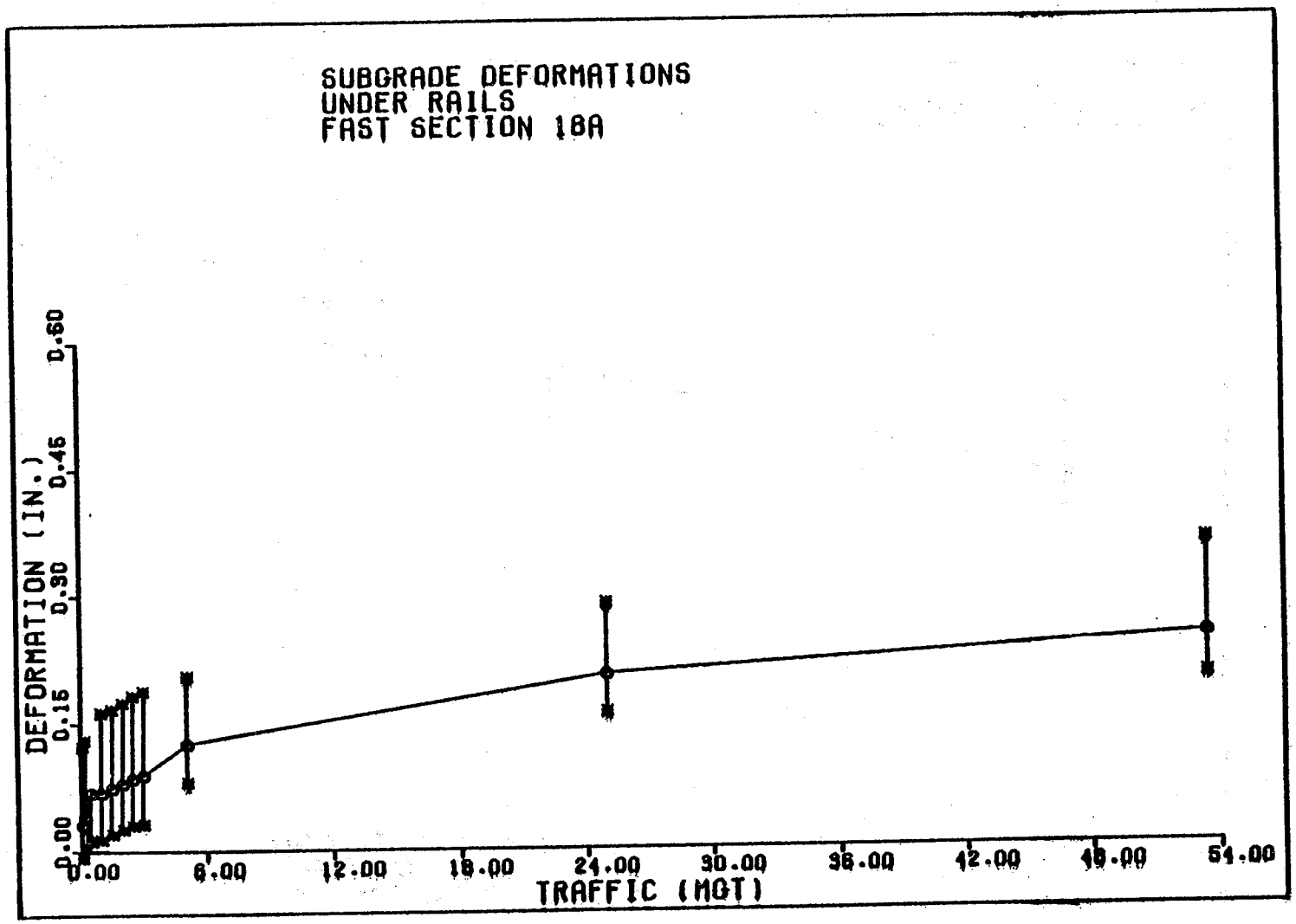

Fig. 5-9. Subgrade Deformations Accumulating with Traffic in FAST Section 18A

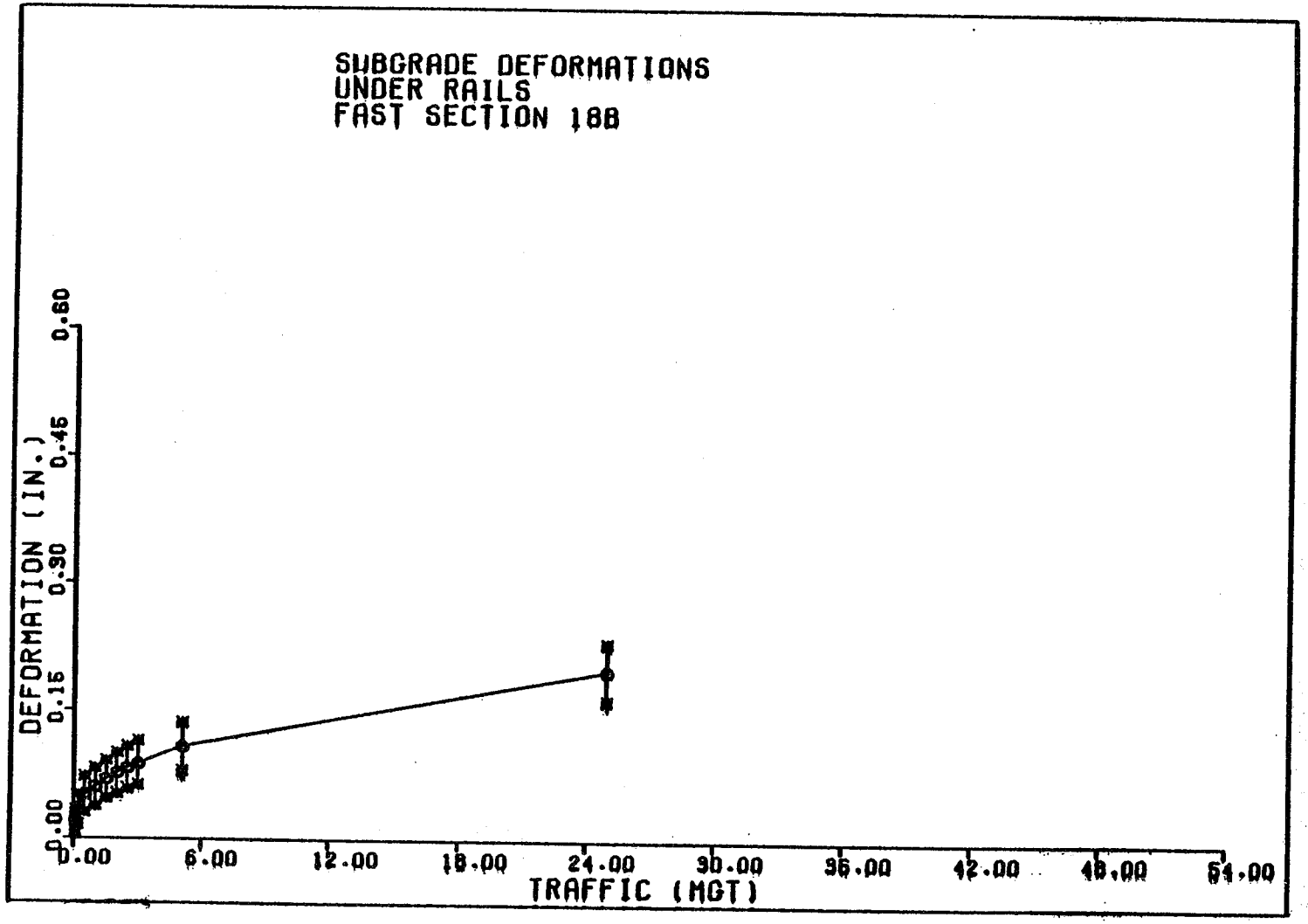

Fig. 5-10. Subgrade Deformations Accumulating with Traffic in FAST Section 18B

higher variation, but the mean values are similar to those in section 18B. Again, section 17E has a greater tie spacing and a greater tie stiffness because this is the concrete tie section.

CHAPTER 6. LABORATORY TRIAXIAL TESTS

Following a brief description of the apparatus and procedures developed for the laboratory triaxial tests, this chapter presents the results of the static and cyclic testing conducted on the FAST granite ballast. Further information on the laboratory equipment can be found in Refs. 1 and 3. A detailed presentation of the testing conditions and results is presented in Ref. 3.

6.1 Apparatus and Procedures

6.1.1 Apparatus

The triaxial cell, pressure controls and volume change device used for both the static and the cyclic tests have been described in Ref. 1. A diagram of the cell is shown in Fig. 6-1.

Loading in the static triaxial tests was accomplished with a 12,000-lb compression machine at a strain rate of 0.05 in./min. The compression machine used is capable of providing various constant rates of strain. The loads were measured by the load cell built into the testing machine.

The vertical deformation readings were taken with a 0.001-in.-sensitivity dial indicator mounted externally to the cell and fixed to the loading piston. The volume change was determined during the test, and pore pressures were monitored to make sure that excess pore pressure did not develop.

Two different closed-loop, servo-controlled testing systems were employed for the cyclic testing. The first series of cyclic tests was performed with a $\pm$ 22 kip force capacity hydraulic actuator with a maximum stroke of 6 in. The servocontroller furnished a haversine time-dependent force. This system has been documented in Ref. 1.

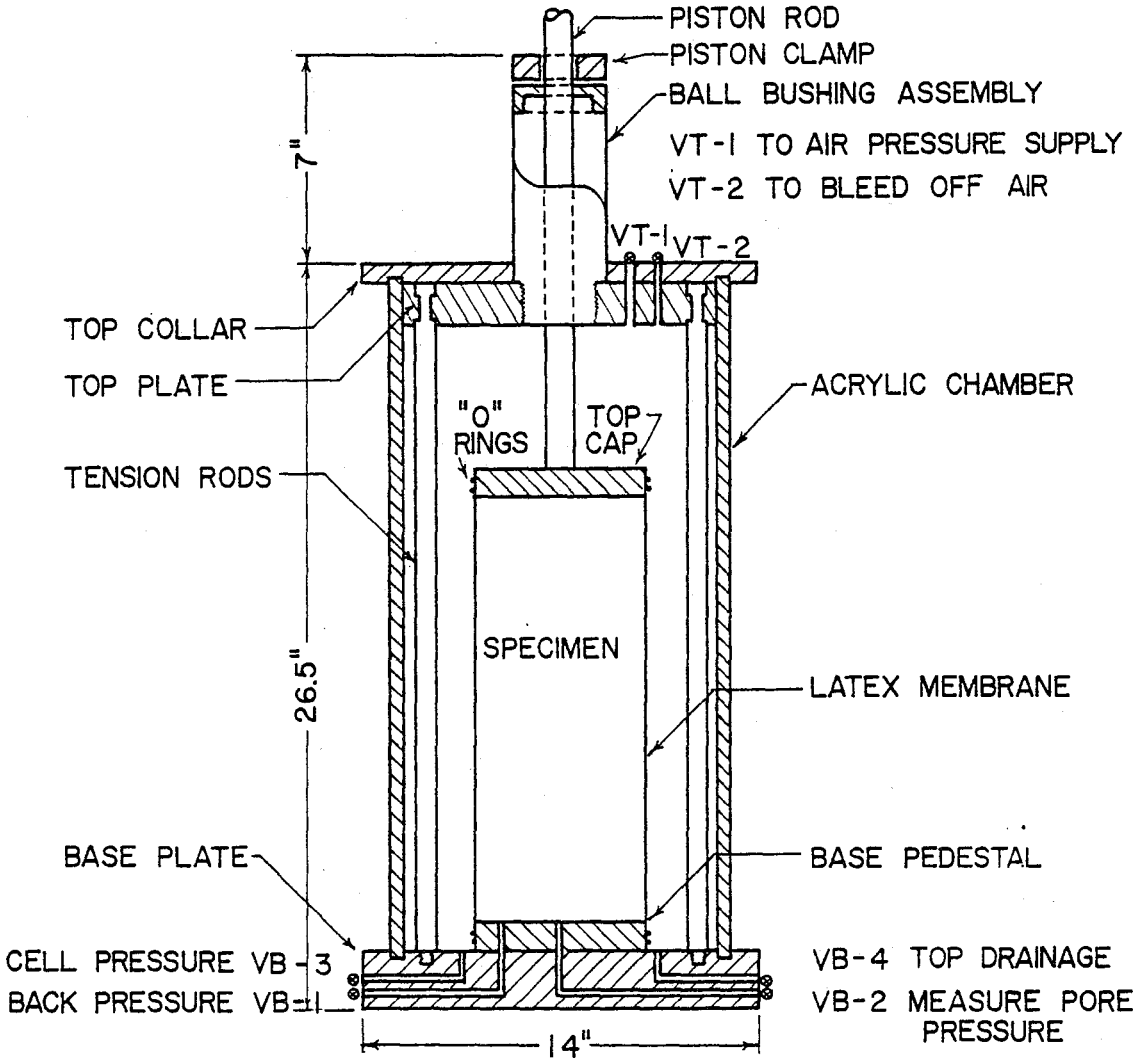

Fig. 6-1. Illustration of Cyclic Triaxial Cell Features

The second series of cyclic tests was performed with a system (Fig. 6-2) having a ± 11 kip force capacity hydraulic actuator with a maximum stroke of 6 in. The load cell, LVDT, servo-controller and hydraulic power supply were similar to those incorporated in the first system. This servo-controller did not have the haversine control function, so a sinusoidal time-dependent force was applied to the samples, together with a static offset equal to half of the peak-to-peak sinusoidal amplitude. The maximum cyclic load was determined from the settings of the calibrated dials on the control panel. The minimum load was always zero.

The sample deformation in the cyclic tests has two components: one which is irrecoverable or permanent, and the other of much smaller magnitude, which is recoverable. These were measured by the same dial gage device used in the static tests. The actuator LVDT is not an accurate indicator of sample deformation because the deformation in the loading frame introduces excessive measurement error. The dial indicator was retracted most of the time during the test to avoid mechanical wear from the large number of load cycles. To obtain readings, the dial indicator was extended again without moving the reference position. With the cycling frequency at 1 Hz, the maximum and minimum displacement readings could be taken manually during oscillation. From these, the elastic and cumulative permanent deformations could be obtained for the existing number of cycles.

6.1.2 Density Determination

It was found that the sample boundary condition for ballast materials plays a crucial role in determining the accuracy of the calculated sample density (Ref. 1). The problem is caused by the difficulty in defining the volume of the large surface voids that should be excluded from the sample volume. Still

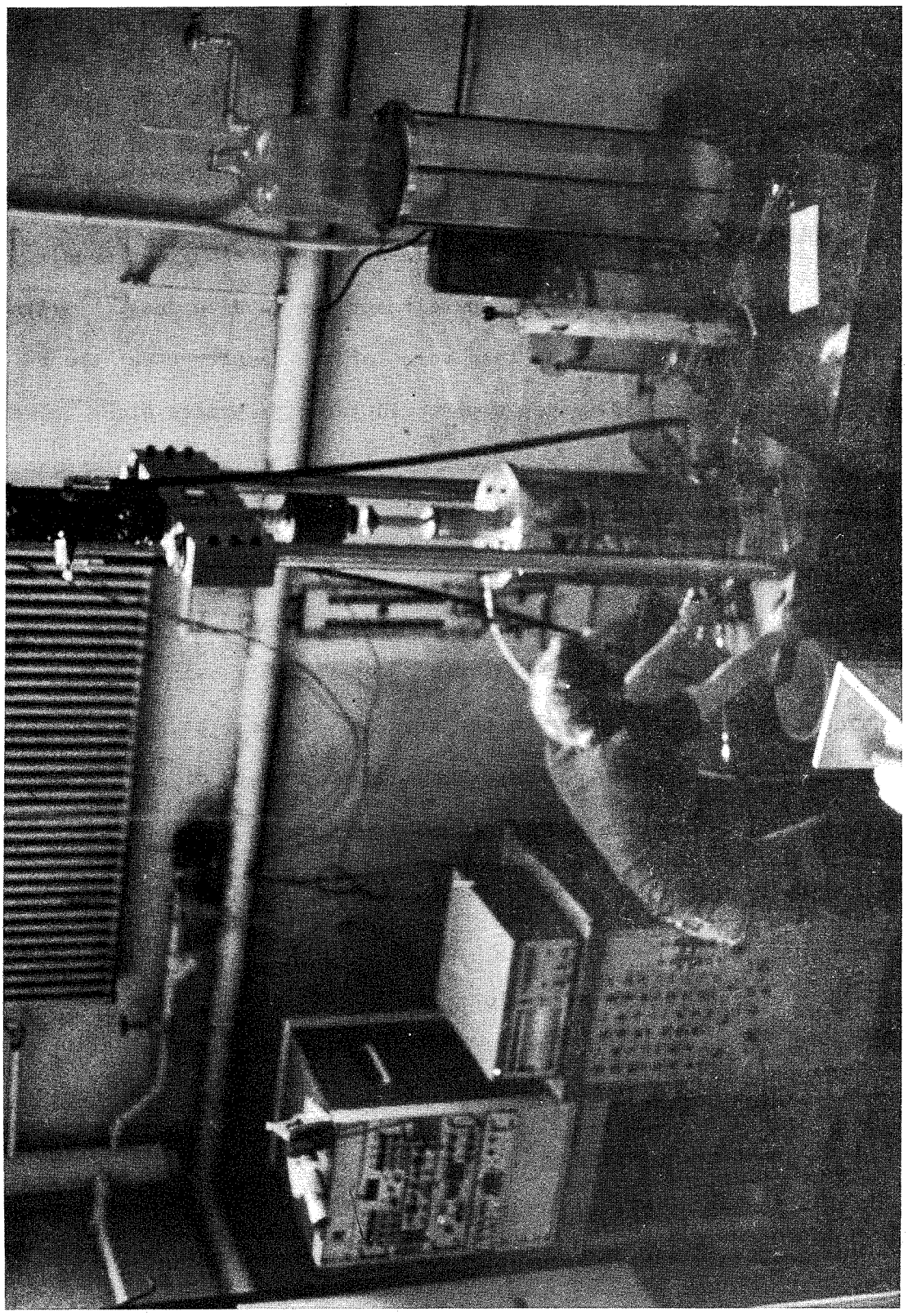

further research is necessary to establish the density correction between the laboratory and the field measurements. Therefore, rather than match the field density values, laboratory sample preparation techniques were devised to represent the observed range from uncompacted to compacted ballast density conditions in the field.

A study of the variation of the in-situ granite ballast density (Ref. 3) showed that under the tie the mean value of the in-situ density at the tie center is 95 lb/cu ft and the mean value of the density under the rail is 105 lb/cu ft. Thus a difference up to 10 lb/cu ft exists along the tie in the ballast. For the crib area, density is more uniform with a mean value of approximately 100 lb/cu ft.

To prepare the laboratory samples, the impact-type hammer compaction method was chosen, which is the same as the method presented in Ref. 1. To establish the amount of compaction, samples were prepared in a 6-in. diameter by 12-in. high container (similar size to the triaxial samples) in three equal layers with the number of blows per layer changed to produce different compactive efforts. The compactive effort is calculated from

$$E = \frac{n\, W_r\, D\, N}{V_c} \quad ,$$

where E = compactive effort in lb-ft/ft^3,

W_r = drop weight = 7.8 lb,

D = drop height = 17 in.,

n = number of layers = 3,

N = number of blows per layer, and

V_c = ballast sample volume in the container.

Figure 6-3 presents the resulting relationships of dry density to

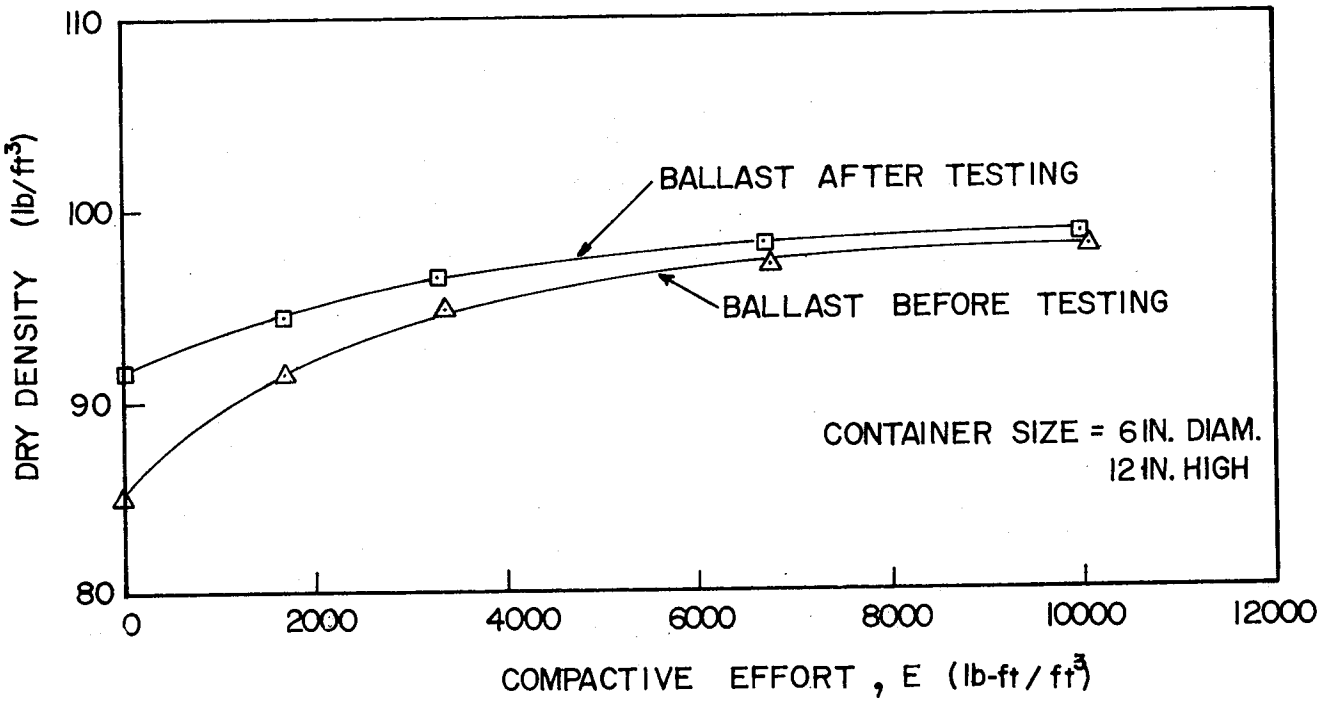

Fig. 6-3. Laboratory Density Test Results for Granite Ballast Samples

compactive effort for two different granite ballast conditions. The ballast before testing is the one that came directly from the quarry without previous usage. The ballast after testing is the same ballast after the completion of the cyclic triaxial tests. The ballast after testing shows a higher unit weight for the same compactive effort, the difference increasing with decreasing compactive effort. According to gradation tests, this difference may have occurred because the ballast after testing had finer particles, apparently from ballast breakdown during the cyclic testing. In general, the laboratory density tests showed good density reproducibility.

In order to represent the observed range of in-situ ballast density states, a lower bound density state was established by preparing laboratory samples without compaction, simulating the uncompacted or loose condition measured in the field. The upper bound density state was established as that produced by a compactive effort of 3378 lb-ft/ft^3 (20 blows per layer, 3 layers), which is the effort in Fig. 6-3 at which the curves start to level off. These two density states will be termed uncompacted and compacted states.

6.1.3 Sample Preparation

The triaxial test samples were 6 in. in diameter. The height was approximately 15 in. in order to minimize the end effects on deformation measurements.

The specimens were prepared in a special split mold that is clamped together and held on the base pedestal. A 0.025-in.-thick latex membrane was stretched inside the mold and fixed at the bottom to the cell base pedestal with o-rings. The mold has two holes in the wall so that a vacuum could be applied to hold the membrane against the mold, thus allowing preparation of a good cylindrical specimen. For the compacted specimens, almost without exception the original membrane was punctured during compaction by the sharp edges of the ballast particles. Therefore it was necessary to roll down a second

latex membrane, 0.012 in. thick, over the original membrane once the mold was removed.

Before connecting the top cap and piston assembly to the sample, the ballast particles were rearranged at the top of the mold to provide a good seat for the piston top cap. The inner membrane was next fixed to the top cap with o-rings and the top drainage was connected to the cell base plate. Then a partial vacuum of about 5 in. of mercury (approximately 2 psi) was applied to the specimen to produce a confining pressure which gives some strength to the specimen. Next, the compaction mold was taken off and the second membrane was rolled down. Additional o-rings were put at top and bottom. The two front rods were put back in place and initial specimen height and diameter measurements were taken. The acrylic chamber of the triaxial cell was then put in place and the cell was sealed by screwing down the top collar plate.

The triaxial cell was then moved to its test position in the loading frame. After the cell was filled with water and a small confining pressure applied (less than 3 psi), the vacuum in the sample was released allowing water from the back pressure reservoir to enter and eventually saturate the sample. Using the bottom and top drainages, the water was flushed out in order to eliminate trapped air bubbles. Once enough water was circulated, cell pressure and back pressures were simultaneously applied in order not to impose any effective confining stresses greater than approximately 3 psi.

With the sample saturated, several attempts were made to obtain high values of the B pore pressure coefficient, defined as $B = \Delta u/\Delta\sigma_1$ with σ_3 = constant. It was necessary, in the majority of the tests, to apply a back pressure of 20 psi to get B values greater than 0.92. Once the B value was achieved, the effective consolidation stress was applied to the sample and

the drainage valve was opened so dissipation of the excess pore pressure could occur.

6.2 Static Test Results

Eleven static triaxial compression tests with constant confining pressures (5 to 20 psi) were performed on the granite ballast. All the static triaxial tests were isotropically-consolidated, drained tests, in which the samples were saturated. Back pressures were applied to the samples to obtain a high percent of saturation so that volume change measurements could be made. Both uncompacted and compacted sample states were included.

Parameters for the Mohr-Coulomb failure criteria were determined for the uncompacted and compacted samples. Hyperbolic fitting curves were developed for the stress-strain and volume change behavior. The influence of the ballast density state on the failure parameters and on the stress-strain and volume change behavior is presented.

6.2.1 Stress-Strain and Strength

The average dry unit weight of the six uncompacted specimens was 95.6 pcf with a coefficient of variation of 2.0% and a range from 93.3 to 98.4 pcf. The average dry unit weight of the five compacted samples was 101.2 pcf with a coefficient of variation of 0.6% and a range from 100.6 to 101.9 pcf. The fact that the coefficient of variation for the two density states is low demonstrates that the preparation techniques used give reproducible results. Assuming a specific gravity of 2.67 (Ref. 24), the average initial void ratio (e_o) for the compacted samples was 0.65 and for the uncompacted samples was 0.74. No correction for boundary void conditions was undertaken.

The angle of internal friction ($\bar{\phi}$) was calculated for each sample assuming that the value of cohesion ($\bar{c}$) was equal to zero. When the confining pressure

was increased, the $\overline{\phi}$ value decreased for both compacted and uncompacted samples (Fig. 6-4). The $\overline{\phi}$ value was always higher for compacted samples than for uncompacted samples at the corresponding confining pressures, the difference increasing with an increase in the confining pressure. Duplicate tests show that this strength parameter is very reproducible in these drained static tests.

The p-q stress paths were plotted for the uncompacted specimens in Fig. 6-5 and for the compacted specimens in Fig. 6-6. These stress paths enable the K_f-line to be determined. Using the relationship $\sin \overline{\phi} = \tan \overline{\alpha}$, the $\overline{\phi}$ value was determined for both types of specimens. The $\overline{\phi}$ value for the compacted samples is 44.4 deg and for the uncompacted samples is 37.8 deg.

From the construction of the K_f-line, it can be seen that an apparent cohesion (intercept) exists for both types of samples because in both cases, the q-intercept ($\overline{a}$) is not equal to zero. The apparent cohesion value for the uncompacted samples ($\overline{c} = \overline{a}/\cos \overline{\phi}$) is 4.8 psi and the value for the compacted samples is 2.8 psi. It is believed that this apparent cohesion is due to particle interlocking. This hypothesis has also been presented by Raymond and Davies (Ref. 55).

The stress-strain and volume change relationships are presented in Fig. 6-7 for the uncompacted samples and in Fig. 6-8 for the compacted samples. The stress-strain plots in the upper part of Figs. 6-7 and 6-8 show that the static tests of the uncompacted and compacted specimens follow the expected trends, i.e., as confining pressure is increased, so does the deviator stress at failure. Also, the deviator stress at failure is greater for the compacted samples than for the uncompacted samples.

The volumetric strain plots in the bottom part of Figs. 6-7 and 6-8 show that this material follows the well-established behavior trends for granular

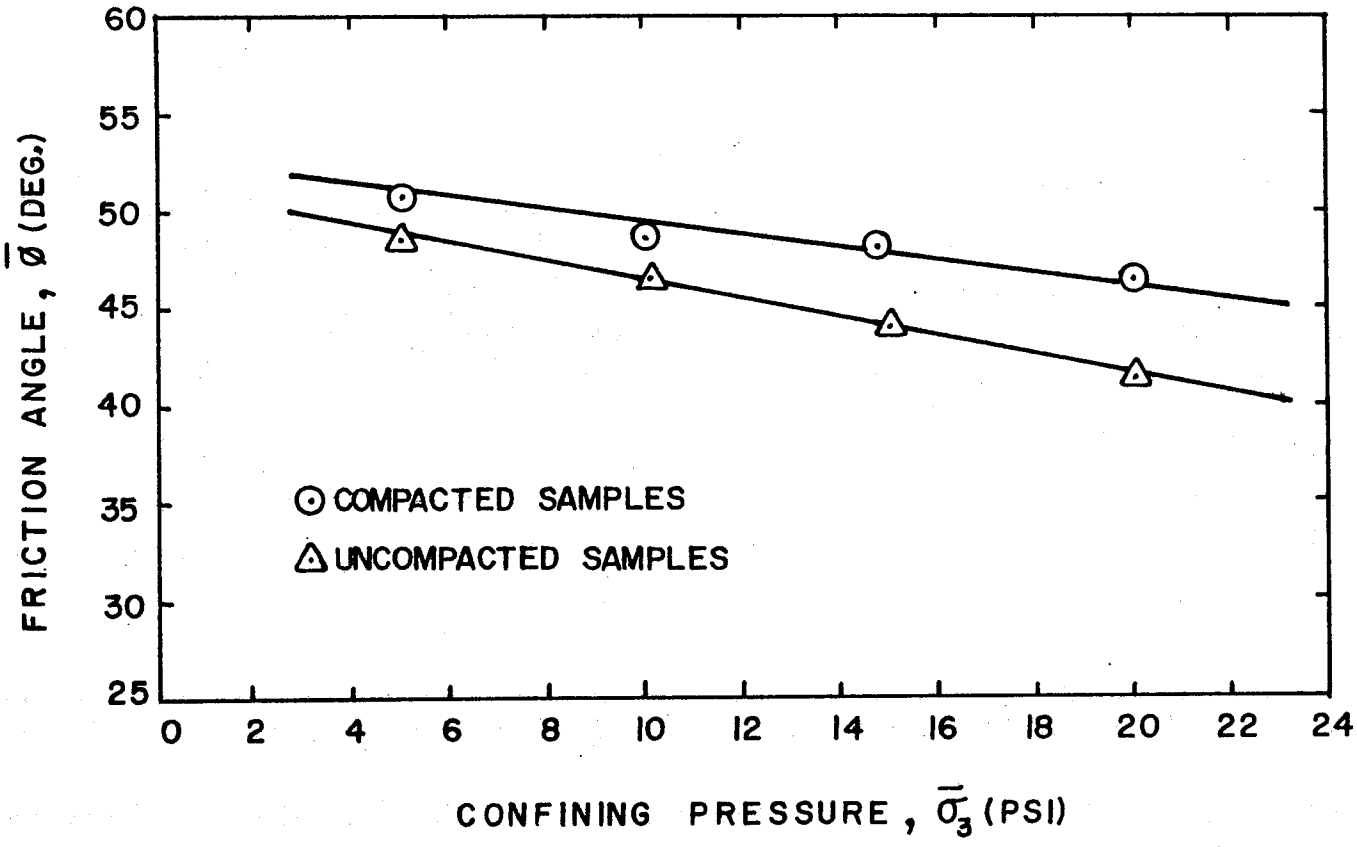

Fig. 6-4. Variation of Angle of Internal Friction with Confining Pressure for Granite Ballast Samples

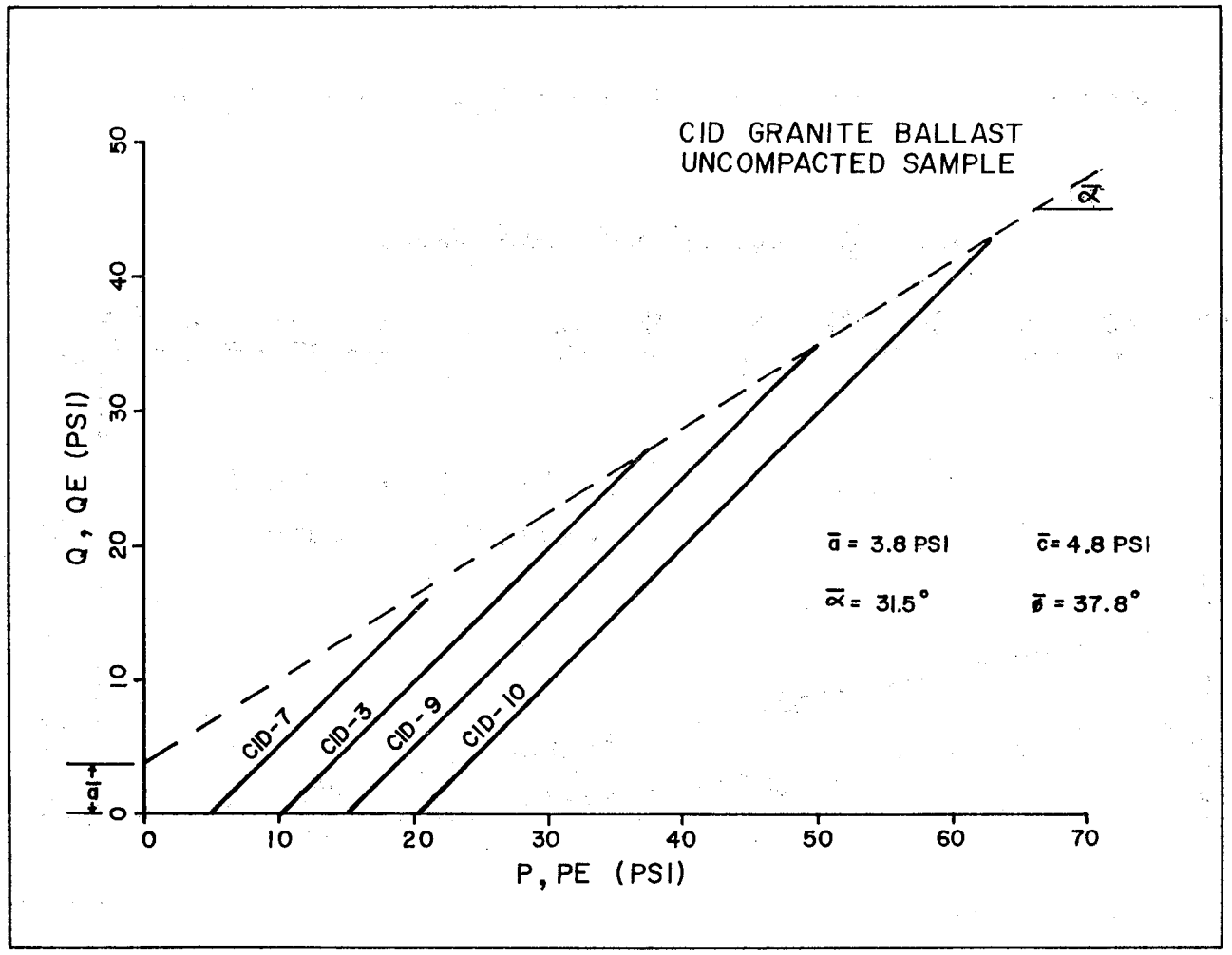

Fig. 6-5. Strength Envelopes for Uncompacted Ballast Samples

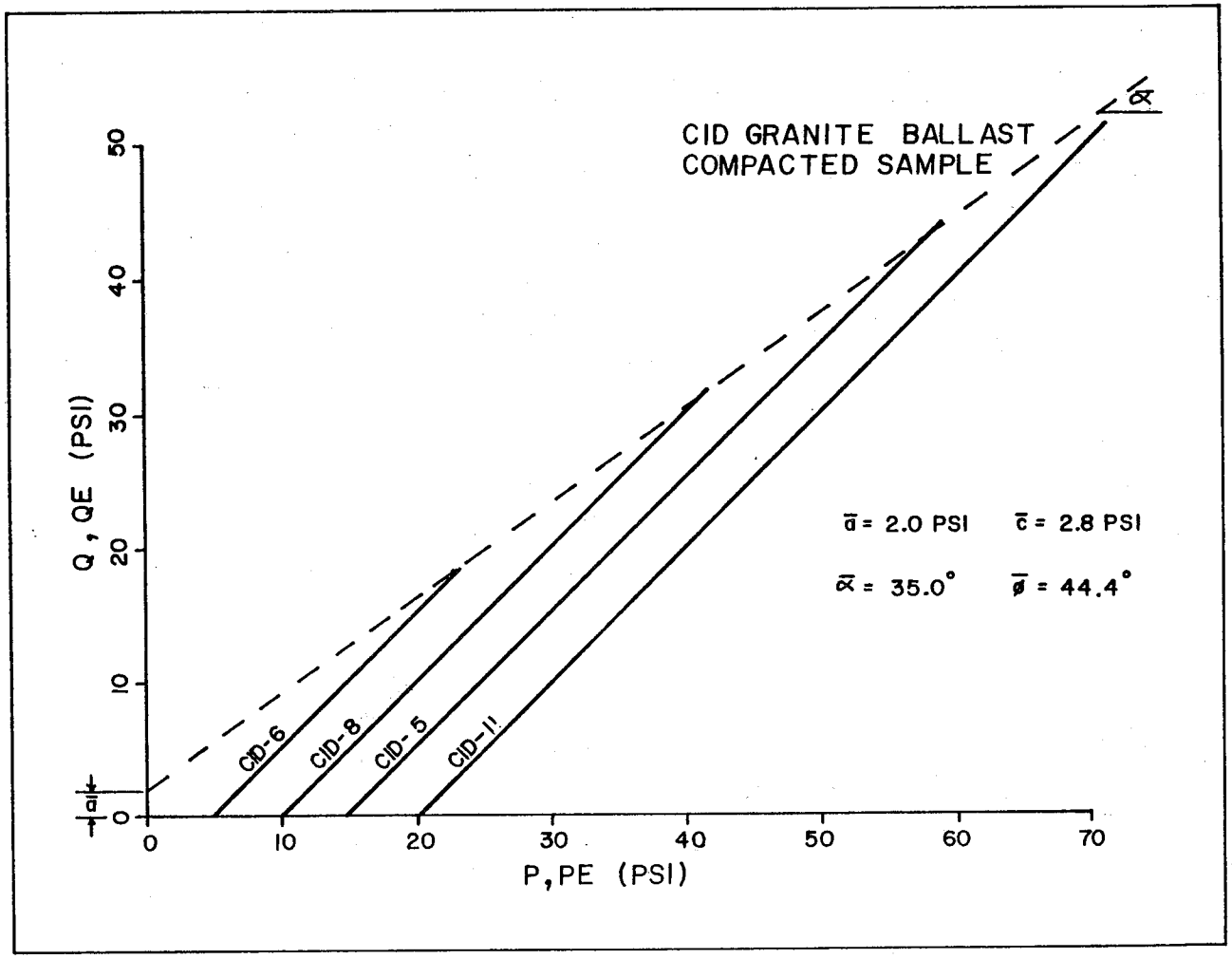

Fig. 6-6. Strength Envelopes for Compacted Ballast Samples

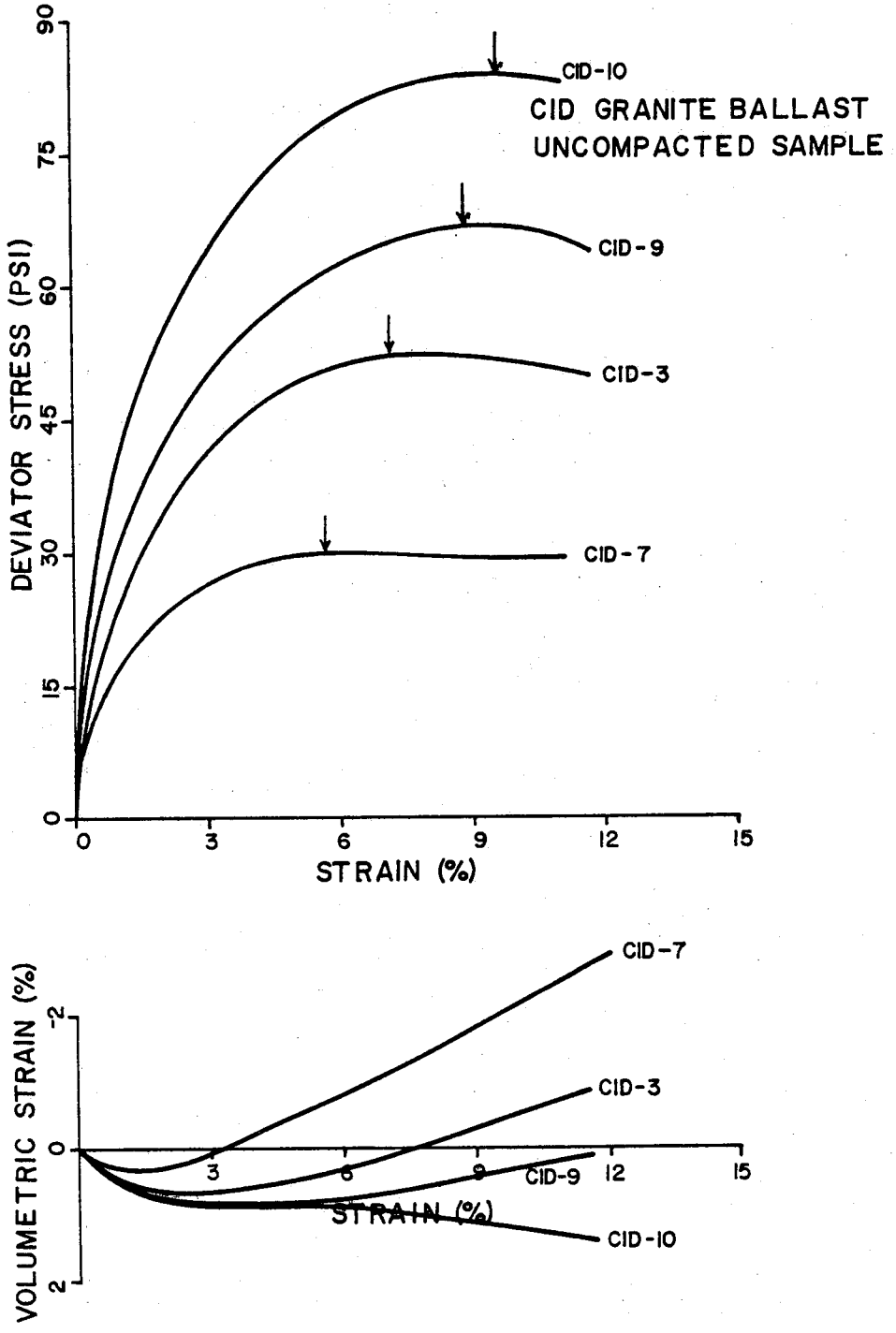

Fig. 6-7. Stress-Volume Change Behavior for Uncompacted Ballast Samples

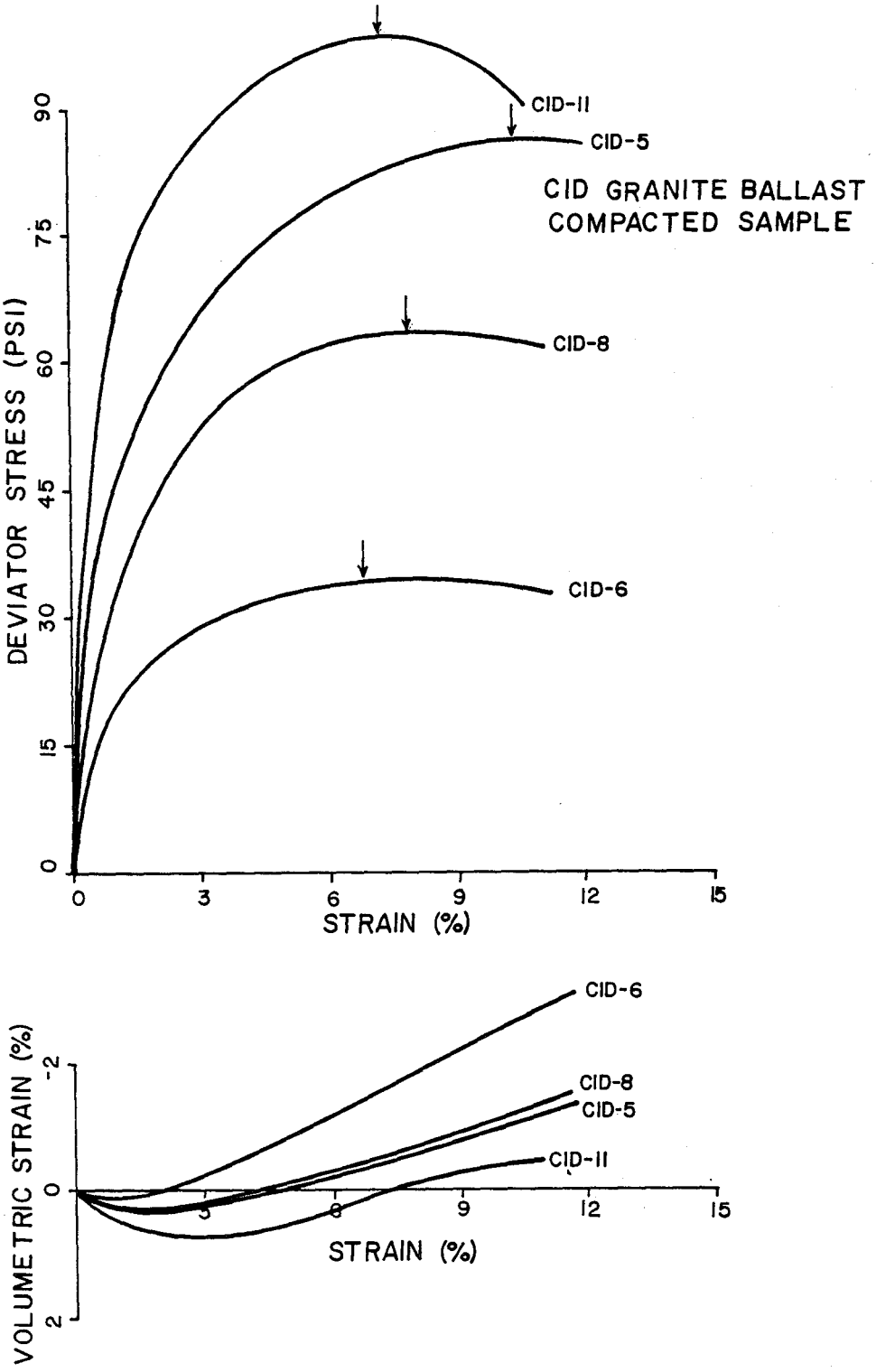

Fig. 6-8. Stress-Volume Change Behavior for Compacted Ballast Samples

material. As the confining pressure is increased, the amount of resulting dilation decreases. The compacted samples tend to dilate at much smaller vertical strains than do uncompacted samples at corresponding confining pressures. These facts indicate that the behavior of granular materials under low confining pressures, as in the case of railway ballast, is very different from that under high confining pressures.

The values of vertical strain at failure are plotted for both the compacted and uncompacted samples as a function of confining pressure in Fig. 6-9. The results of these tests follow the trends which one would expect. As the confining pressure is increased, the vertical strain at which the sample fails also increases. The compacted samples have greater vertical strains at failure than do uncompacted samples at confining pressures lower than 15 psi. Thereafter, the trend seems to be reversed, and is in accordance with the behavior of granular materials under moderate to high confining pressures. The relationships for both types of samples, i.e., compacted and uncompacted, are non-linear. It is important to point out that near failure, particle slippage was noticed making the determination of the axial strain at failure difficult.

Figure 6-10 shows the relationship between deviator stress and confining pressure for the uncompacted and compacted samples. As the confining pressure is increased, so does the amount of deviator stress required for failure. The relationship is linear for the compacted samples which, obviously, require a greater deviator stress for failure than do the uncompacted samples. The difference in deviator stress at failure between compacted and uncompacted samples increases with increasing confining pressure. This fact was also pointed out by Raymond and Davies (Ref. 55).

Volumetric strain is considered to be positive when the total volume is

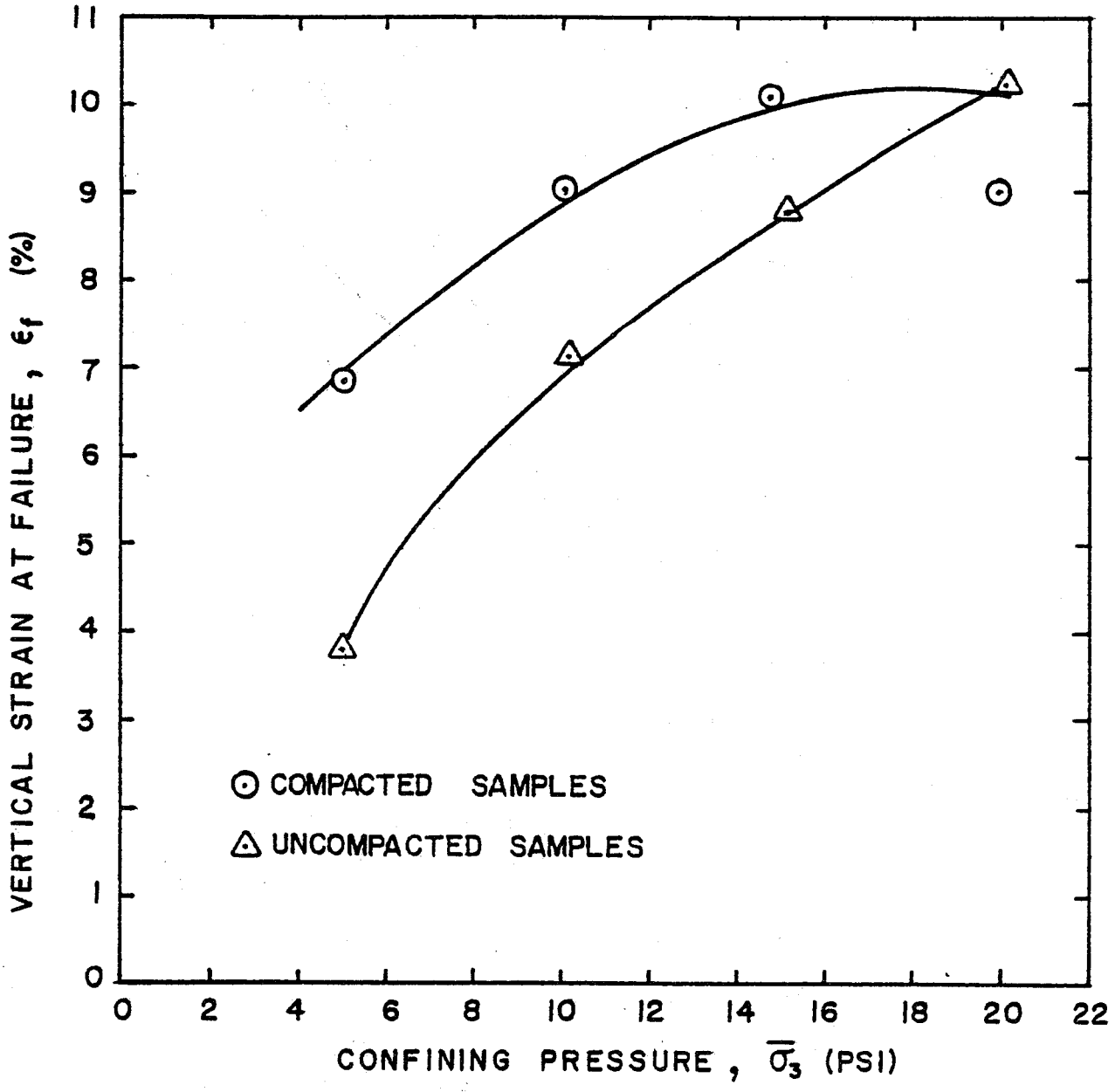

Fig. 6-9. Variation of Vertical Strain at Failure with Confining Pressure for Granite Ballast Samples

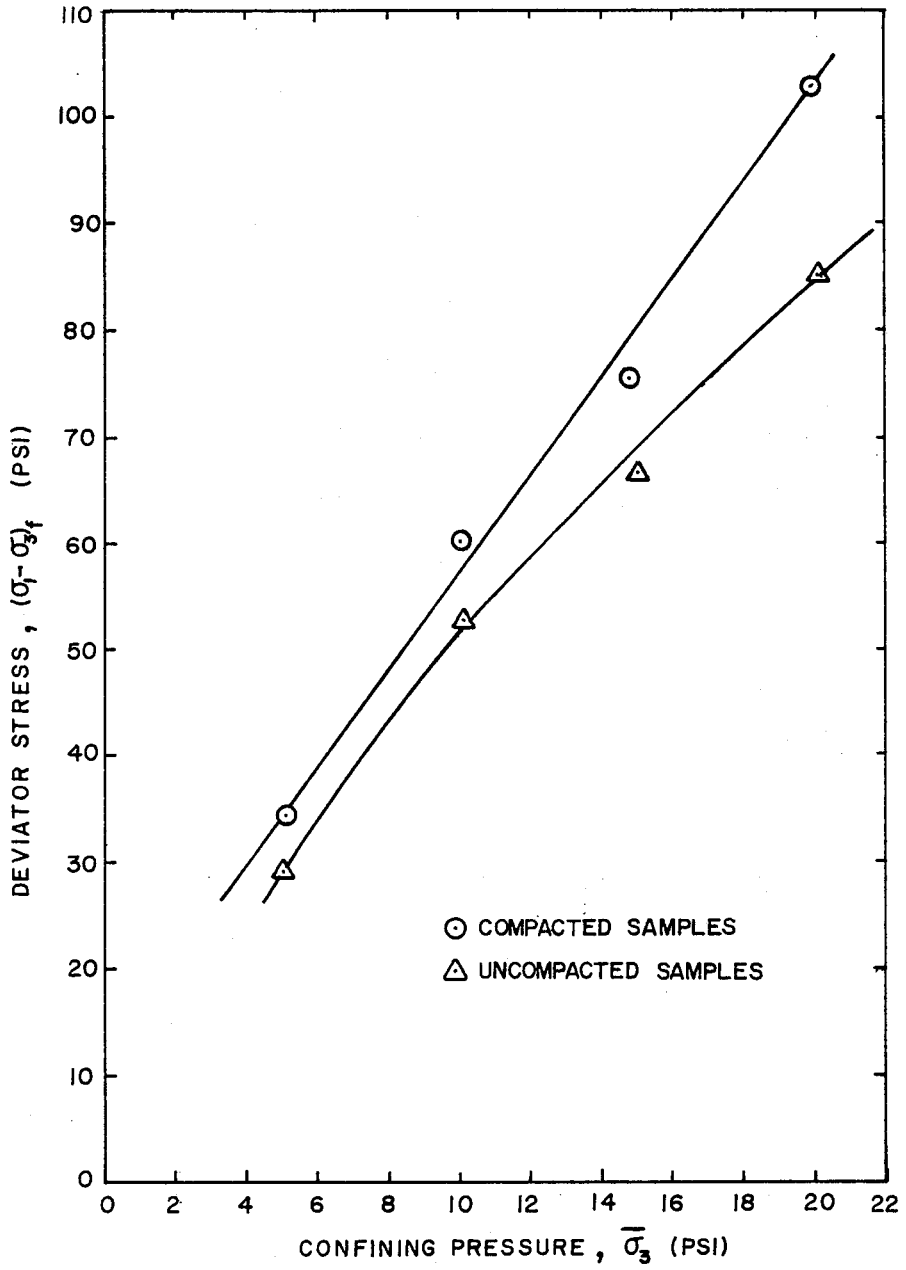

Fig. 6-10. Variation of Deviatoric Stress at Failure with Confining Pressure for Granite Ballast Samples

reduced and negative when there is a volume increase. The volumetric strains at failure are plotted for both compacted and uncompacted samples as a function of confining pressure in Fig. 6-11. As the confining pressure was increased, the volumetric strain changed from dilative to compressive, the uncompacted samples having a greater tendency than the compacted samples, as expected.

6.2.2 Hyperbolic Parameters

The initial Poisson's ratio, ν_i, and the final Poisson's ratio, ν_f, for both compacted and uncompacted samples are plotted against confining pressure in Fig. 6-12 and 6-13, respectively. Although there is scatter on the data, the general trend is that both initial and final Poisson's ratio decrease with increasing confining pressures, and that the initial Poisson's ratio is not affected by the ballast density.

The hyperbolic representation was applied to the stress-strain and volume change-strain data obtained from the ballast static triaxial tests. The equations involved in hyperbolic fitting are documented in Ref. 3. A typical linearized form of the hyperbolic plots for the stress-strain curve, shown in Fig. 6-14, indicates that the behavior is approximately hyperbolic. However, the volume change relationship was not.

Table 6-1 presents a summary of the parameters derived from the hyperbolic equations. Once again, duplicate tests show good reproducibility as far as initial tangent modulus, E_i, and ultimate deviator stress, $(\sigma_1-\sigma_3)_{ult}$, are concerned. The values of R_f vary between 0.74 and 0.98. These values are in agreement with the values given by Raymond and Davies (Ref. 55).

The logarithm of the initial tangent modulus, E_i, as computed from the hyperbolic model, is plotted in Fig. 6-15 as a function of the logarithm of

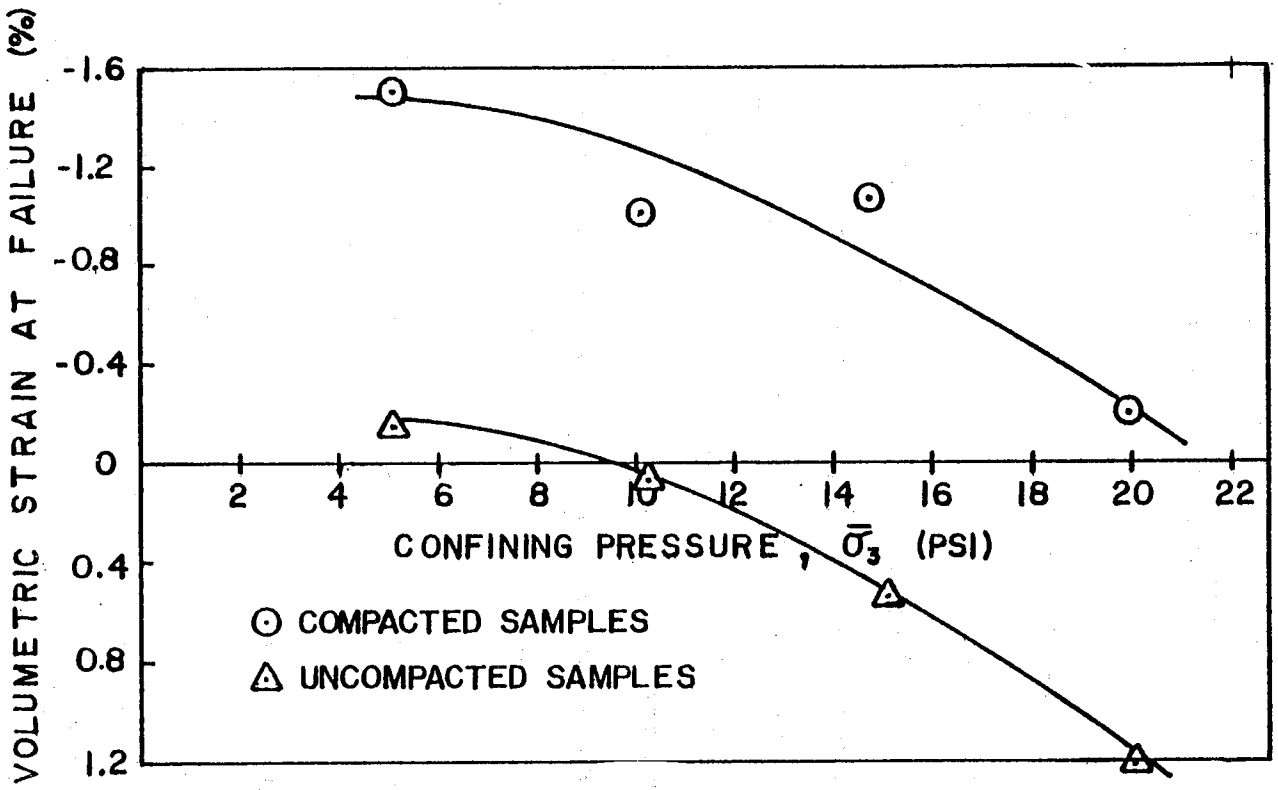

Fig. 6-11. Variation of Volumetric Strain at Failure with Confining Pressure for Granite Ballast Samples

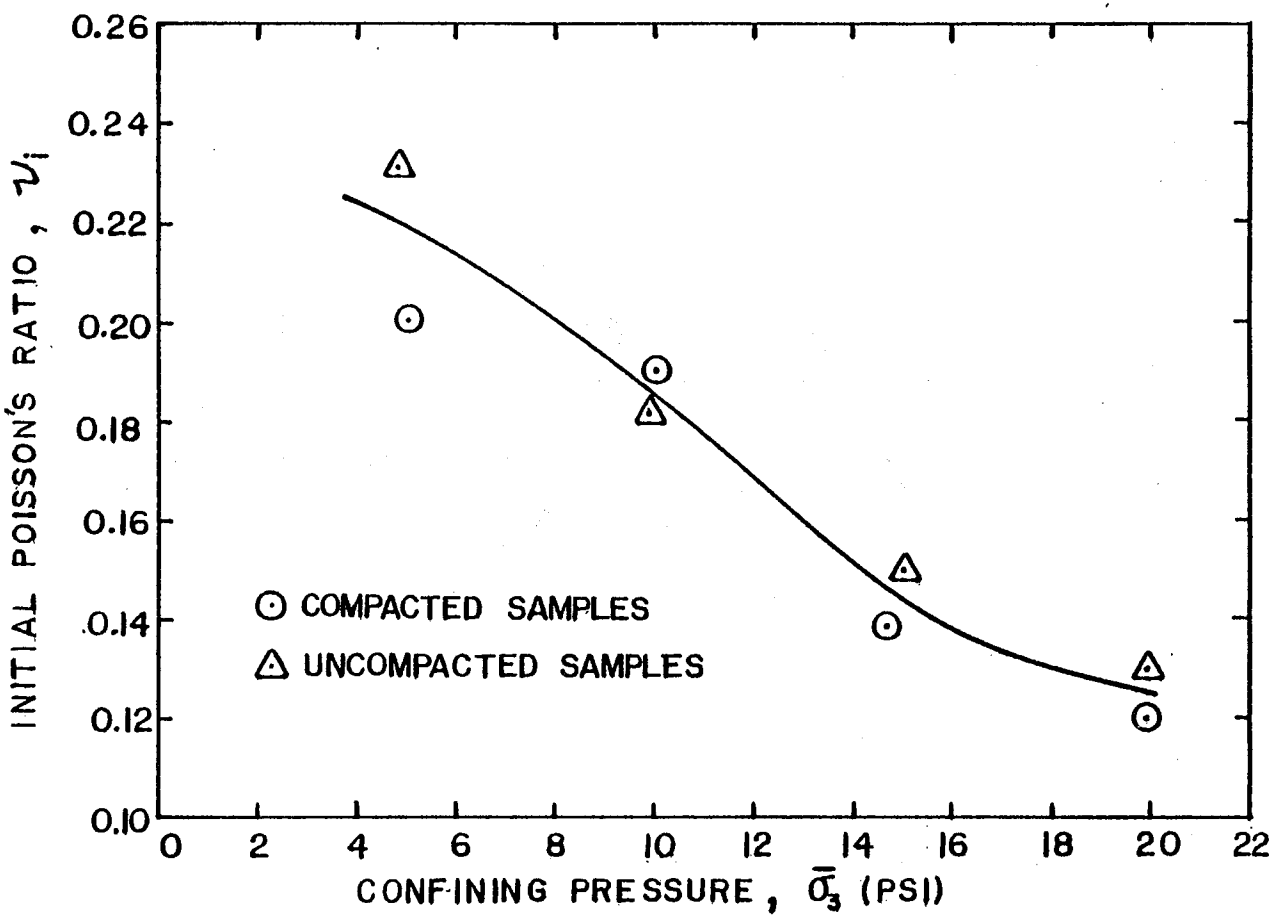

Fig. 6-12. Variation of Initial Tangent Poisson's Ratio with Confining Pressure for Granite Ballast Samples

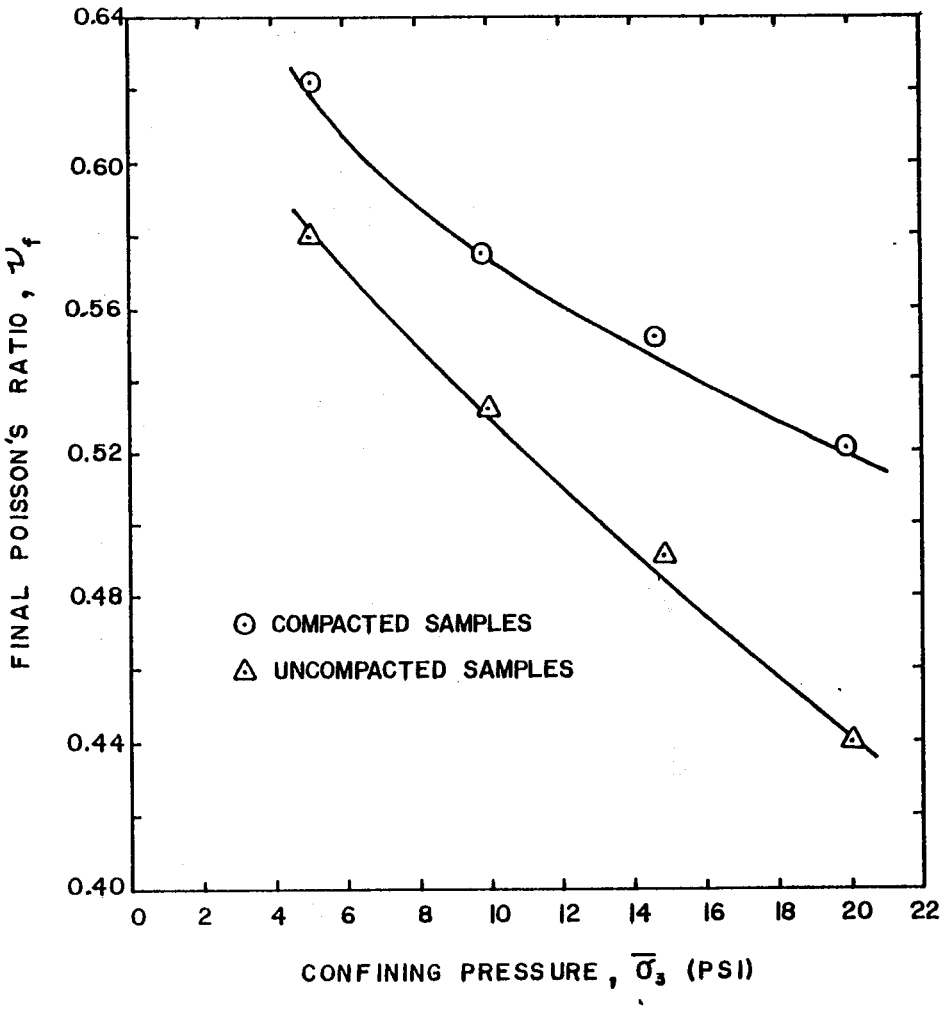

Fig. 6-13. Variation of Final Tangent Poisson's Ratio with Confining Pressure for Granite Ballast Samples

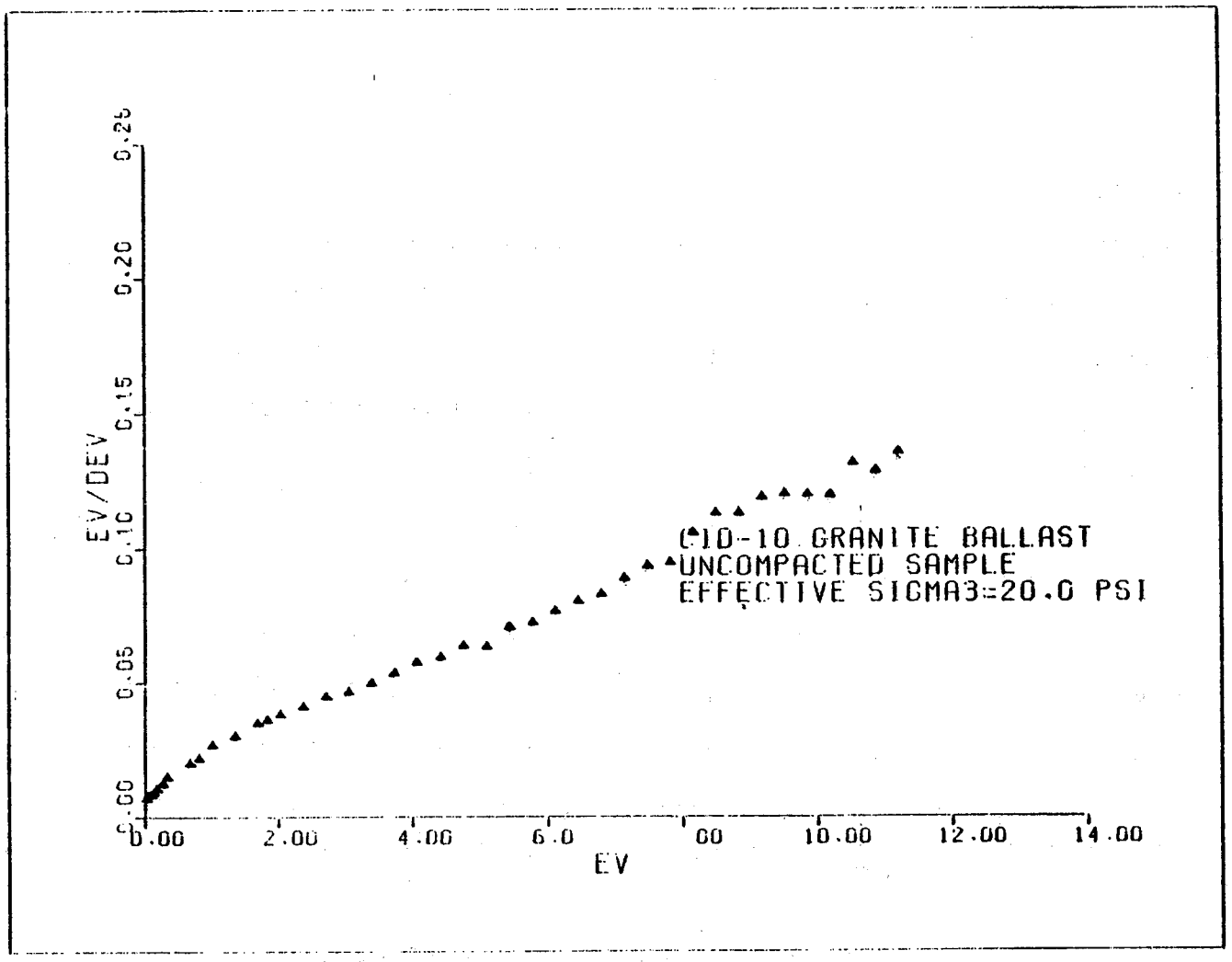

Fig. 6-14. Stress-Strain Hyperbolic Representation for Test CID-10

Table 6-1. Results of the Hyperbolic Fit

Test Number	Condition	E_i (psi)	$(\sigma_1-\sigma_3)_{ult}$ (psi)	$(\sigma_1-\sigma_3)_f$ (psi)	$R_f = \frac{(\sigma_1-\sigma_3)_f}{(\sigma_1-\sigma_3)_{ult}}$	$\bar{\sigma}_3$ (psi)	ν_i	ν_f
CID-1	Compacted	9000	69.0	60.5	0.88	10.01	0.20	0.53
CID-2	Uncompacted	6250	65.4	61.7	0.94	15.38	0.16	0.47
CID-3	Uncompacted	3850	71.4	52.7	0.74	10.16	0.18	0.53
CID-4	Uncompacted	3450	44.8	37.7	0.84	5.01	0.21	0.56
CID-5	Compacted	10000	100.0	85.6	0.86	14.79	0.14	0.55
CID-6	Compacted	6700	35.7	34.3	0.96	5.01	0.20	0.64
CID-7	Uncompacted	3330	35.1	29.1	0.83	5.01	0.23	0.58
CID-8	Compacted	8197	66.7	60.5	0.91	10.01	0.19	0.57
CID-9	Uncompacted	5500	74.1	66.7	0.90	15.05	0.15	0.49
CID-10	Uncompacted	5900	100.0	85.2	0.85	20.02	0.13	0.44
CID-11	Compacted	12500	105.3	102.7	0.98	19.99	0.12	0.52

For Uncompacted Samples (CID-3, CID-7, CID-9, CID-10)

$$E_i = 1500\ (\bar{\sigma}_3)^{0.46} \qquad R_f = 0.82$$

For Compacted Samples (CID-5, CID-6, CID-8, CID-11)

$$E_i = 3000\ (\bar{\sigma}_3)^{0.46} \qquad R_f = 0.91$$

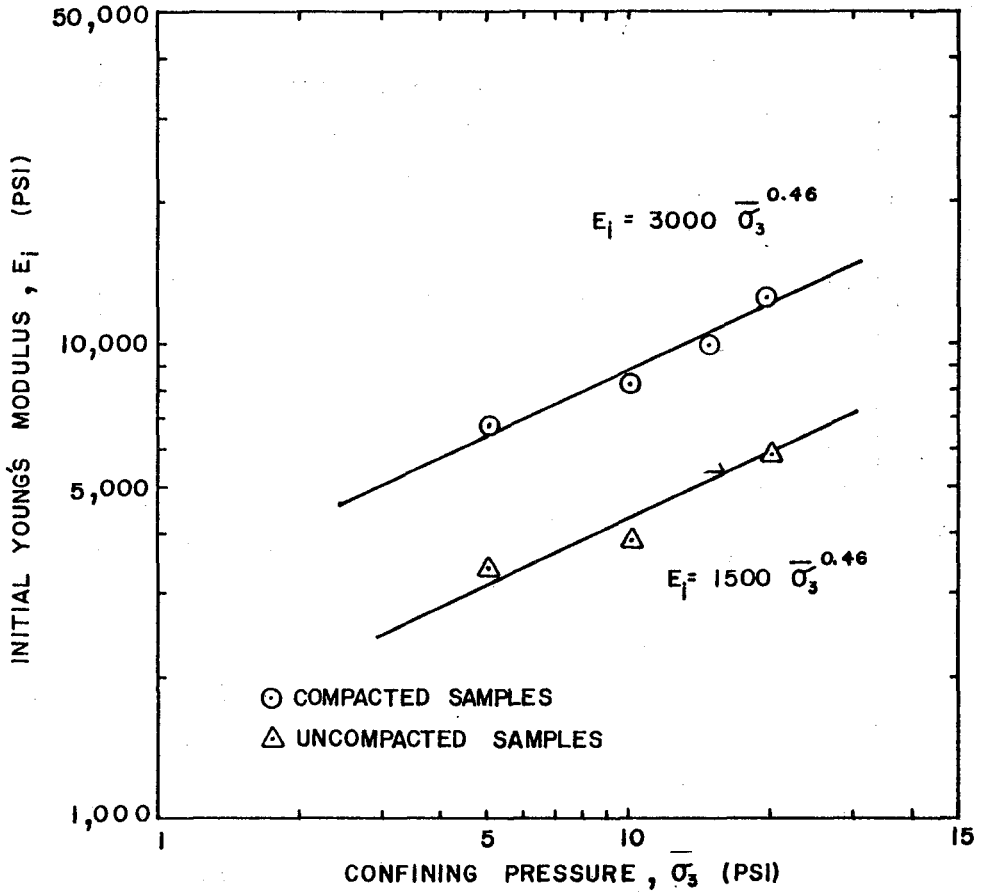

Fig. 6-15. Variation of Initial Young's Modulus with Confining Pressure for Granite Ballast Samples

the confining pressure, for both compacted and uncompacted samples. Naturally, the compacted samples have a greater initial tangent modulus than do the uncompacted samples. Generally, the relationship between these two can be represented as $E_i = K(\bar{\sigma}_3)^n$. A linear regression analysis using this functional relationship gave for compacted samples

$$E_i = 3000\ (\bar{\sigma}_3)^{0.46} \quad ,$$

and for uncompacted samples

$$E_i = 1500\ (\bar{\sigma}_3)^{0.46} \quad .$$

6.3 Cyclic Test Results

Forty-three cyclic triaxial tests with constant confining pressures (5 to 20 psi) were performed on granite ballast samples obtained from the FAST track in Pueblo, Colorado. The cyclic tests, with the exception of test CYD-16, were isotropically-consolidated, drained tests with saturated samples under back pressure. Test CYD-16 was run with a dry sample to evaluate moisture effects on the resilient and permanent deformation behavior. As in the case of static testing, both uncompacted and compacted sample states were prepared to simulate the range of ballast density that was measured in the field.

The sample preparation techniques used for the cyclic triaxial testing were primarily the same as those for the static triaxial testing. However, in the cyclic triaxial tests after the consolidation stage was completed, some water was drained out of the cell chamber to provide an air cushion inside the top of the cell which permits the rapid movement of the loading piston without causing changes in the cell pressure. The cell pressure was created in this situation by air pressure applied to the top of the cell. Five different confining pressures were used, nominally 5, 7, 10, 15 and 20 psi.

The first sixteen cyclic tests (preliminary series) were performed at the State University of New York at Buffalo (SUNYAB) using a ± 22 kip force capacity hydraulic actuator, providing a haversine motion. The remainder of the cyclic testing (final series) was performed at the University of Massachusetts at Amherst (UMass) using a ± 11 kip force capacity hydraulic actuator providing a sinusoidal motion.

The average dry unit weight of the fourteen uncompacted samples was 94.6 pcf with a coefficient of variation of 2.6% and a range from 92.1 to 100.1 pcf. The average dry unit weight of the twenty-seven compacted samples was 100.5 pcf with a coefficient of variation of 1.9% and a range from 98.0 to 104.9 pcf. The average initial void ratio for the uncompacted samples was 0.76, and for the compacted samples was 0.67. These are in good agreement with the dry unit weight and initial void ratio results for the static triaxial testing.

The data taken after a selected number of cycles during each test were reduced using a computer code written to determine the values of vertical elastic strain and resilient modulus (deviatoric stress divided by the vertical elastic strain), vertical permanent strain and volumetric permanent strain (accumulated volumetric strain at the end of each cycle).

6.3.1 Resilient Behavior

Only resilient modulus results are presented. Unfortunately the resilient Poisson's ratio was not possible to determine with the available apparatus. The volume change device was designed primarily to measure permanent volumetric deformation and not resilient volumetric deformation. For future work, the apparatus should be modified in such a way that the measurement of the resilient lateral strain is possible.

During the first series of tests, the device for holding the external dial indicator on the cell was found not rigid enough for the measurement of resilient vertical deformation. Thus it was decided not to use the resilient modulus results from the first series.

The preliminary series results carried to 10,000 cycles confirmed that there was not a large difference in the resilient behavior of granular material whether it was saturated or dry. Because the only available method to determine the lateral permanent strain with the present apparatus was through the measurement of both the volumetric and vertical permanent strains, it was decided to continue testing in the final series with saturated samples. In the final series, the number of cycles of load application was increased to 100,000 in order to simulate increased traffic conditions.

Most samples were tested with just one combination of confining pressure and cyclic deviator stress. This is termed single-staged tests. However, for two samples, a whole series of combinations were tested in sequence. This is termed multi-staged tests. Multi-staged tests have been commonly used in the past for economic reasons.

The following observations were made concerning the resilient modulus results:

1. For single-staged tests, the resilient modulus continued to increase with increasing number of cycles. However, for the multi-staged tests the resilient modulus achieved a constant value even for a small number of load applications.
2. Figure 6-16, representing 10,000 cycles, shows that the uncompacted samples give a smaller resilient modulus than the compacted samples for a given bulk stress. Similar results were found at other numbers of cycles.

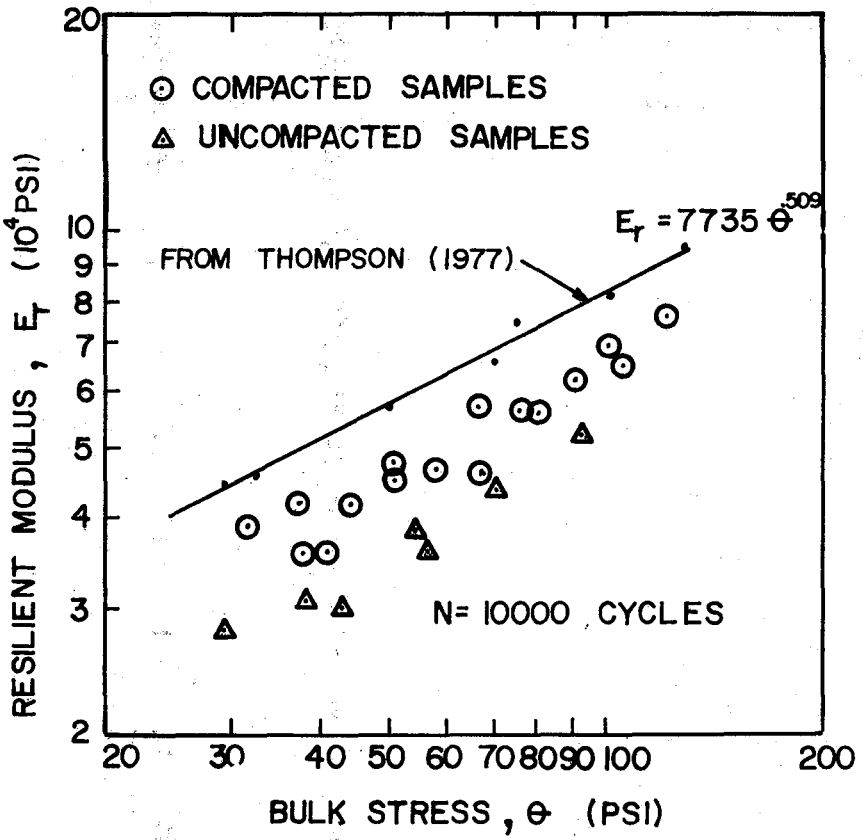

Fig. 6-16. Comparison of Resilient Modulus from Samples in Final Series

3. The values of the FAST granite ballast resilient modulus obtained by Thompson (Ref. 24) are also presented in Fig. 6-16. The results of Thompson indicate a higher resilient modulus for the same material in a compacted state than the UMass results.
4. The resilient modulus results from single-staged tests indicated more dispersion than the results from multi-staged tests. This seems logical because the single-staged tests use a different specimen each time in contrast to the multi-staged tests.

Linear regression analysis of the final series of single-staged tests was undertaken using UMass SPSS program (Statistical Package for the Social Sciences, from Nie, et al., Ref. 56). The 17 compacted and 7 uncompacted samples were treated separately. Two different independent variables were chosen to perform the regressions. These were the effective confining pressure, $\bar{\sigma}_3$, and the bulk stress, Θ. For both cases, arithmetic, log-log and semi-log relationships were investigated.

Figure 6-16 related the resilient modulus to the log of the bulk stress. For comparison, Fig. 6-17 presents the arithmetic relationship of the resilient modulus with the bulk stress for 10,000 cycles for both the compacted and uncompacted samples. There is a difference of about 10,000 psi in the resilient modulus of the uncompacted and compacted samples.

The following conclusions were drawn from the results of the resilient modulus study:

1. It is very important to minimize errors in the measurement of the axial resilient deformation in the triaxial test. The resilient modulus values determined from the first series of tests were not considered in the analysis due to an inaccuracy in these measurements.

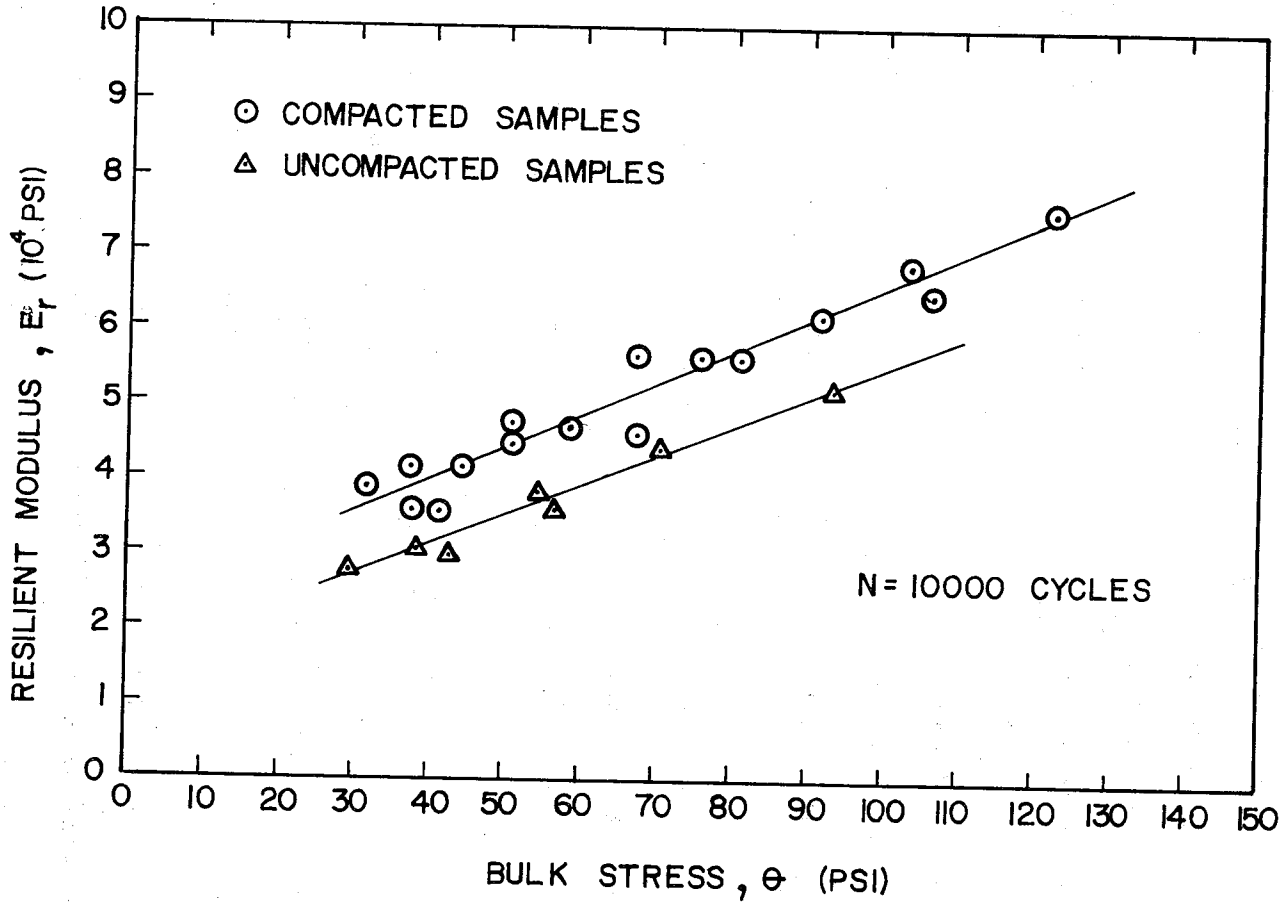

Fig. 6-17. Arithmetic Relationship of E_r as a Function of θ for the Final Test Series

2. Based on the results of the final series of tests, it can be concluded that the resilient modulus is better correlated to the bulk stress than to the confining pressure. However, for a small number of cycles, the modulus is better correlated to the confining pressure than to the bulk stress.
3. Arithmetic relationships between E_r and Θ give as high or higher coefficient of determination (R^2) than the previously postulated log-log relationships.
4. The initial density of the sample affects the resilient modulus, giving the compacted samples a higher modulus than the uncompacted samples.
5. For single-staged tests, the resilient modulus keeps increasing with the number of cycles. This situation is different for multi-staged tests such as those presented in the literature where constant values of resilient modulus are achieved within a few cycles.
6. Further apparatus development is recommended to measure both the axial and lateral resilient strain directly on the sample, so the resilient Poisson's ratio can also be determined.

6.3.2 Permanent Deformation Behavior

In this section, only vertical (axial) permanent strain results from cyclic testing will be presented. During cyclic testing, volumetric permanent strain measurements were also made. Assuming that the sample deforms like a cylinder, the lateral permanent strains can be calculated from the vertical and volumetric permanent strains.

Different parameters were tried to correlate the data, such as the shear stress level and the confining pressure. However, the measured values of the

vertical permanent strain were found to be best represented by a function of the stress ratio $\Delta q/q_f$ (the ratio of maximum applied shear stress to maximum shear stress at failure for the same confining pressure) and the effective confining pressure, $\bar{\sigma}_3$.

Figure 6-18 presents the results for uncompacted samples after the first load application for both the preliminary and final series. Figure 6-19 presents the corresponding results for the compacted samples. Similar graphs have been obtained for cycle numbers 10, 100, 1000, 10,000 and 100,000. These figures show that, for a given number of cycles of load application, the vertical permanent strain increases with increasing stress ratio. For a given number of cycles, the relationship between the vertical permanent strain with the stress ratio seems to be nonlinear. For moderate to high stress ratios, the confining pressure seems to have an effect in the development of permanent strain. The effect of the confining pressure is not noticeable for low stress ratios.

The vertical permanent strain values were normalized by dividing them by the confining pressure $\bar{\sigma}_3$. Figure 6-20 presents the plot of normalized vertical permanent strain $\varepsilon_1 / \bar{\sigma}_3$ against stress ratio $\Delta q/q_f$ for the uncompacted and compacted samples after the first load applications. Similar plots can be obtained for cycles 10, 100, 1000, 10,000 and 100,000. Even though there is some scatter in the data, the effects of the degree of compaction, stress ratio $\Delta q/q_f$, and effective confining pressure $\bar{\sigma}_3$ can be seen. It should be pointed out that these relationships have been developed for the specific range of confining pressures, 5 to 20 psi. Further investigation is required to extend these relationships to lower and higher confining pressures.

Figure 6-20 can be used to predict vertical permanent strains for uncompacted and compacted samples after the first cycle of load for a given stress

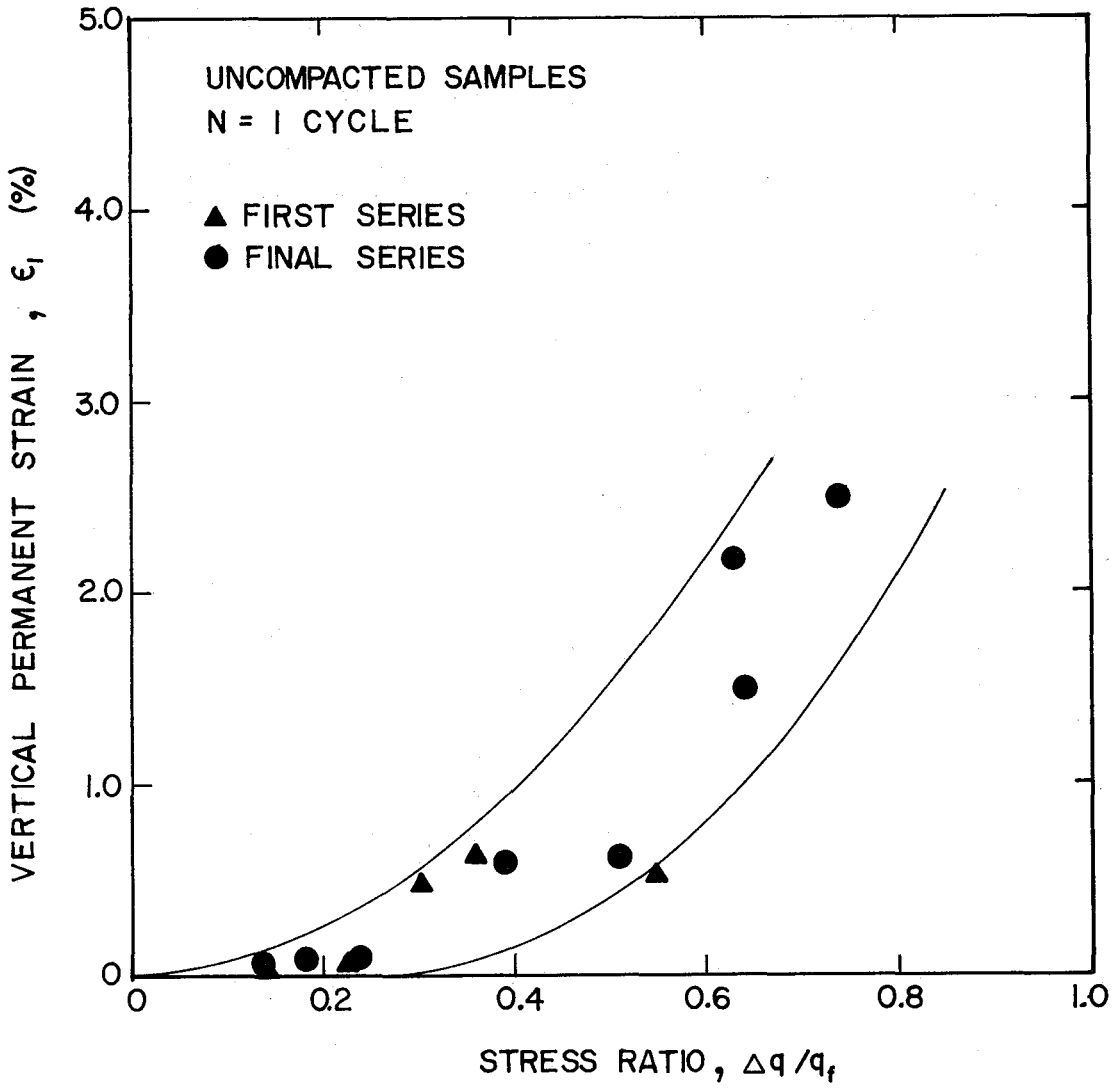

Fig. 6-18. Permanent Vertical Strain as a Function of Stress Ratio for Uncompacted Samples After One Cycle

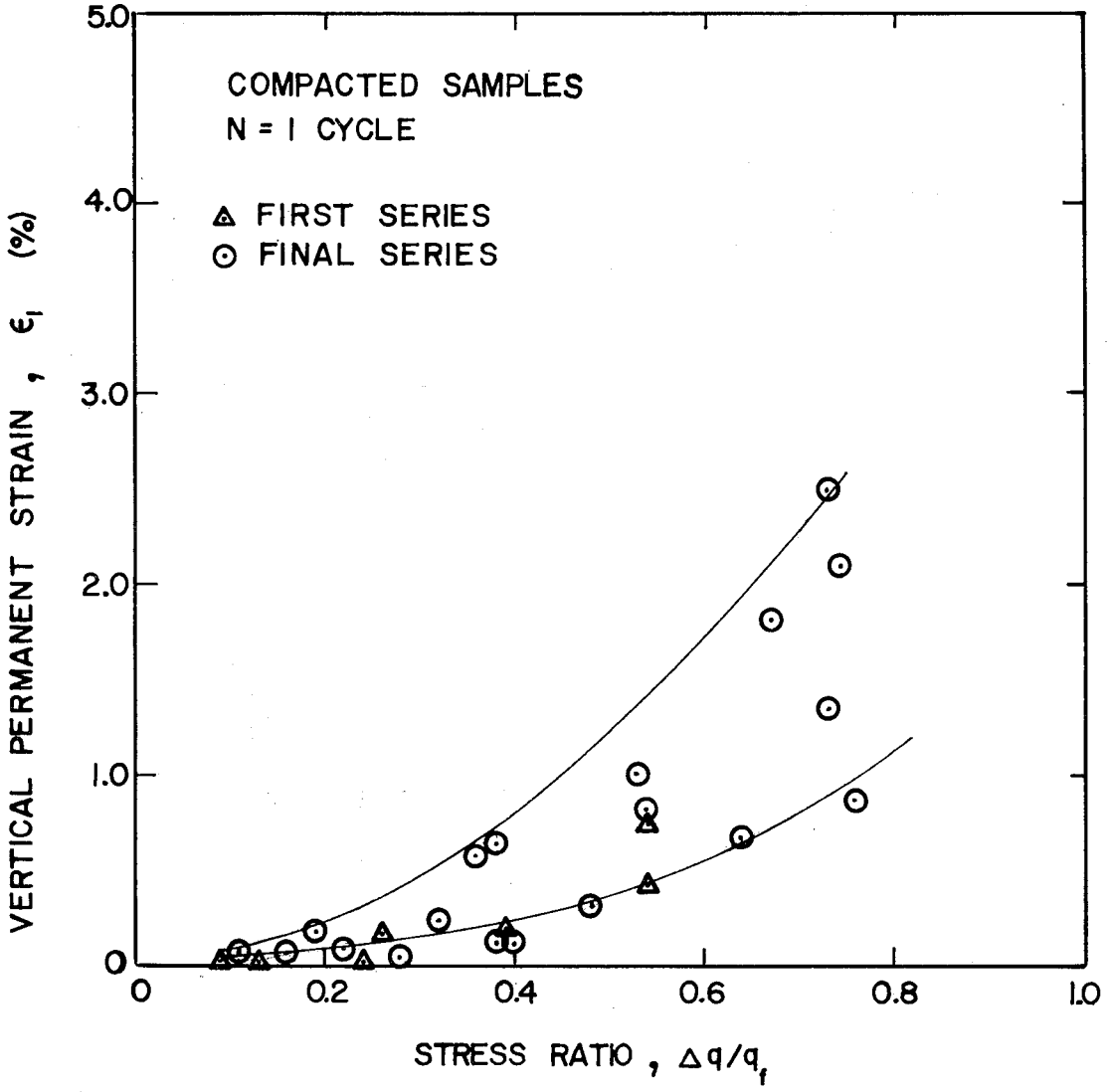

Fig. 6-19. Vertical Permanent Strain as a Function of Stress Ratio for Compacted Samples After One Cycle

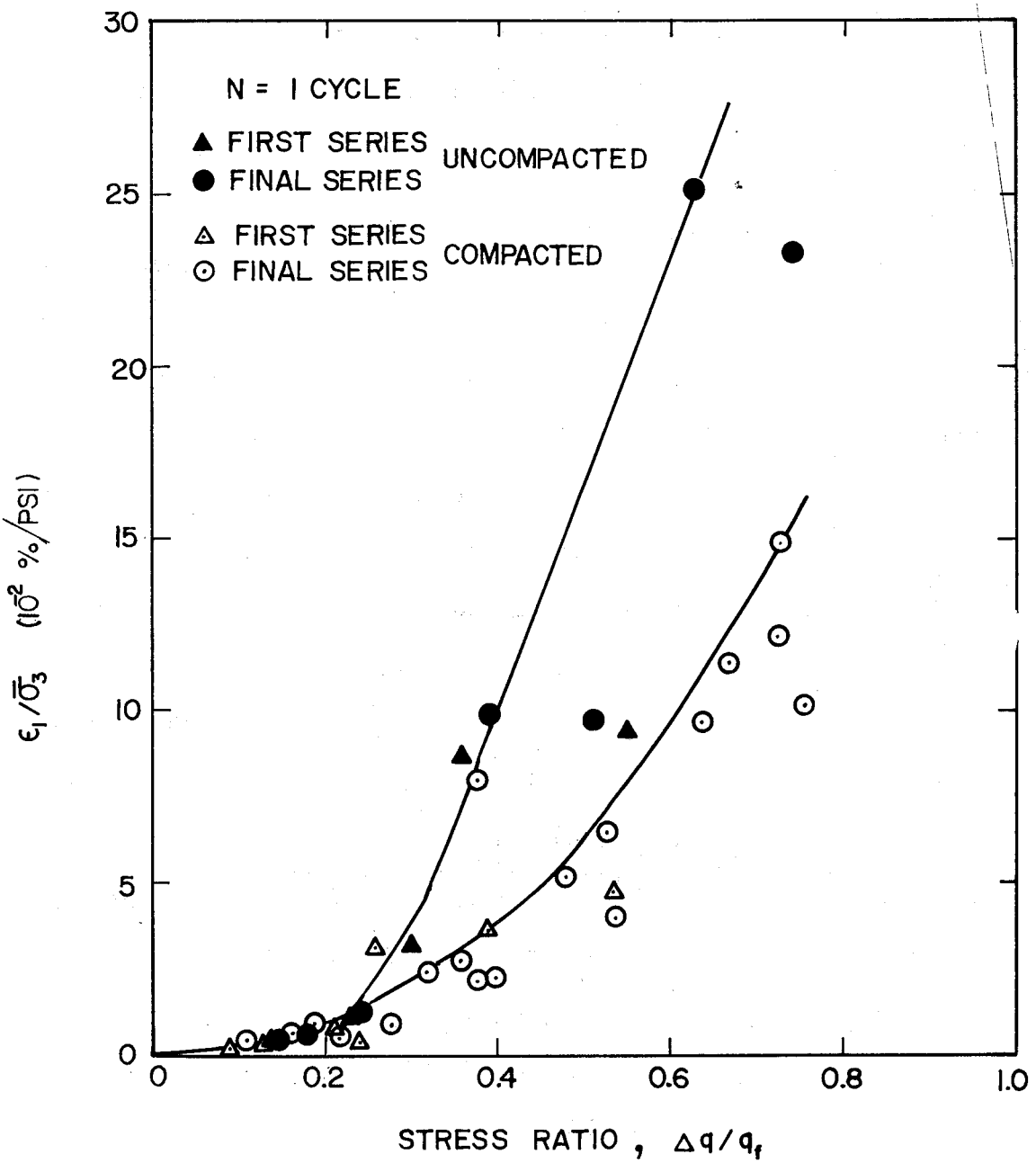

Fig. 6-20. Normalized Vertical Permanent Strain as a Function of Stress Ratio for Uncompacted and Compacted Samples After One Cycle

ratio, $\Delta q/q_f$, and a given confining pressure, $\bar{\sigma}_3$. Similar curves for other numbers of cycles can be developed. However, the results indicated that the vertical permanent strain after N cycles can be predicted from the vertical permanent strain after the first cycle. This observation is in accordance with previously published results by ORE (Ref. 45) and Shenton (Ref. 46).

Due to the importance of the determination of the vertical permanent deformation after the first cycle, during the final series of tests the first cycle was applied by manual operation of the testing machine. The successive load applications in the final series of tests were done using the sinusoidal wave form from the function generator of the servo-controlled system. Only the results from the final series of tests will be presented in this section.

Figure 6-21 presents the relationship between the vertical permanent strains from the first cycle to the vertical permanent strains at the tenth, hundredth, thousandth, ten thousandth and hundred thousandth cycle, respectively. It can be seen in this figure that independently of the degree of compaction or stress condition, straight lines passing through the origin can be developed for these relationships. However, some nonlinearity was observed with the curves at larger numbers of load applications.

Both linear and nonlinear regression analyses were undertaken with these data using the SPSS package (Ref. 56) in order to establish relationships between ε_N, ε_1 and N. The linear regression equation determined was

$$\varepsilon_N = \varepsilon_1(1 + 0.19 \log N).$$

There is excellent similarity between this equation and the equation

$$\varepsilon_N = \varepsilon_1(1 + 0.2 \log N)$$

presented in Refs. 45 and 46 for different ballasts tested in England.

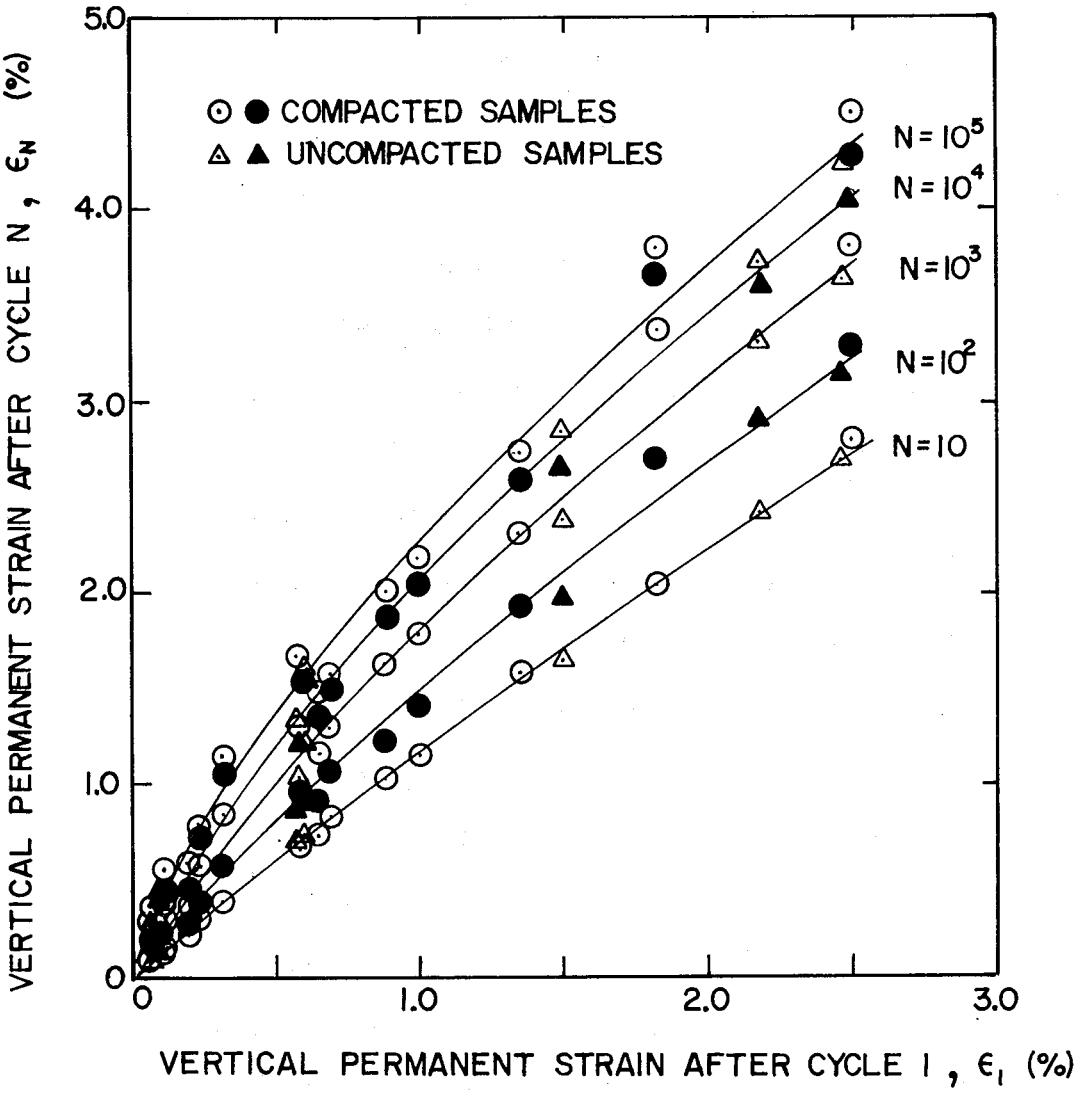

Fig. 6-21. Relationships Between the Vertical Permanent Strains at the First and the Nth Cycles

Because Fig. 6-21 presented some nonlinearities at higher values of N, nonlinear regressions of the form $\varepsilon_N = K_1\varepsilon_1 + K_2\varepsilon_1^2$ were tried at the different cycle numbers. Using a nonlinear regression of the first order, the expression determined to predict ε_N based on ε_1 and N is

$$\varepsilon_N = (0.85 + 0.38 \log N)\varepsilon_1 + (0.05 - 0.09 \log N)\varepsilon_1^2.$$

The above analysis shows that the vertical permanent deformation at any cycle, ε_N, can be predicted as a function of the number of cycles of load application, N, and the vertical permanent deformation after the first cycle, ε_1, independently of the state of stress and degree of compaction of the specimen. Linear and nonlinear expressions have been presented.

The remainder of this section will consider the prediction of ε_1. Figure 6-20 presented a way to predict the values of ε_1 for a given stress ratio, $\Delta q/q_f$ and a confining pressure, $\overline{\sigma}_3$. A different approach using the results of the static testing will also be presented.

The stress-strain relationship in the static tests was shown to be represented by hyperbolic equations. The parameters required are presented in Ref. 3. The results of the cyclic or repeated load testing give vertical permanent strain measured at the end of the first cycle. There is a difference between the predicted value of vertical strain using hyperbolic equations and the measured value of vertical strains after the first cycle. This difference is the resilient or recoverable strain in the first cycle. If the resilient strain in the first cycle is added to the vertical permanent strain at the end of the first cycle, a comparison can be made with the predicted values from the hyperbolic relationships which represent the strain before unloading.

The relationship of vertical strain for a given stress level and degree of compaction given by the hyperbolic expression is

$$\varepsilon_V = \frac{\sigma_1 - \sigma_3}{\left[1 - \frac{(\sigma_1-\sigma_3)R_f(1-\sin\bar{\phi})}{2\,\bar{c}\cos\bar{\phi} + 2\bar{\sigma}_3\sin\bar{\phi}}\right] K(\bar{\sigma}_3)^n}$$

where the terms have been defined in Ref. 3. For the uncompacted samples, $\bar{c}$ = 4.8 psi, $\bar{\phi}$ = 37.8 deg, R_f = 0.82, K = 1500 (developed for psi units), and n = 0.46. For the compacted samples, $\bar{c}$ = 2.8 psi, $\bar{\phi}$ = 44.4 deg, R_f = 0.91, K = 3000 (developed for psi units), and n = 0.46.

It is postulated that the value of ε_1 can be predicted by subtracting ε_{r_1} (resilient strain at the first cycle) from ε_V (axial strain predicted by hyperbolic modelling). The only value missing in this method is ε_{r_1}. Another method to obtain ε_1 can be by performing a static test up to the maximum level of shear stress and then unload the first cycle to measure ε_1. The relationship between ε_1 and ε_N has been presented previously. Thus the values of ε_N can be predicted if the degree of compaction of the ballast is known and also the stress state.

The measured values of ε_{r_1} in the cyclic testing program have been plotted against the stress ratio $\Delta q/q_f$ in Fig. 6-22. Even though it can be noticed that the degree of compaction and confining stress will influence the value of ε_{r_1}, a first approximation curve has been fitted to the data that provides a means to predict ε_{r_1} based on the stress ratio $\Delta q/q_f$. This relationship is clearly nonlinear.

The following conclusions are drawn from the permanent deformation analysis:

1. The degree of compaction is a very important parameter in the development of permanent vertical strain of ballast materials. The uncompacted samples will develop more vertical permanent strain than compacted samples.

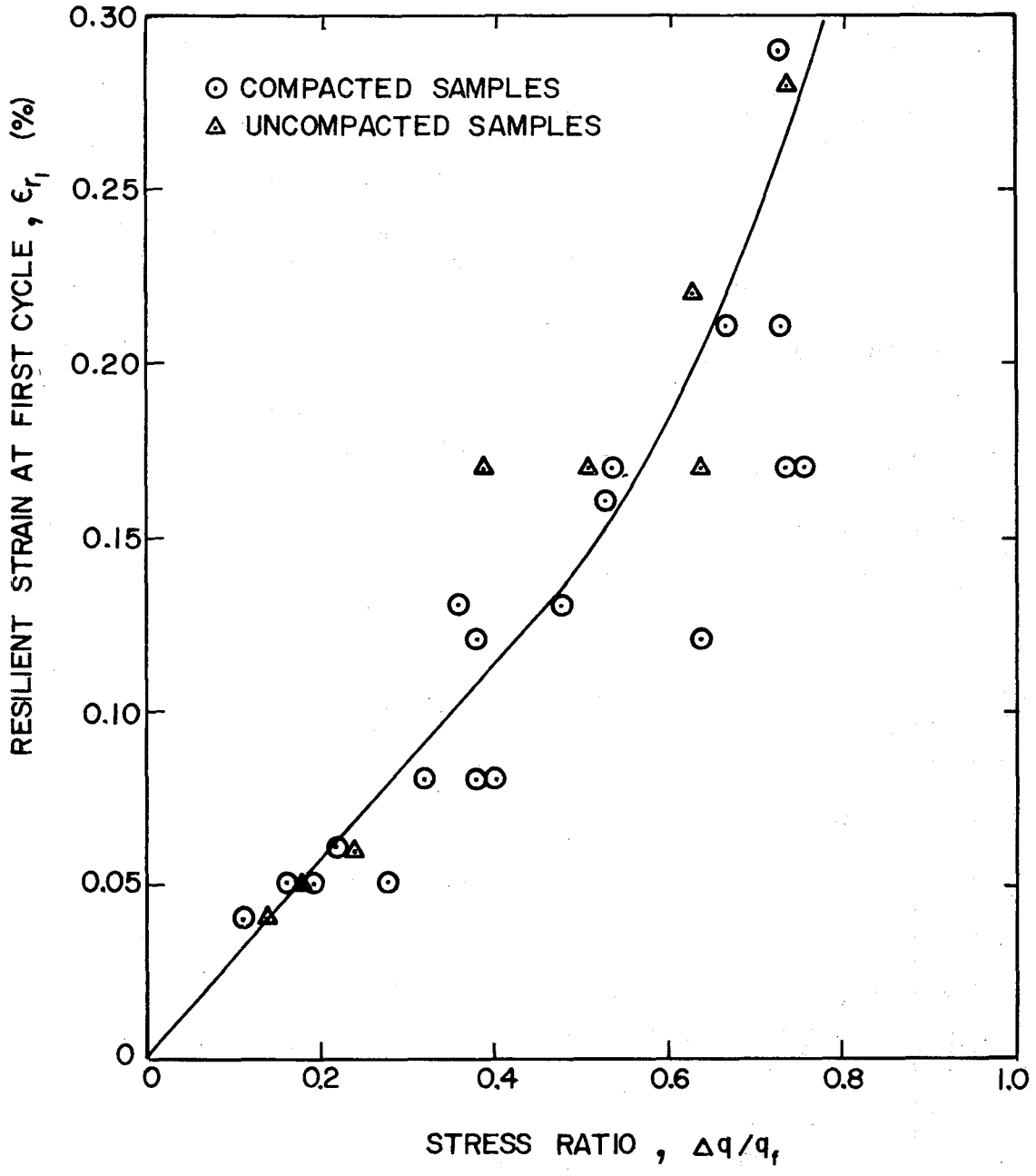

Fig. 6-22. Variation of the Resilient Strain at the First Cycle with Stress Ratio $\Delta q/q_f$

2. The vertical permanent strain of both uncompacted and compacted samples can be normalized with respect to the confining pressure. The higher the stress ratio $\Delta q/q_f$, the higher the development of permanent strain.
3. The development of the permanent deformation of ballast reduces considerably as the number of cycles increases. The vertical permanent strain after a given number of cycles can be predicted by a linear or nonlinear function of N, and the strain at the end of the first cycle.
4. The vertical strain at the end of the first cycle ε_1 can be predicted from the static testing results.
5. By virtue of 3 and 4, a means is provided to predict the vertical permanent deformation of ballast material after any cycle by knowing the degree of compaction, number of cycles of load application, the stress conditions, and the static stress-strain behavior.

CHAPTER 7. PREDICTION METHODOLOGY

This chapter presents the methodology for predicting the permanent deformation behavior of railroad track. The methodology is based on the GEOTRACK model and laboratory testing. The validity is determined by comparison with the measured values at the FAST track. The presentation is limited to the prediction of the granite ballast strain. Further study is necessary for the subballast strain and subgrade permanent deformation in all sections, and for the limestone and traprock ballast strain.

7.1 Method of Prediction

Figure 4-15 presented the two equivalent triaxial stress paths, CB and DE, at the middle of the ballast layer for FAST section 18B. Table 7-1 gives the confining pressures and deviatoric stresses represented by those two stress paths for the three granite ballast sections.

For each stress path, values of the $\Delta q/q_f$ ratio are calculated for both the uncompacted and compacted conditions by the following relationship:

$$\frac{\Delta q}{q_f} = \frac{(\sigma_1-\sigma_3)}{(\sigma_1-\sigma_3)_f} = \frac{(\sigma_1-\sigma_3)}{\left[\frac{2\,\bar{c}\cos\bar{\phi} + 2\bar{\sigma}_3\sin\bar{\phi}}{1-\sin\bar{\phi}}\right]} \qquad (7\text{-}1)$$

From the static triaxial test results for the uncompacted samples, $\bar{c}$ = 4.8 psi and $\bar{\phi} = 37.8^{o}$, and for the compacted samples, $\bar{c}$ = 2.8 psi and $\bar{\phi} = 44.4^{o}$. Table 7-2 presents the $\Delta q/q_f$ ratios obtained for both the uncompacted and the compacted samples of sections 17E, 18A and 18B.

The values of the vertical permanent deformation after the first cycle, ε_1, can be predicted by two methods: 1) using the cyclic test results from

Table 7-1. Stress Conditions for Equivalent Stress Paths at the Middle of the Granite Ballast Layers

Section	Stress Path CB		Stress Path DE	
	$\overline{\sigma}_3$ (psi)	$\sigma_1-\sigma_3$ (psi)	$\overline{\sigma}_3$ (psi)	$\sigma_1-\sigma_3$ (psi)
Section 17E: Ballast Depth = 14 in. Concrete Tie	6.8	13.4	3.5	13.4
Section 18A: Ballast Depth = 21 in. Wooden Tie	4.9	16.2	3.0	16.2
Section 18B: Ballast Depth = 15 in. Wooden Tie	6.3	16.7	3.5	16.7

Table 7-2. Confining Pressure and Stress Ratios for Equivalent Stress Paths at the Middle of the Ballast Layer

Section	Stress Path CB		Stress Path DE	
	$\bar{\sigma}_3$ (psi)	$\Delta q/q_f$	$\bar{\sigma}_3$ (psi)	$\Delta q/q_f$
	a) Uncompacted Samples			
17E	6.8	0.33	3.5	0.44
18A	4.9	0.46	3.0	0.56
18B	6.3	0.42	3.5	0.54
	b) Compacted Samples			
17E	6.8	0.30	3.5	0.45
18A	4.9	0.45	3.0	0.59
18B	6.3	0.39	3.5	0.56

Section 6.3.2, or 2) using the hyperbolic parameters from the static triaxial tests in Section 6.2.2. Both methods were used and the results compared.

Figure 7-1 presents the contours of constant strain after the first cycle ε_1 for the compacted samples of the FAST granite ballast based on Fig. 6-20. For the range of confining stresses tested (5 to 20 psi), and for small values of ε_1, the contour line tends to be horizontal. This was the reason for normalizing the permanent strains with the confining stress in Fig. 6-20. However, for values of confining pressure lower than 5 psi, the lines of constant strain should tend to zero. This is accomplished by having ε_1 be a function of $\Delta q/q_f$, obtained by putting $\bar{\sigma}_3$ = 5 psi in Fig. 6-20. The resulting relationship in Fig. 7-2 is recommended for confining pressures in the range from zero to 5 psi.

Table 7-3 presents the predicted values of the permanent deformation after the first cycle ε_1 for the stress paths CB and DE, and for the uncompacted and compacted samples.

Table 7-4 presents the predicted values of ε_1 using the static test hyperbolic parameters from Section 6.2.2. To accomplish this, the axial strain, ε_v, with the deviator stress applied is calculated. The resilient strain in the first cycle from Fig. 6-22 is subtracted to obtain an estimate of the permanent strain that would develop at the end of the first cycle after removing the deviator stress. Thus, $\varepsilon_1 = \varepsilon_v - \varepsilon_{r_1}$, where ε_v is determined from

$$\varepsilon_v = \frac{\sigma_1-\sigma_3}{\left[1 - \frac{(\sigma_1-\sigma_3)\ R_f\ (1-\sin\bar{\phi})}{2\bar{c}\cos\bar{\phi} + 2\bar{\sigma}_3 \sin\bar{\phi}}\right] K\bar{\sigma}_3^{\,n}} \qquad (7\text{-}2)$$

A good agreement between the two methods can be noticed from the comparison of results presented in Tables 7-3 and 7-4. As expected, the stress path DE

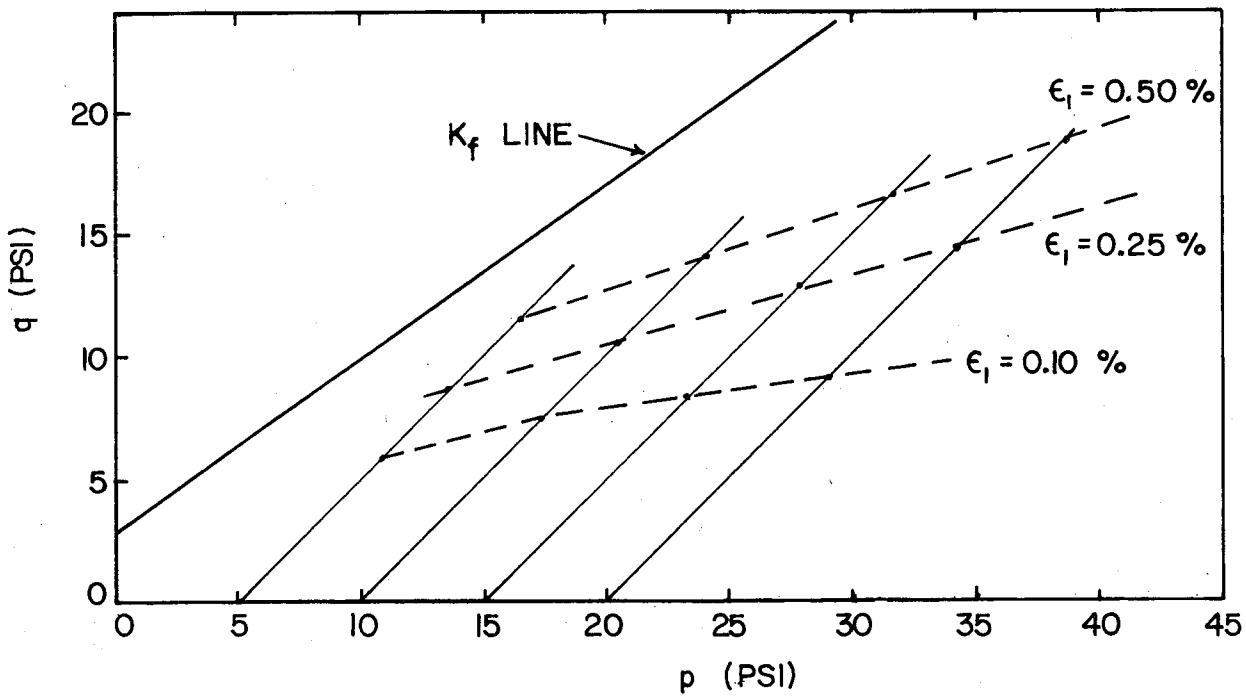

Fig. 7-1. Contours of Equal Strain after the First Cycle for Compacted Samples of Granite Ballast

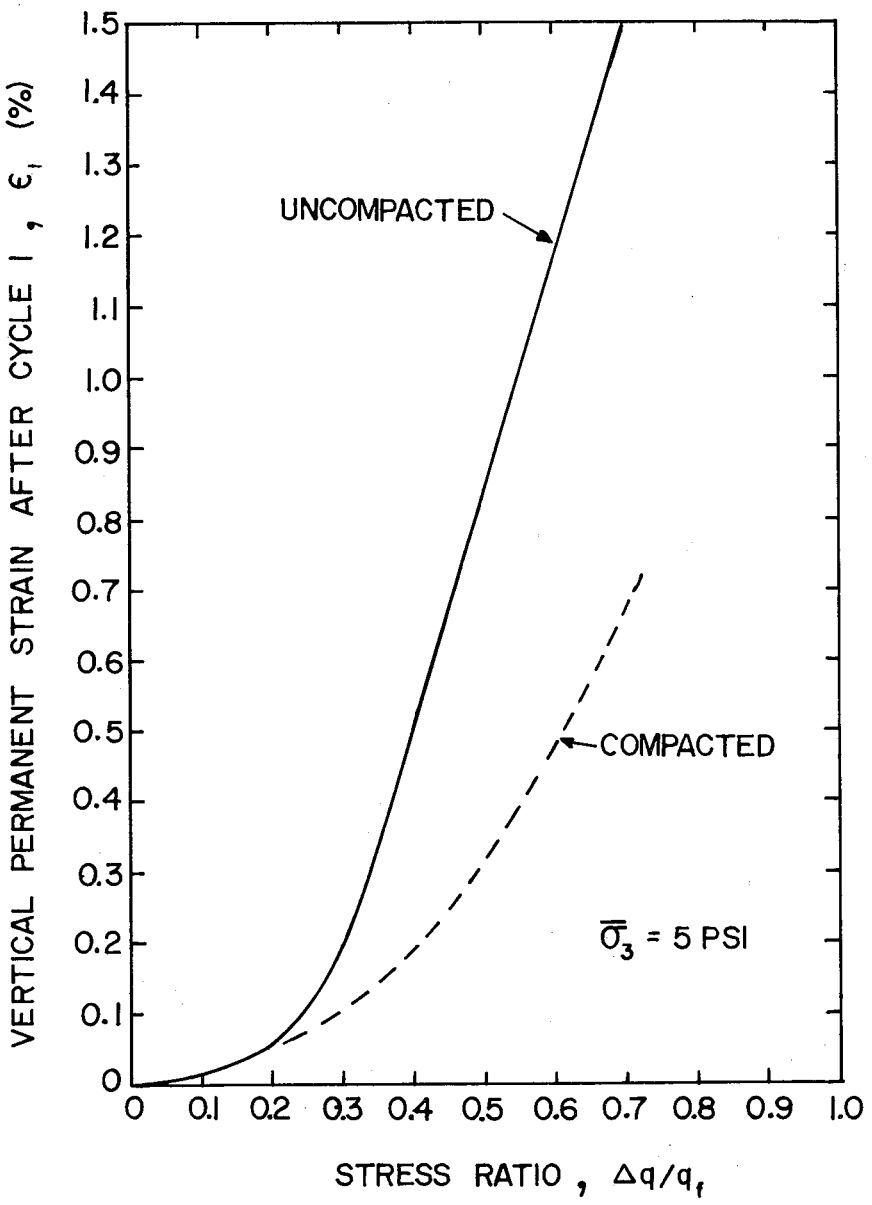

Fig. 7-2. Vertical Permanent Strain after the First Cycle as a Function of Stress Ratio and Degree of Compaction to be Used for Confining Pressures of 5 psi and Less

Table 7-3. Prediction of ϵ_1 Based on Confining Pressures and Stress Ratios at the Middle of the Ballast Layer

Section	Stress Path CB		Stress Path DE	
	$\bar{\sigma}_3$ (psi)	ϵ_1 (%)	$\bar{\sigma}_3$ (psi)	ϵ_1 (%)
	a) Uncompacted Samples			
17E	6.8	0.270	3.5	0.630
18A	4.9	0.690	3.0	1.030
18B	6.3	0.570	3.5	0.960
	b) Compacted Samples			
17E	6.8	0.110	3.5	0.250
18A	4.9	0.250	3.0	0.460
18B	6.3	0.180	3.5	0.400

Table 7-4. Prediction of ε_1 Based on Static Testing Results

Section	Stress Path CB: ε_v (%) − ε_{r_1} (%) = ε_1 (%)	Stress Path DE: ε_v (%) − ε_{r_1} (%) = ε_1 (%)
	a) Uncompacted Samples	
17E	0.507 − 0.090 = 0.417	0.786 − 0.120 = 0.666
18A	0.835 − 0.130 = 0.705	1.205 − 0.160 = 1.045
18B	0.728 − 0.115 = 0.613	1.123 − 0.155 = 0.968
	b) Compacted Samples	
17E	0.254 − 0.080 = 0.174	0.425 − 0.130 = 0.295
18A	0.440 − 0.130 = 0.310	0.703 − 0.175 = 0.528
18B	0.370 − 0.110 = 0.260	0.638 − 0.160 = 0.478

develops more permanent strain after the first cycle than stress path CB. Also, the uncompacted ballast state produces larger permanent strains after the first cycle than the compacted state.

As was presented in Section 6.3.2, the values of permanent strain after the application of N cycles (ε_N) can be predicted based on the values of ε_1 and N. Linear and nonlinear equations were presented. The linear equation is

$$\varepsilon_N = \varepsilon_1(1 + 0.19 \log N), \tag{7-3}$$

and the nonlinear equation is

$$\varepsilon_N = (0.85 + 0.38 \log N)\varepsilon_1 + (0.05 - 0.09 \log N)\varepsilon_1^2. \tag{7-4}$$

Tables 7-5, 7-6 and 7-7 present the predictions of ε_N for sections 17E, 18A and 18B, respectively. Values at 1, 10, 100, 1000, 10,000, 100,000 and 1,000,000 cycles are presented for the CB and DE stress paths for both the uncompacted and compacted conditions. These values have been derived based on ε_1 from Table 7-3 and N, the number of cycles.

From a comparison of the permanent strain values for sections 18A and 18B, the wooden tie sections, it can be seen that the methodology predicts larger permanent strains for section 18A which has the 21-in. ballast layer, than for section 18B, which has the 15-in. ballast layer. This prediction is in agreement with the larger measured values for section 18A presented in Chapter 5. On the other hand, the predicted values for the concrete tie section 17E are smaller than the predicted values for the wooden tie sections. The measured values for the concrete tie section are higher than the measured values for the wooden tie sections. As shown in Chapter 4, the stress distribution along the tie is different for the concrete and wooden tie sections. The stiffer concrete tie follows the distribution of a rigid foundation with stresses higher at the edges than in the center. The wood tie follows a distribution of a flexible

Table 7-5. Prediction of ε_N for Section 17E at the Middle of the Ballast Layer

a) Uncompacted Sample, ε_N (%)

	Stress Path CB		Stress Path DE	
Cycle N	Linear	Nonlinear	Linear	Nonlinear
1	0.270	0.270	0.630	0.630
10	0.321	0.329	0.750	0.759
100	0.373	0.425	0.869	0.963
1000	0.424	0.521	0.989	1.166
10,000	0.475	0.617	1.109	1.370
100,000	0.527	0.713	1.229	1.574
1,000,000	0.578	0.809	1.348	1.777

b) Compacted Sample, ε_N (%)

	Stress Path CB		Stress Path DE	
Cycle N	Linear	Nonlinear	Linear	Nonlinear
1	0.110	0.110	0.250	0.250
10	0.131	0.135	0.298	0.305
100	0.152	0.176	0.345	0.394
1000	0.173	0.216	0.393	0.484
10,000	0.194	0.257	0.440	0.573
100,000	0.215	0.298	0.488	0.663
1,000,000	0.235	0.338	0.535	0.752

Table 7-6. Prediction of ε_N for Section 18A at the Middle of the Ballast Layer

a) Uncompacted Sample, ε_N (%)

	Stress Path CB		Stress Path DE	
Cycle N	Linear	Nonlinear	Linear	Nonlinear
1	0.690	0.690	1.030	1.030
10	0.821	0.830	1.226	1.224
100	0.952	1.049	1.421	1.520
1000	1.083	1.268	1.617	1.816
10,000	1.214	1.488	1.813	2.112
100,000	1.346	1.707	2.009	2.408
1,000,000	1.477	1.926	2.204	2.704

b) Compacted Sample. ε_N (%)

	Stress Path CB		Stress Path DE	
Cycle N	Linear	Nonlinear	Linear	Nonlinear
1	0.250	0.250	0.460	0.460
10	0.298	0.305	0.547	0.557
100	0.345	0.394	0.635	0.713
1000	0.393	0.484	0.722	0.869
10,000	0.440	0.573	0.810	1.025
100,000	0.488	0.663	0.897	1.180
1,000,000	0.535	0.752	0.984	1.336

Table 7-7. Prediction of ε_N for Section 18B at the Middle of the Ballast Layer

a) Uncompacted Sample, ε_N (%)

	Stress Path CB		Stress Path DE	
Cycle N	Linear	Nonlinear	Linear	Nonlinear
1	0.570	0.570	0.960	0.960
10	0.678	0.688	1.142	1.144
100	0.787	0.875	1.325	1.426
1000	0.895	1.063	1.507	1.708
10,000	1.003	1.250	1.690	1.990
100,000	1.112	1.438	1.872	2.271
1,000,000	1.220	1.625	2.054	2.553

b) Compacted Sample, ε_N (%)

	Stress Path CB		Stress Path DE	
Cycle N	Linear	Nonlinear	Linear	Nonlinear
1	0.180	0.180	0.400	0.400
10	0.214	0.220	0.476	0.486
100	0.248	0.286	0.552	0.623
1000	0.283	0.351	0.628	0.761
10,000	0.317	0.417	0.704	0.898
100,000	0.351	0.482	0.780	1.036
1,000,000	0.385	0.548	0.856	1.174

foundation, with the stresses higher under the rail. For the prediction methodology, the representative or average point for the ballast layer is taken at the middle of the layer directly under the rails for both the concrete and wood tie sections. Later in this chapter, a different representative point for the ballast layer of the concrete tie section will be considered. Further research is recommended in the determination of representative points in the concrete and wood tie sections.

7.2 Comparison of Measured and Predicted Strains

The measured values of the permanent strain and deformations of the ballast, subballast and subgrade have been presented in Chapter 5. The measured values indicate that the ballast strains in section 17E (concrete tie) are higher than the ballast strains in the wooden tie sections. The measured values for the 21-in. ballast layer, wooden tie section are higher than those in the 15-in. ballast layer section.

The main emphasis of this report is the prediction of ballast strains. The prediction of the subballast strains and subgrade deformations is more straightforward because the stress paths imposed on these layers by the passing trains are close to those produced in the repeated load triaxial testing. This is not the case for the ballast layer, where truly three-dimensional conditions exist and large variations of stresses within the layer are developed. The problem is further complicated because the model employed predicts tension zones at the bottom of the ballast layer that are impossible to simulate in the triaxial test, and in fact, cannot actually occur in the ballast.

The measured values have been taken in the field as a function of MGT (million gross tons) of accumulated traffic. A conversion from MGT values to equivalent number of cycles of load application is necessary. After studying the dynamic records available and recognizing that each axle pair in a truck acts

nearly as a single load cycle, it was decided that two cycles of load would be imposed by each car of the train. Each car was assumed to weigh 131.6 tons. Thus each 65.8×10^{-6} MGT is assumed to represent 1 cycle of load.

The records of dynamic measurement at FAST shows that partial unloading occurs between axles and trucks. The effect of partial unloading was not investigated, but according to Shenton (Ref. 46), partial unloading will produce more permanent strain.

Figures 7-3 through 7-5 present the comparison of the measured values of the permanent strain in the ballast layer with the predicted values using the equivalent stress paths at the middle of the ballast layer under the rails for sections 17E, 18A and 18B, respectively. The predicted values are based on Eq. 7-4. Both stress paths and both ballast states are presented. As can be seen in the figures, both the stress path and the degree of compaction have an effect on the predicted values of permanent strain. The in-situ ballast condition is probably between the uncompacted and compacted states prepared in the laboratory.

Permanent strains predicted by stress paths CB and DE are plotted in Figs. 7-3 to 7-5. The actual in-situ stress path AB is different than either stress path CB or DE. This can be a reason for disagreement between the measured and predicted permanent strains in the ballast layer. It is recommended that further equipment development be undertaken to permit tests following the stress path AB in the laboratory. This involves the capability of cycling the confining pressure in phase with the cycling of the deviatoric stress.

The best agreement between predicted and measured results is given by section 18B, the wooden tie section with 15 in. of ballast. The measured values are closer to the predicted values using stress path DE. Also, a density

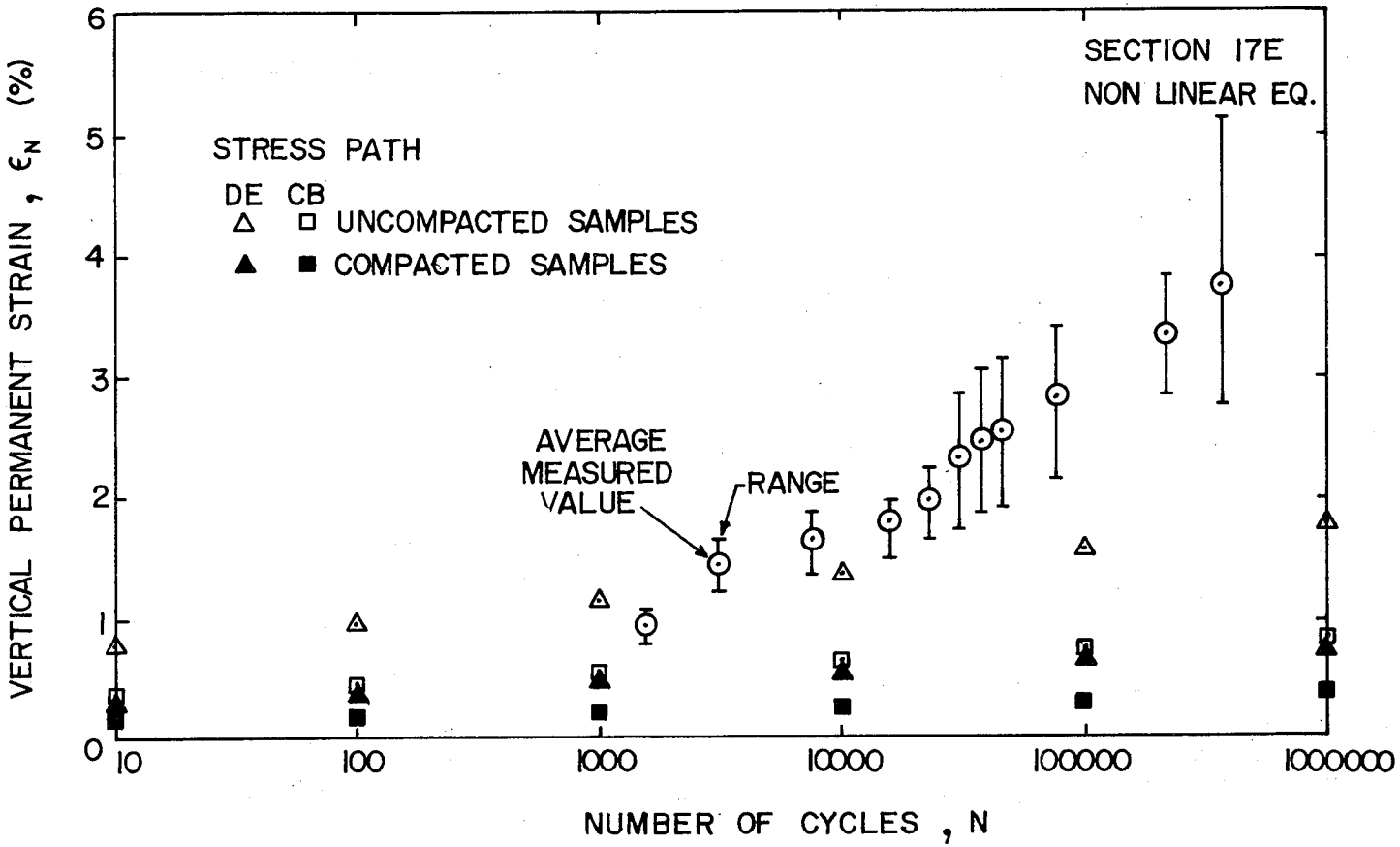

Fig. 7-3. Comparison of Predicted and Measured Values of Ballast Permanent Strain for Section 17E

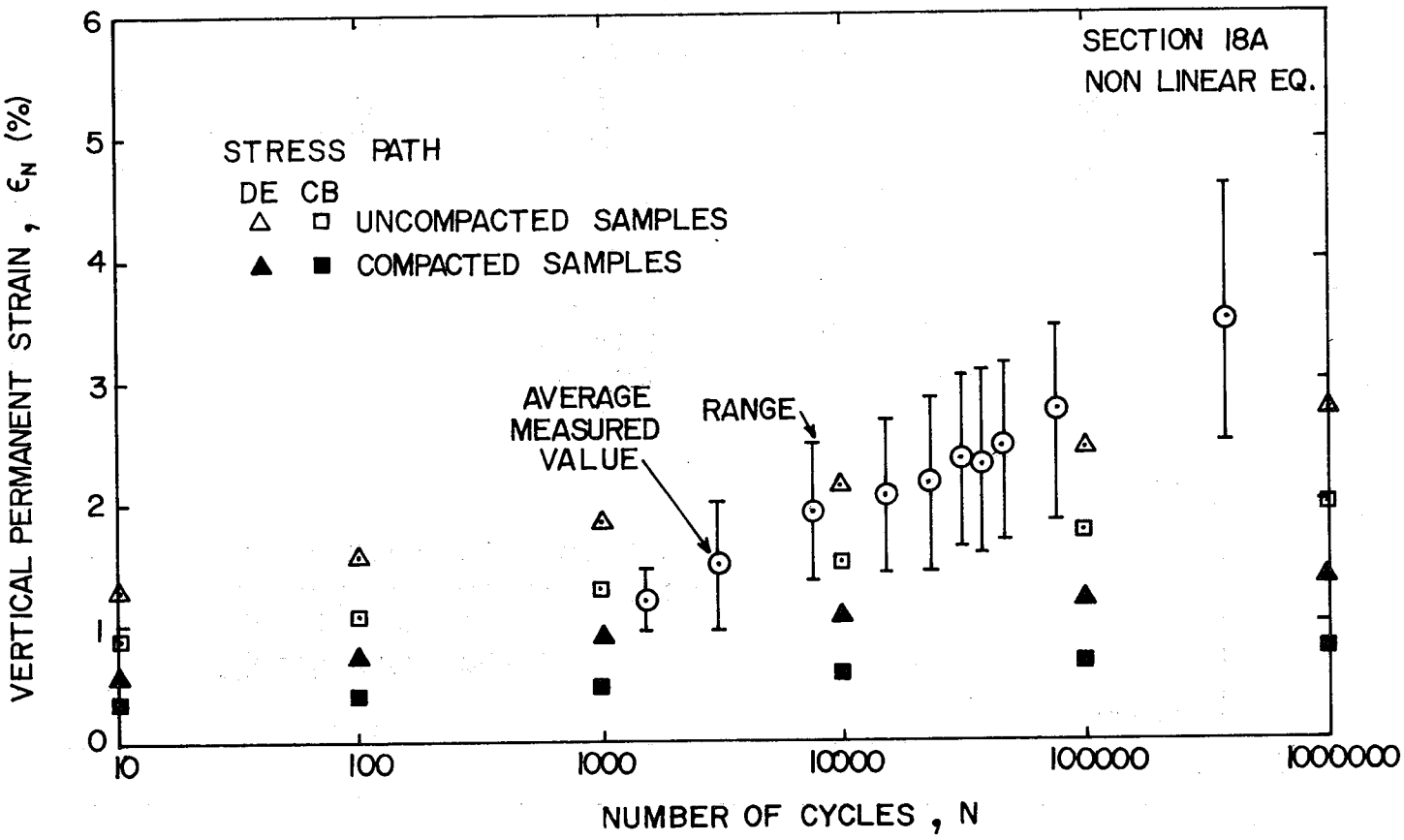

Fig. 7-4. Comparison of Predicted and Measured Values of Ballast Permanent Strain for Section 18A

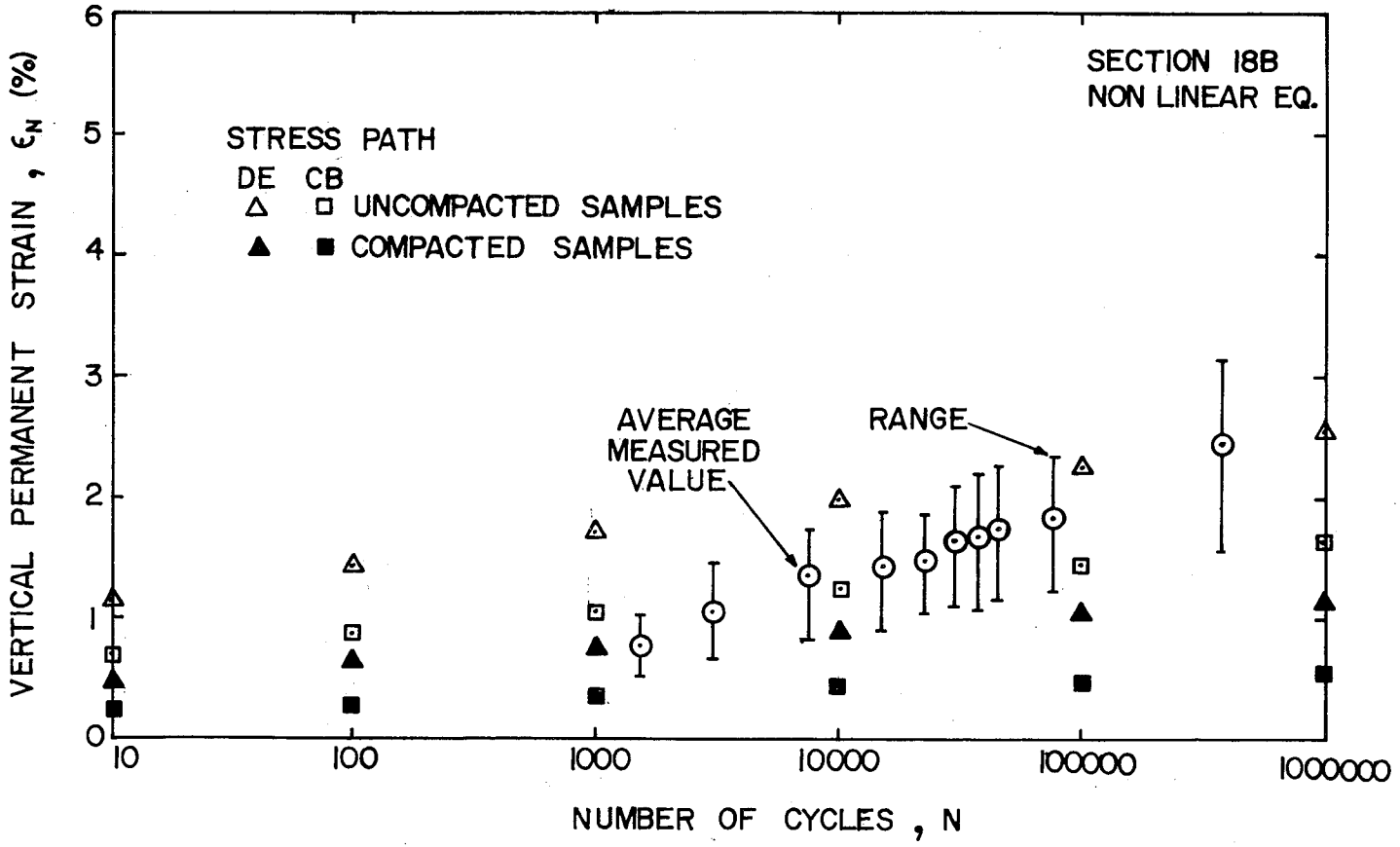

Fig. 7-5. Comparison of Predicted and Measured Values of Ballast Permanent Strain for Section 18B

condition between the uncompacted and compacted states is best representing the field behavior. It should be mentioned that most of the laboratory testing was taken to a maximum of 100,000 cycles, representing 6.5 MGT's. Further research is recommended to extend the number of laboratory load applications to at least 1 million cycles, representing 65.8 MGT's.

It is noticed in Fig. 7-5 that the slope of the curve of measured permanent strain with number of cycles is steeper than the slope of the curves of predicted values of permanent strain with number of cycles. Further verification of this fact is necessary by subjecting laboratory samples to larger number of cycles of load applications.

An intermediate degree of agreement is obtained for section 18A (Fig. 7-4) which is the deeper ballast layer on wooden ties. More permanent strain is predicted for this section than for section 18B, which is the shallower ballast depth on wooden ties. The prediction seems to worsen with further application of loading cycles.

The poorest prediction is for section 17E (Fig. 7-3), which is the concrete tie section. The permanent strain is underpredicted by a factor of 2 at the higher load applications. As was previously mentioned, further study is recommended, in particular to properly determine the representative point with the different stress distribution in the ballast produced by concrete and wooden ties.

7.3 Discussion of Comparison

Further studies were undertaken for section 17E, the concrete tie section that gave the poorest prediction. Because the concrete tie section develops a different stress distribution along the tie than the wooden tie sections, a different representative point under the end of the tie was chosen. Because the

stresses are higher under the ends than under the center of the concrete tie, the representative point was taken near the end of the tie. The depth of the new representative point was also at the middle of the ballast layer.

Figure 7-6 presents the new equivalent stress paths CB and DE for the concrete tie section 17E. Only the results produced by stress path CB will be analyzed. Stress path DE creates a condition near to failure in this case.

The same procedure previously presented for predicting ε_1 for both uncompacted and compacted density conditions was undertaken. Table 7-8 presents the prediction of ε_N for stress path CB for the uncompacted and compacted samples using the linear and nonlinear equations, Eqs. 7-3 and 7-4. Figure 7-7 presents the prediction values of ballast strain using the new representative point. A comparison of Figs. 7-3 and 7-7 indicates that there is a better agreement using this representative point under the tie ends than under the rail for the concrete tie section. Therefore, the prediction values for section 17E are improved.

Some of the factors that could contribute to the disagreement of the predicted and measured values of the ballast permanent strain are:

1. There is a high variability in the field data of the measured response of the ballast.
2. The computer model predicts a tension zone at the bottom of the ballast layer, in accordance with multi-layer theory. The ballast material cannot take tension, therefore failure states are produced in the equivalent stress paths. The computer model does not incorporate a failure criteria that can redistribute the stresses.
3. The three-dimensional state of stress in the ballast layer is converted to an equivalent axisymmetrical state. This stress path cannot be reproduced by conventional laboratory testing equipment.

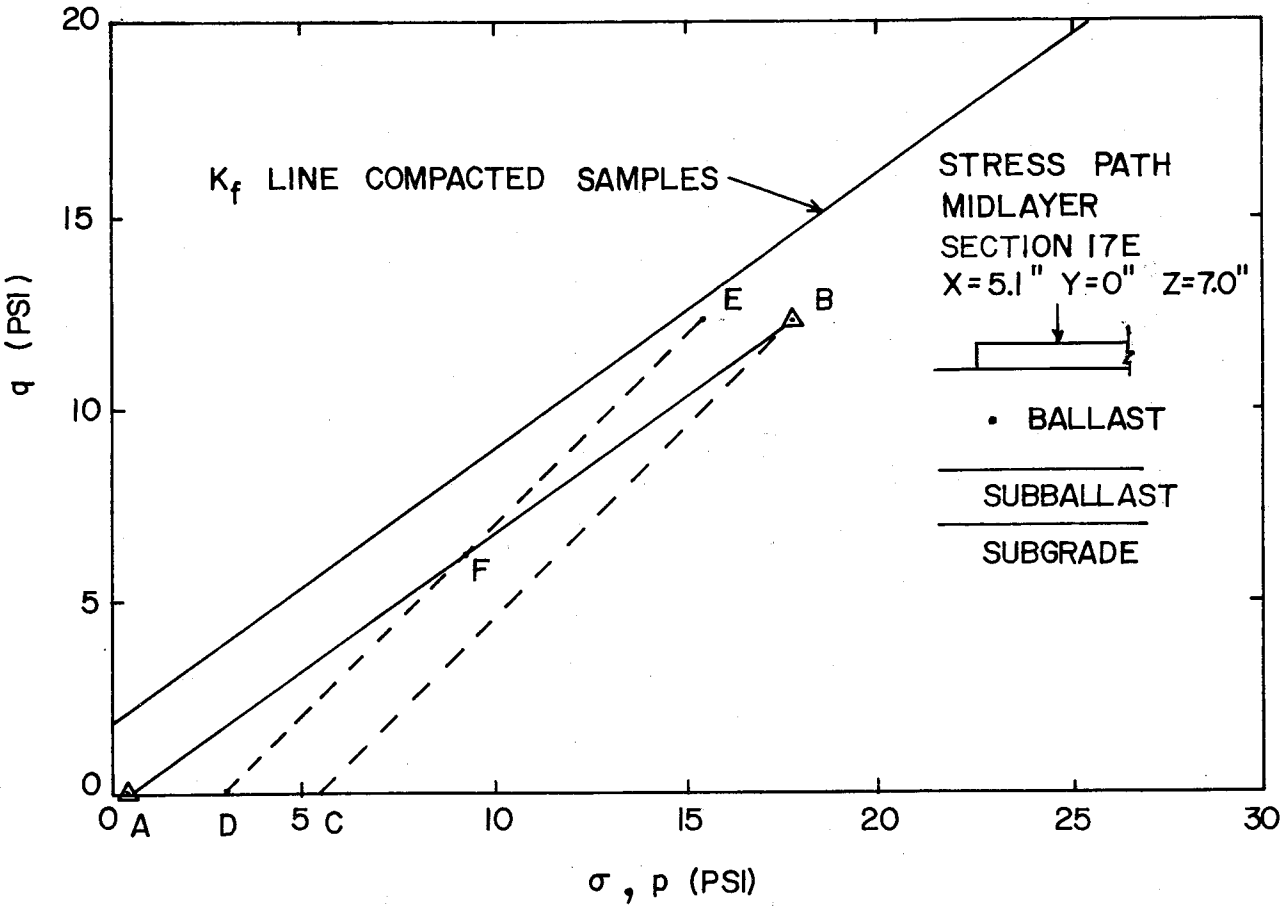

Fig. 7-6. Stress Paths for the Middle of the Ballast Layer at the End of the Tie in Section 17E

Table 7-8. Prediction of ε_N for Section 17E
(Mid-layer x = 5.1 in.)

a) Uncompacted Sample, ε_N (%)

	Stress Path CB	
Cycle N	Linear	Nonlinear
1	1.360	1.360
10	1.618	1.599
100	1.877	1.949
1000	2.135	2.299
10,000	2.394	2.650
100,000	2.652	3.000
1,000,000	2.910	3.350

b) Compacted Sample, ε_N (%)

	Stress Path CB	
Cycle N	Linear	Nonlinear
1	0.530	0.530
10	0.631	0.641
100	0.731	0.817
1000	0.832	0.993
10,000	0.933	1.169
100,000	1.034	1.345
1,000,000	1.134	1.521

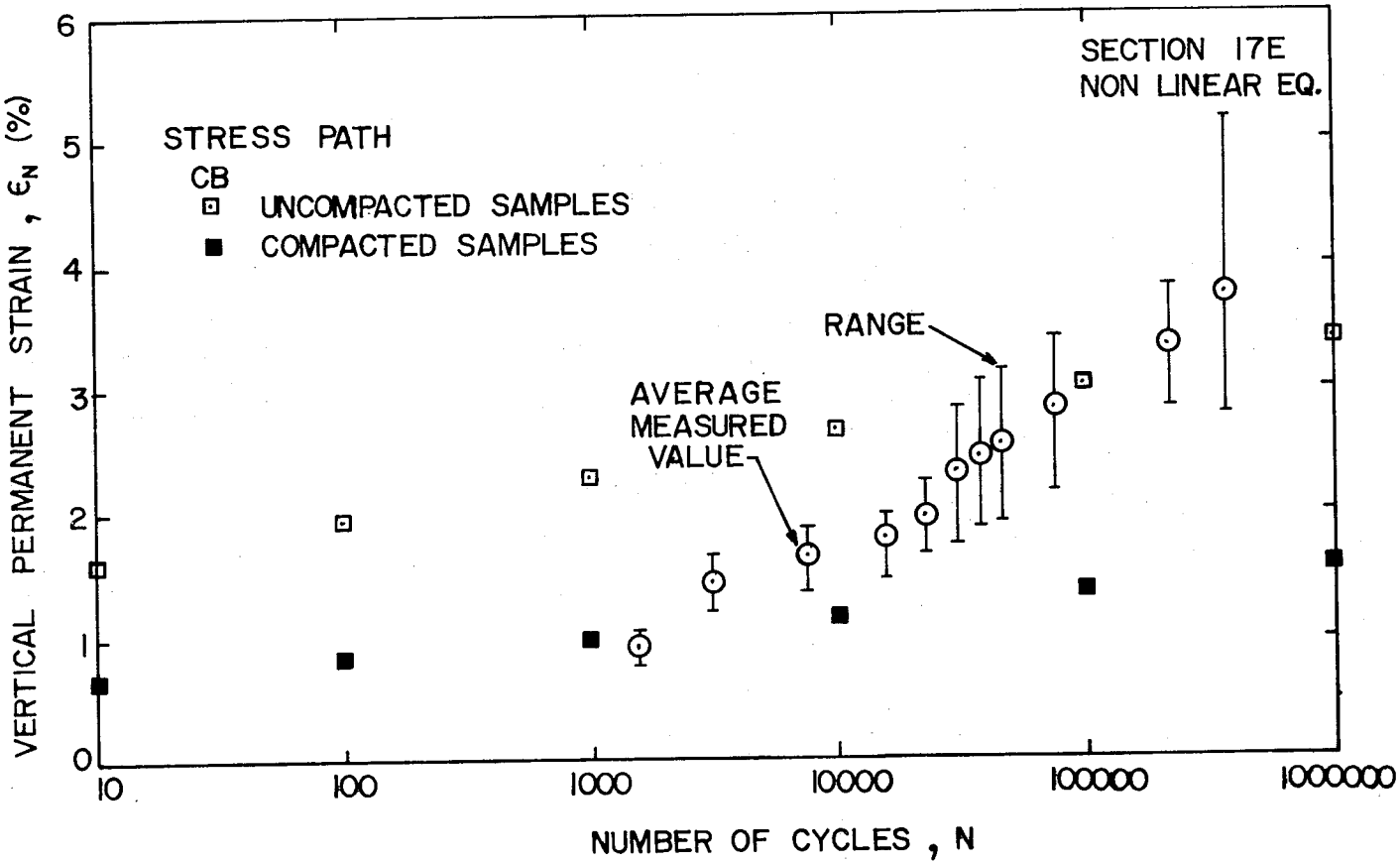

Fig. 7-7. Comparison of Predicted and Measured Values of Ballast Permanent Strain for Section 17E for a Representative Point Under the Tie Ends

4. The representative point in the ballast layer requires further study. It was demonstrated that the concrete and wood tie sections do not have the same representative point.
5. The cyclic laboratory testing used sinusoidal waves to simulate the conditions imposed by the passing trains. Partial unloading was not taken into consideration.
6. The laboratory testing was constrained to a small number of load applications up to 100,000 cycles. It is necessary to extend the number of cycles of load application to simulate larger accumulation of traffic.

Further methodology validation needs to be undertaken for the subballast strains and subgrade deflections as well as the limestone and traprock ballasts at FAST.

CHAPTER 8. SUMMARY AND CONCLUSIONS

The need for maintenance of track is assumed to be represented by the amount of permanent deformation caused by repeated cycles of loading on the ballast and underlying layers. The development of a theory for predicting this permanent deformation was the objective of this study.

Field observations showed that the roadbed strains in the track structure caused by train loads were essentially elastic, although the modulus of the materials are dependent on the stress level. After considering available computer models for representing the elastic response of the track structure, a new model, GEOTRACK, was developed that was economical to use and contained the essential features of the system. The model was shown to be in reasonable agreement with field results.

Laboratory triaxial test apparatus was developed to measure the properties of the ballast materials. Static tests were conducted with constant confining pressure and increasing axial load to determine the stress-strain and strength behavior of granite ballast over a range of density states representing field conditions. Repeated load or cyclic triaxial tests were conducted with the same confining pressure and density conditions to measure the resilient modulus and rate of permanent strain development. An important finding was that the cumulative permanent axial strain after any cycle of loading was a function only of the strain after the first cycle and the number of cycles. This relationship was not affected by the ballast type or density state. As a consequence, the development of permanent strains can even be approximately predicted by static test results.

To make a prediction of permanent compression in the ballast for a given set of track and traffic conditions, the stress state at the middepth of the

ballast layer beneath the tie is calculated using the GEOTRACK model. The stress-dependent elastic modulus of each of the layers is the resilient modulus determined from the triaxial tests. The three-dimensional state of stress in the unloaded condition and with the designated axle load over the tie is used to define the stress paths to which the ballast layer is subjected with each axle load cycle. These stress paths then define equivalent stress states for the constant-confining-pressure cyclic triaxial tests. The axial strains in the triaxial test for these stress states are assumed to represent the vertical strains in the ballast layer. The particular values of stress in a given case will determine the magnitude of permanent ballast strain after a designated number of cycles of a specified axle load. The ballast layer compression is equal to the product of this strain and the layer thickness.

Using this approach, ballast permanent strains were predicted as a function of train traffic (defined by the number of tons of train loading) for the granite ballast sections of the FAST track. The predicted results were in approximate agreement with the field results.

The methodology developed in this study appears to provide a reasonable and rational approach for permanent deformation prediction of track. The method can take into account the main factors influencing the deformation behavior, including axle load and number of cycles, rail and tie characteristics, and properties and thickness of the ballast and underlying layers. However, at the present time the model only represents uniform track settlement rather than the differential settlement that causes the need for maintenance. In the continuation of this study, consideration will be given to extending the theory to provide a means of predicting the nonuniform behavior.

REFERENCES

1. Selig, E.T., Chang, C.S., Adegoke, C.W. and Alva-Hurtado, J.E., "A Theory for Track Maintenance Life Prediction," Final Report on First Year of Study, prepared for USDOT, Report No. DOT-RSPA-DPB-50-79-22, August, 1979.

2. Adegoke, C.W., "Elastic and Inelastic Deformation Response of Track Structures Under Train Loads," Ph.D. Dissertation, Department of Civil Engineering, State University of New York at Buffalo, December, 1978.

3. Alva-Hurtado, J.E., "A Methodology to Predict the Elastic and Inelastic Behavior of Railroad Ballast," Ph.D. Dissertation, Department of Civil Engineering, University of Massachusetts at Amherst, May, 1980.

4. Yoo, T.S. and Selig, E.T., "Field Observations of Ballast and Subgrade Deformations in Track," Transportation Research Board, Transportation Research Record No. 733.

5. Chang, C.S., Adegoke, C.W. and Selig, E.T., "A Study of Analytical Models for Track Support System," TRB, Transportation Research Record No. 733.

6. Selig, E.T., Yoo, T.S., Adegoke, C.W., and Stewart, H.E., "Status Report - Ballast Experiments, Intermediate (175 MGT) Substructure Stress and Strain Data," Prepared for USDOT, Transportation Systems Center, Cambridge, Massachusetts, September, 1979.

7. Seed, H.B., Chan, C.K., and Monismith, C.L., "Effects of Repeated Loading on the Strength and Deformation of Compacted Clay," Proceedings, Highway Research Board, Vol. 34, pp. 541-558, 1955.

8. Morris, J., Haas, R.C.G., Reilly, P. and Hignell, E.T., "Permanent Deformations in Asphalt Pavements Can be Predicted," Proceedings, American Association of Paving Technologists, Volume 43, pp. 41-76, 1974.

9. McLean, D.B. and Monismith, C.L., "Estimation of Permanent Deformation in Asphalt Concrete Layers Due to Repeated Traffic Loading," TRB, Transportation Research Record No. 510, pp. 14-30, 1974.

10. Freeme, C.R. and Monismith, C.L., "The Analysis of Permanent Deformation in Asphalt Concrete Pavement Structures," Proceedings, 2nd Conference on Asphalt Pavements for Southern Africa, 1974.

11. Snaith, M.S., "Permanent Deformation Characteristics of a Dense Bitumen Macadam," Ph.D. Thesis, University of Nottingham, England, 1973.

12. Barksdale, R.D., "Repeated Load Test Evaluation of Base Coarse Materials," Georgia Institute of Technology, May, 1972.

13. Olowokere, D.O., "Strength and Deformation of Railway Ballast Subject to Triaxial Loading," M.Sc. Thesis, Department of Civil Engineering, Queen's University, Canada, 1975.

14. Knutson, R.M., "Factors Influencing the Repeated Load Behavior of Railway Ballast," Ph.D. Thesis, University of Illinois at Urbana-Champaign, 1976.

15. Edris, E.V., "Dynamic Properties of Subgrade Soils, Including Environmental Effects," Master's Thesis, Texas A & M University, May, 1976.

16. Kondner, R.L. and Zelasko, J.S., "A Hyperbolic Stress-Strain Formulation for Sands," Proceedings, Second Pan-American Conference on Soil Mechanics and Foundations Engineering, Brazil, Vol. I, pp. 289-324, 1963.

17. Duncan, J.M. and Chang, C.Y., "Nonlinear Analysis of Stress and Strain in Soils," Proceedings, Journal of the Soil Mechanics and Foundations Division, ASCE, Volume 96, SM5, September, 1970.

18. Dehlen, H.L., "The Effect of Nonlinear Material Response on the Behavior of Pavements Subjected to Traffic Loads," Ph.D. Thesis, University of California at Berkeley, 1969.

19. Huang, Y.H., "Stresses and Displacements in Nonlinear Soil Media," Proceedings, JSMFD, ASCE, Vol. 94, SMI, January, 1968.

20. Chou, Y.T., "An Iterative Layered Elastic Computer Program for Rational Pavement Design," Report No. FAA-RD-75-226, U.S. Army Engineer Waterways Experiment Station, Vicksburg, Mississippi, February, 1976.

21. Seed, H.B., Mitry, F.G., Monismith, C.L. and Chan, C.K., "Prediction of Pavement Deflections from Laboratory Repeated Load Tests," Report No. TE-65-6, Soil Mechanics and Bituminous Materials Research Laboratory, University of California at Berkeley, October, 1965.

22. Hicks, R.G. and Monismith, C.L., "Factors Influencing the Resilient Response of Granular Materials," Highway Research Record No. 345, 1971.

23. Brown, S.F., Lashine, A.K.F. and Hyde, A.F.L., "Repeated Load Triaxial Testing of a Silty Clay," Geotechnique, Vol. 25, No. 1, pp. 95-114, 1975.

24. Thompson, M.R., "FAST Ballast and Subgrade Materials Evaluation," Interim Report Prepared by the University of Illinois for U.S. DOT Federal Railroad Administration, Report No. FRA/ORD-77/32, December, 1977.

25. Barksdale, R.D. and Hicks, R.G., "Material Characterization and Layered Theory for Use in Fatigue Analysis," Highway Research Board Special Report 140, January, 1973.

26. Burmister, D.M., "The General Theory of Stresses and Displacements in Layered Systems," Journal of Applied Physics, Vol. 16, No. 2, 1945.

27. Desai, C.S. and Abel, J.F., "Introduction to the Finite Element Method," Van Nostrand, 1972.

28. Barksdale, R.D., "Laboratory Evaluation of Rutting in Base Coarse Materials," Proceedings, Third International Conference on the Structural Design of Asphalt Pavements, pp. 161-174, London, England, 1972.

29. Hargis, L.L., "A Study of Strain Characteristics in a Limestone Gravel Subjected to Repetitive Load," Master's Thesis, Texas A & M University, 1963.

30. Haynes, J.H. and Yoder, E.J., "Effects of Repeated Loading on Gravel and Crushed Stone Base Coarse Materials Used in the AASHTO Road Test," Highway Research Record No. 39, 1963.

31. Hicks, R.G., "Factors Influencing the Resilient Properties of Granular Materials," Ph.D. Thesis, University of California at Berkeley, 1970.

32. Allen, J.J., "The Effects of Non-Constant Lateral Pressures on the Resilient Properties of Granular Materials," Ph.D. Thesis, University of Illinois at Urbana, 1973.

33. Morgan, J.R., "The Response of Granular Materials to Repeated Loading," Proceedings, Third Conference of the Australian Road Research Board, pp. 1178-1192, 1966.

34. Shackel, B., "Repeated Loading of Soils---, A Review," Australian Road Research 5, (3), pp. 22-49, 1973.

35. Brown, S.F., "Repeated Load Testing of a Granular Material," Journal of the Geotechnical Engineering Division, Vol. 100, No. 7, ASCE, 1974.

36. Robnett, Q.L., Thompson, M.R., Knutson, R.M. and Tayabji, S.D., "Development of a Structural Model and Materials Evaluation Procedures," Ballast and Foundation Materials Research Program, University of Illinois at Urbana, Report No. FRA-OR&D-76-255, July, 1976.

37. Robnett, Q.L., Thompson, M.R. and Hay, W.W., "Ballast and Foundation Materials Research Program," University of Illinois at Urbana, July, 1975.

38. Brown, S.F. and Hyde, A.F.L., "Significance of Cyclic Confining Stress in Repeated-Load Triaxial Testing of Granular Material," TRB, Transportation Research Record No. 537, pp. 49-57, 1975.

39. Dunlap, W.A., "Deformation Characteristics of Granular Materials Subjected to Rapid Repetitive Loading," Research Report 27-4, Texas Transportation Institute, 1966.

40. Seed, H.B., Mitry, F.G., Monismith, C.L. and Chan, C.K., "Prediction of Flexible Pavement Deflections from Laboratory Repeated Load Tests," National Cooperative Highway Research Program, Report No. 35, Highway Research Board, Washington, D.C., 1967.

41. Thompson, O.O., "Evaluation of Flexible Pavement Behavior with Emphasis on the Behavior of Granular Layers," Ph.D. Thesis, University of Illinois at Urbana, 1969.

42. Allen, J.J. and Thompson, M.R., "Resilient Response of Granular Materials Subjected to Time-Dependent Lateral Stresses," Transportation Research Record No. 510, pp. 1-13, 1974.

43. Kalckeff, I.V. and Hicks, R.G., "A Test Procedure for Determining the Resilient Properties of Granular Materials," Journal of Testing and Evaluation, ASTM, Vol. 1, No. 6, pp. 472-479, November, 1973.

44. Boyce, J.R., Brown, S.F. and Pell, P.S., "The Resilient Behavior of a Granular Material Under Repeated Loading," Proceedings, Australian Road Research Board, Vol. 8, pp. 8-19, 1976.

45. Office for Research and Experiments, International Union of Railways, "Stresses in the Rails, the Ballast and in the Formation Resulting from Traffic Loads," Question D71, Report No. 10, Vols. 1 and 2, Utrecht, Holland, 1970.

46. Shenton, M.J., "Deformation of Railway Ballast Under Repeated Loading," Soil Mechanics Section, British Railways Research Department, 1974.

47. Lade, P.V. and Duncan, J.M., "Stress-Path Dependent Behavior of Cohesionless Soil," Journal of the Geotechnical Engineering Division, GT1, ASCE, January, 1976.

48. Raymond, G.P. and Williams, D.R., "Repeated Load Triaxial Tests on a Dolomite Ballast," JGED, GT7, ASCE, pp. 1013-1029, July, 1978.

49. Hyde, A.K.L., "Repeated Load Triaxial Testing of Soils," Ph.D. Thesis, University of Nottingham, England, 1974.

50. Transportation Research Board, "Soil Mechanics: Rutting in Asphalt Pavements, Embankments on Varved Clays, and Foundations," Transportation Research Record No. 616, Washington, D.C., 1976.

51. Monismith, C.L., "Rutting Prediction in Asphalt Concrete Pavements - A State-of-the-Art," Symposium on Predicting Rutting in Asphalt Concrete Pavements, Transportation Research Board, Washington, D.C., 1976.

52. Monismith, C.L. and Finn, F.N., "Flexible Pavement Design: State-of-the-Art, 1975," Transportation Engineering Journal, TE1, ASCE, January, 1975.

53. Van de Loo, P.J., "A Practical Approach to the Prediction of Rutting in Asphalt Pavements-The Shell Method," Annual Meeting of the Transportation Research Board, Washington, D.C., 1976.

54. Brown, S.F., "Improved Framework for Predicting Permanent Deformation in Asphalt Layers," TRB, Transportation Research Record No. 537, pp. 18-38, 1975.

55. Raymond, G.P. and Davies, J.R., "Triaxial Tests on Dolomite Railroad Ballast," JGED, GT6, pp. 737-751, June, 1978.

56. Nie, N.H., Hull, C.H., Jenkins, J.G., Steinbrenner, K. and Bent, D.H., "SPSS Statistical Package for the Social Sciences," 2nd Edition, McGraw Hill, 1975.

*U.S. GOVERNMENT PRINTING OFFICE : 1981 0-729-786/2134

REQUEST FOR FEEDBACK TO
The DOT Program Of University Research

This booklet is intended to serve as a reference source for transportation analysts, planners and operators. Your comments will be reviewed by the persons responsible for writing and publishing this material. Feedback is extremely important in improving the quality of research results, the transfer of research information, and the communication link between the researcher and the user.

YES	NO	
☐	☐	Did you find the report useful for your particular needs? If so, how?
☐	☐	Did you find the research to be of high quality?
☐	☐	Were the results of the research communicated effectively by this report?
☐	☐	Do you think this report will be valuable to workers in the field of transportation represented by the subject area of the research?
☐	☐	Are there one or more areas of the report which need strengthening? Which areas?
☐	☐	Would you be interested in receiving further reports in this area of research? If so, fill out form on other side.

Please furnish in the space below any comments you may have concerning the report. We are particularly interested in further elaboration of the above questions.

COMMENTS

Thank you for your cooperation. No postage necessary if mailed in the U.S.A.

RESEARCH INTEREST

PLEASE CHECK YOUR AREAS OF INTEREST. YOU WILL BE NOTIFIED AS NEW REPORTS ARE PUBLISHED.

TRANSPORTATION

- ☐ Air
- ☐ Highway
- ☐ Maritime & Ports
- ☐ Mass Transit
- ☐ Pipeline
- ☐ Rail

ECONOMIC REGULATION

- ☐ Air Carrier
- ☐ Motor Carrier
- ☐ Railroads

TRANSPORTATION STUDIES IN SPECIAL AREAS

- ☐ Advanced Technology
- ☐ Energy
- ☐ Environment
- ☐ Facilities & Terminals
- ☐ Hazardous Materials
- ☐ Safety
- ☐ Tunnelling
- ☐ Construction, Rehabilitation & Maintenance
- ☐ Efficiency, Productivity & Innovation
- ☐ Elderly, Handicapped & Disadvantaged
- ☐ Freight, Goods Movement & Commodity Flow
- ☐ Modeling - Demand, Supply & Traffic
- ☐ Rural Development, Planning & Policy
- ☐ Urban Development, Planning & Policy

☐ OTHER (PLEASE LIST) _____

_____

_____

U.S. DEPARTMENT OF TRANSPORTATION
Research and Special Programs Administration
Washington, D.C. 20590

NO POSTAGE NECESSARY IF MAILED IN THE UNITED STATES

BUSINESS REPLY MAIL

FIRST CLASS PERMIT NO. G-126

POSTAGE WILL BE PAID BY ADDRESSEE

OFFICE OF UNIVERSITY RESEARCH
Attn: HELEN L. ENGRUM (DPB-50)
U.S. DEPARTMENT OF TRANSPORTATION
400 Seventh Street, S.W.
Washington, D.C. 20590

PLEASE LIST YOUR NAME AND ADDRESS.

NAME _____

TITLE _____

ORGANIZATION _____

STREET _____

CITY, STATE, ZIP CODE _____

U.S. Department
of Transportation

**Research and
Special Programs
Administration**

400 Seventh St., S.W.
Washington, D.C. 20590

Official Business
Penalty for Private Use $300

Postage and Fees Paid
Research and Special
Programs
Administration
DOT 513